

POLITECNICO DI TORINO MASTER DEGREE IN ENVIRONMENTAL AND LAND ENGINEERING

TRACK: CLIMATE CHANGE

DEPARTMENT OF ENVIRONMENT, LAND AND INFRASTRUCTURE ENGINEERING (DIATI)

Defining Embodied Emissions for Concentrated Solar System, in the framework of the PYSOLO project

Supervisor:		
Prof.Matteo PRUSSI		
	By:	
	Marvam KARRAR	s312270

October 2025

Acknowledgements

I would like to express my deepest gratitude to my supervisor, Professor Matteo Prussi, for granting me the invaluable opportunity to contribute to this innovative and ambitious project. His unwavering support, insightful guidance, and enthusiasm have been instrumental throughout my research journey. His confidence in my abilities and his encouragement at every stage have continually motivated me to strive for excellence.

I am sincerely thankful to Francesco Barracco, Joao Victor De Oliveira Pontes, and Payam Danesh, Ph.D. candidates at the Politecnico di Torino, for their valuable advice, technical support, and collaborative spirit. Their contributions greatly enriched the quality and depth of this work.

My appreciation also extends to Clarisse Lorreyte, Justin Eckstein, and Karolina Wirtz-Duerlich at DLR for their sustained assistance and for providing essential data related to the rotary kiln. I am equally grateful to Ferdinand Kähler at NOVA for his constructive input on the life cycle assessment and his thoughtful, practical advice.

I acknowledge with gratitude the German Aerospace Center (DLR) and all PYSOLO project collaborators for their generous technical support, data sharing, and valuable insights, which were pivotal to the progress of this research. Their dedication to innovation and sustainability has provided a strong foundation for this work.

Finally, I wish to thank my family. Although physically distant during this period, their unconditional love, encouragement, and unwavering belief in me have been a constant source of strength. Their emotional support has been a cornerstone of both my personal and academic journey.

Abstract

This thesis presents a cradle-to-grave Life Cycle Assessment (LCA) of the solar subsystem within the PYSOLO project—Pyrolysis of biomass by concentrated solar power—a Horizon Europe initiative. The aim of the study is to assess the environmental performance of the solar subsystem, which comprises the heliostat field and the solar particle receiver, in enabling pyrolysis within the PYSOLO process. A key innovation of the system is the use of particle heat carriers (PHCs)—including silica sand, bauxite, and olivine—within a rotary kiln reactor that functions both as the solar receiver and the heat transfer medium in a central tower configuration. Once heated, the particles are transferred to a downstream pyrolysis reactor.

The solar subsystem analyzed in this study consists of a heliostat field of mirrored, sun-tracking devices that concentrate sunlight, and a rotary kiln solar receiver adapted for the PYSOLO application. The system is designed to provide 15 kW of thermal power to the rotary kiln, using a five-heliostat configuration to ensure reliable operation under realistic solar conditions. Three operational scenarios are compared, each employing a different PHC material.

For this LCA, the functional unit (FU) is defined as 1 kWh of useful thermal energy delivered to the particle bed in the rotary kiln. System lifetime production is parameterized by a Net Functional Unit (NFU) case of 98,550 kWh, corresponding to a laboratory baseline equivalent to 2 h/day operation over 15 years. This definition enables consistent normalization of all material, energy, and emissions flows across scenarios. Since PHCs are continuously reused inside the kiln, only the replacement material required to compensate for wear and loss is considered as an input, allowing more precise comparisons between scenarios.

As the system is still under development, the analysis relies on numerical simulations, engineering assumptions, and scaled estimates rather than measured operational data. The LCA was conducted using OpenLCA in accordance with ISO 14040/44, applying the Ecoinvent v3.10 database supplemented with custom data. The assessment covers the full life cycle of the solar subsystem, from construction and operation to end-of-life, and evaluates six environmental impact categories using the ReCiPe 2016 Midpoint (H) method, with emphasis on greenhouse gas emissions, non-renewable energy use, land use, and water consumption.

The results indicate that heliostat construction is the dominant contributor to environmental impacts across all categories. In the climate change category, contributions are similar for all three particle heat carriers, with heliostat construction accounting for 57% of emissions, followed by heliostat operation (25%), rotary kiln construction (12%), and end-of-life stages of heliostats and rotary kilns (4% and 1%, respectively). Rotary kiln operation contributes only 1%. Human toxicity is almost entirely driven by heliostat construction (77%), with smaller shares from rotary construction (12%) and heliostat operation (11%). In terms of material resource use (for bauxite), heliostat construction contributes 48%, rotary kiln construction 32%, heliostat operation 16%, and rotary operation 4%, while end-of-life stages remain negligible. For land use (with sand), heliostat construction again dominates (62%), followed by heliostat operation (25%), rotary kiln construction (9%), and end-of-life stages (3% for heliostats and 1% for the kiln), with rotary operation having no significant influence. Overall, while the choice of particle heat carrier (bauxite, sand, or olivine) results in minor variations within specific categories, the environmental profile is consistently shaped primarily by heliostat construction.

Despite relying on scaled assumptions, this study provides the first comprehensive environmental profile for the PYSOLO solar-biomass integration. It identifies key environmental hotspots,

evaluates the influence of design parameters, and offers guidance for improving the sustainability of future PYSOLO deployments.

Contents

A	cknov	vledgement	j
Al	bstrac	t	ii
Li	st of]	Figures	vii
Li	st of '	Tables	ix
Li	st of A	Abbreviations	X
1	Intr	oduction	1
	1.1	Background and Context	1
	1.2	Problem Statement	4
	1.3	Objectives of the Thesis	4
	1.4	Research Questions	6
	1.5	Scope and Limitations	6
	1.6	Thesis Structure	6
2	Tecl	nnological Background	8
	2.1	PYSOLO components	8
	2.2	Concentrated Solar Power Technologies	9
		2.2.1 Types of CSP Systems	9
		2.2.2 Thermal Energy Storage (TES) and Dispatchability	10
		2.2.3 Deployment Trends and Strategic Importance	11
	2.3	Rotary Kiln Receiver Design	11
		2.3.1 Concept and Operating Principle	12
		2.3.2 Receiver Configuration	13
		2.3.3 Materials and Mechanical Construction	13
		2.3.4 Thermal Performance and Operating Conditions	14
		2.3.5 Simulation and Experimental Validation	15
	2.4	Particle Heat Carriers (PHCs)	16
		2.4.1 Functional Requirements	16
		2.4.2 Common Materials in Literature	16
		2.4.3 Particle Selection for PYSOLO	17
	2.5	Jülich Solar Tower Facility	18
		2.5.1 Overview of the Jülich Solar Tower Facility	18
		2.5.2 Retrofitting History and Field Performance at Jülich	19
		2.5.3 Control System and Operational Management	20
		2.5.4 Tower Infrastructure and Experimental Platforms	21
		2.5.5 Advances in Heliostat Design and Material Properties	22
3	Syst	em Overview	23
	3.1	System Configuration	23
		3.1.1 Power from Individual Heliostats	23

CONTENTS

		3.1.2	Sensitivity to Less Favorable Conditions	24
		3.1.3	System Operational Lifetime and Energy Delivery	24
		3.1.4	Heat Delivered to the Kiln	25
		3.1.5	Solar Power Requirements	25
		3.1.6	Scaling to Lifetime	26
	3.2	PHC S	Scenarios	27
4	IC	N / - 41	3-1	21
4			odology	31
	4.1 4.2		nd Scope	31 31
			onal Unit	
	4.3 4.4		Cycle Phases	32 32
	4.4	4.4.1	are and Databases	32
		4.4.1	Allocation procedures	32
		4.4.2	Cut-off rules	32
	15		Data quality	
	4.5		n Boundaries	33
	4.6	4.6.1	ycle Inventory (LCI)	34
			Heliostat Construction	35 47
		4.6.2	Heliostat Operation and Maintenance	
		4.6.3	Heliostat End-of-Life	49
		4.6.4	Rotary kilo Construction	52
		4.6.5 4.6.6	Rotary kiln Operation	58 58
		4.6.7	Process Representation and Custom PHC Flows	64
		4.0.7	Rotary Killi Elid-of-Life	0-
5	Res	ults		66
	5.1	Impact	t Analysis	66
		5.1.1	Total Impacts before Normalization	67
		5.1.2	Normalized Results per Functional Unit	67
		5.1.3	Comparison Across PHC Materials	68
	5.2	Contril	bution Analysis of Subsystem	68
			Contribution Analysis of the Whole System with Bauxite as the Particle	68
		5.2.2	Contribution Analysis of the Whole System with Sand as the Particle	71
		5.2.3	Contribution Analysis of the Whole System with Olivine as the Particle	74
	5.3	Proces	s and Flow Contribution Analysis in the Entire System	76
	5.4	Hotspo	ot Analysis with Sankey Diagrams	86
		5.4.1	Bauxite	86
		5.4.2	Sand	90
	5.5	Summ	ary of Results	98
6	Disc	cussion a	and Optimization	99
	6.1		al and Design Efficiency	99
	6.2		tional Improvements	99
	6.3	_	f-Life and Circularity	99
	6.4		egative Emissions Potential	99
	6.5		retation (ISO 14044)	99
_	~	•		4 0 ·
7	Con	clusion	and Future work	101

CONTENTS	vi

7.1	Summary of Contributions	101
7.2	Limitations of the Study	101
7.3	Recommendations for Future Research	101

List of Figures

1.1	General concept of the solar Pyrolysis PYSOLO process	3
2.1	Simplified schematic of the CSP-based and hybrid pyrolysis plants, with dashed lines showing hybrid operation when solar heat is unavailable	8
2.2	Diagrams illustrating the four CSP systems that have been scaled up to pilot and demonstration levels	1(
2.3	solar rotary kiln reactor at the DLR	12
2.4	a) Key geometric aspects of rotary kiln design b) Particle flow patterns in rotating drums as Froude number increases	12
2.5	Simulation of the Rotary Kiln for the PYSOLO Project	14
2.5	Xenon lamps used in the spotlight facility in Cologne for rotary kiln testing	15
2.7	Over 2,000 Mirrors in Front of Solar Towers in Jülich, Germany	18
2.8	Synhelion heliostats with linear actuators and new kinematics, each having four mirror facets (mirrors by Flabeg; frame and canting by KAM	20
2.9	The solar thermal tower power plant at DLR Jülich is shown on the left, while	20
	the Multifocus Tower, which has been utilized for testing advanced solar technologies since 2020, is on the right	22
4.1	System boundary of the solar subsystem in the PYSOLO project, showing key materials, manufacturing, transport, operation, and end-of-life; downstream im-	
	pacts beyond thermal energy delivery are excluded	34
4.2	Cutaway view illustrating the rotary components 2.5	52
5.1	Impact Amounts for Different PHCs	68
5.2	Contribution of Each Process to Human Toxicity in the Bauxite-Based System	
	Operation	69
5.3	Contribution of Each Process to Climate Change in the Bauxite-Based System Operation	70
5.4	Contribution of Each Process to Material Resources in the Bauxite-Based Sys-	
	tem Operation	70
5.5	Contribution of Each Process to Human Toxicity in the Sand-Based System Operation	72
5.6	Contribution of Each Process to Climate Change in the Sand-Based System	
	Operation	72
5.7	Contribution of Each Process to Land use in the Sand-Based System Operation.	73
5.8	Contribution of Each Process to Human Toxicity in the Olivine-Based System	
	Operation	75
5.9	Contribution of Each Process to Climate Change in the Olivine-Based System	
	Operation	75
5.10	Comparison of Normalized Total Impact Contributions for the Climate Change	
	Category Among Three PHCs	76
5.11	Comparison of Normalized Total Impact Contributions for the Energy resources: non-renewable, fossil Category Among Three PHCs	79
5.12	Comparison of Normalized Total Impact Contributions for the Material resources	
	Category Among Three PHCs	81

5.13	Comparison of Normalized Total Impact Contributions for the Land use Category Among Three PHCs	82
5.14	Comparison of Normalized Total Impact Contributions for the Water use Category Among Three PHCs	84
5.15	Comparison of Normalized Total Impact Contributions for the Human Toxicity	
	Category Among Three PHCs	86
5.16	Human Toxicity Hotspot Analysis with Sankey Diagram Using Bauxite as the	
	PHC	88
5.17	Climate Change Hotspot Analysis with Sankey Diagram Using Bauxite as the	
	PHC	90
5.18	Human Toxicity Hotspot Analysis with Sankey Diagram Using sand as the PHC.	91
5.19	Climate Change Hotspot Analysis with Sankey Diagram Using sand as the PHC.	93
5.20	Human Toxicity Hotspot Analysis with Sankey Diagram Using Olivine as the	
	PHC	95
5.21	Climate Change Hotspot Analysis with Sankey Diagram Using Olivine as the	
	PHC	97

List of Tables

3.1	Summary of laboratory-scale lifetime values	27
3.2	Specific Heat Capacities of Materials	28
3.3	Inventory Values for Circulating Particles	30
3.4	Summary Table — Material Requirements Per Functional Unit	30
4.1	Electric motor, small, assembled (heliostat actuator type)	38
4.2	Materials, Energy Inputs, Transport, and Waste in Heliostat Manufacturing (5	
	units, Synhelion DAWN design, Jülich)	42
4.3	Transport Details of Materials and Components in Heliostat Manufacturing	46
4.4	Comprehensive breakdown of material and energy transfers, maintenance pro-	
	cedures, and waste outputs associated with the heliostat operation system through-	
	out a 15-year lifespan	48
4.5	Material flows at end-of-life for heliostat systems, including inputs, recycling,	
	and waste outputs	51
4.6	Material transport assumptions (to DLR Cologne)	55
4.7	Detailed Material, Process Inputs, Waste, and Outputs for Rotary Kiln Construction and Assembly (using Ecoinvent flows).	57
4.8	Processed Particle Heat Carriers (PHCs) – Custom Flows	62
4.9	Initial Stock Processes for Processed Particle Heat Carriers (PHCs) — Custom	
	Flows	62
4.10	Rotary kiln operation (lifetime totals; per PHC scenario; normalized to FU in	
	results)	63
4.11	End-of-Life Flows for Rotary Kiln	65
5.1	Pre-Normalization Environmental Impact Assessment of Various Processes	66
5.2	Normalized Results of Environmental Impact Assessment	67

List of Abbreviations

Al₂O₃: Aluminium Oxide

AOD: Argon Oxygen Decarburization

CaSiO₃: Calcium Silicate

CO (fossil): Carbon monoxide (fossil origin)

CFD-DEM: Computational Fluid Dynamics - Discrete Element Method

DNI: Direct Normal Irradiance

DLR: Deutsches Zentrum für Luft und Raumfahrt

EAF: Electric Arc Furnace

EJ: Exajoule (a unit of energy, $1 \text{ EJ} = 10^{18} \text{ Joules}$)

EPD: Environmental Product Declaration

EU: European Union GHG: Greenhouse Gases HF: Hydrogen fluoride HCl: Hydrogen chloride

Inconel 600: Nickel-Chromium Alloy 600

J: Joule (unit of energy) kWh: Kilowatt-hour

LCA: Life Cycle Assessment LCI: Life Cycle Inventory

LCIA: Life Cycle Impact Assessment LCOE: Levelized Cost of Electricity

LHV: Lower Heating Value

MJ: Megajoule

NFU: Net Functional Unit NOx: Nitrogen oxides

PYSOLO: PYrolysis of biomass by concentrated SOLar pOwer

PTC: Parabolic Trough Collectors

PHC: Particle Heat Carrier

PV: Photovoltaic

S1.4841: Stainless Steel Alloy (AISI 314)

S355: Structural Steel Grade S355

SiO₂: Silicon Dioxide

TES: Thermal Energy Storage

V4A: Stainless Steel Alloy (similar to AISI 316)

1 Introduction

1.1 Background and Context

The decarbonisation of high-temperature industrial processes is essential to meet global climate targets, especially since the industrial sector accounted for 37% of global energy consumption in 2022, amounting to 166 EJ (approximately 46,000 TWh or 3,970 Mtoe), up from 34% in 2002. This increase has been driven largely by growth in energy-intensive subsectors. Industrial heat demand is projected to rise 16% globally from 2023 to 2028, with China and India responsible for more than half of this growth. Despite efforts to increase renewable heat use, fossil fuel consumption for industrial heat is expected to continue rising, contributing to higher CO2 emissions. Renewable heat sources such as solar thermal and biomass are expanding but still represent only a fraction of total heat consumption in industry, highlighting the pressing need for accelerated deployment of clean heat technologies[1, 2, 3].

Energy demand in the industrial sector continued to grow in 2024 and 2025, with electricity and natural gas playing significant roles driven by increased cooling demands, electrification of industrial processes, and digitalization. Global energy demand rose by 2.2% in 2024, with electricity demand surging 4.3%, largely met by renewables like solar PV and nuclear power. Fossil fuels, particularly natural gas, remain major fuels for industry but with a growing role for renewables and cleaner technologies. The industrial heat pump market, for example, is expected to expand significantly through 2035 as decarbonization efforts intensify and regulations drive adoption. These trends underscore a transitional phase where rising industrial energy demand coexists with emerging decarbonization technologies, emphasizing the urgent need for broader implementation of clean energy solutions to curb emissions from the industrial sector[2].

Sectors such as cement, steel, glass, and chemicals rely heavily on fossil fuels—primarily coal, natural gas, and oil—to achieve these conditions. The combustion of these fuels produces significant direct carbon dioxide emissions, while upstream extraction and transportation further contribute to environmental impacts. Achieving long-term carbon neutrality therefore necessitates deep reductions in fossil-derived process heat.

Transitioning to renewable high-temperature heat presents technical challenges. Electrification through resistance or induction heating is highly efficient but demands large-scale renewable electricity generation and extensive infrastructure upgrades. Biomass combustion offers renewable heat but can compete with other land uses and still produces particulates and other pollutants. Concentrated Solar Power (CSP) has emerged as one of the few renewable technologies capable of delivering heat above 500°C directly, without the need for intermediate energy conversion.

CSP technologies use mirrors or lenses to focus sunlight onto a receiver, converting solar radiation into thermal energy. This heat can be stored in thermal storage systems or applied directly to industrial processes. Four main CSP configurations are in commercial use: parabolic troughs, parabolic dishes, linear Fresnel reflectors, and solar towers Figure 2.2.

Among these, solar tower systems are particularly well suited for high-temperature processes due to their high concentration ratios and the ability to centralise thermal collection at an elevated receiver. Concentration ratios above 1000 suns have been demonstrated, enabling receiver outlet temperatures exceeding 1000 °C[4].

Parallel to developments in CSP, biomass pyrolysis has attracted increasing attention as a thermochemical route for producing renewable fuels and carbon-rich products. Pyrolysis involves heating biomass in the absence of oxygen, yielding a mixture of bio-oil, biochar, and pyrogas. These products have multiple applications: bio-oil can be upgraded to transport fuels, biochar can improve soil carbon content, and pyrogas can be used for process heating or electricity generation. Conventional pyrolysis systems supply the required heat either by combusting a portion of the biomass feedstock or by using fossil fuels, which reduces overall carbon savings.

The PYSOLO project integrates these two technologies in a novel solar-driven rotary kiln[5]. Instead of transferring concentrated solar radiation directly to the biomass, the system uses Particle Heat Carriers (PHCs)—granular solids such as silica sand, bauxite, or olivine—as an indirect heat transfer medium. PHCs are heated in a solar receiver using CSP, then conveyed into the pyrolysis kiln where they release stored heat to the biomass. This approach has several potential advantages:

- Uniform heat transfer to the biomass bed
- Reduced risk of biomass charring or hot-spot formation compared to direct irradiation
- Flexibility in receiver operation independent of kiln rotation
- Potential for thermal buffering to smooth fluctuations in solar input

By combining CSP with PHCs, PYSOLO aims to demonstrate a continuous, fully renewable pyrolysis process capable of producing valuable bio-products without the need for fossil-derived heat input. This thesis evaluates the environmental performance of the proposed system through Life Cycle Assessment (LCA), focusing on the material and energy requirements of the solar subsystem and its integration with the pyrolysis process.

While inspired by the SOLPART project[6]—a European initiative that demonstrated high-temperature particle receivers for industrial calcination—the PYSOLO rotary kiln has been fundamentally re-engineered at the German Aerospace Center (DLR) to meet the specific thermal and chemical requirements of biomass pyrolysis. Modifications include changes in materials, geometry, insulation, and operational strategies.

Currently at Technology Readiness Level 4, the PYSOLO system comprises two integrated subsystems. The first is a solar particle receiver, which heats PHCs using concentrated solar radiation. The second is a pyrolysis reactor, equipped with a particle—char separator to enable continuous biomass processing. This circulating-particle configuration allows high-temperature operation without internal heat exchangers, improving scalability and thermal efficiency[5].

An important modelling consideration is that Particle Heat Carriers (PHCs) are not consumed during normal operation but continuously circulated in the kiln. Therefore, the initial inventory required to fill the system is treated as a one-time construction input, while only the small amounts lost and replaced due to attrition (make-up mass) are counted during the operation phase. This distinction avoids double-counting and provides a realistic picture of resource requirements over the system's lifetime.

A notable feature of PYSOLO is its operational flexibility. During solar hours, the process operates on direct sunlight or preheated PHCs. When solar input is unavailable, heat can be

supplied by combusting by-products (pyrogas or biochar) or via electric induction using surplus renewable electricity. Additionally, the system can provide grid-balancing services by converting pyrogas to electricity during peak demand periods or by storing excess renewable electricity as thermal energy. Such versatility supports integration into decentralised, low-carbon energy networks.

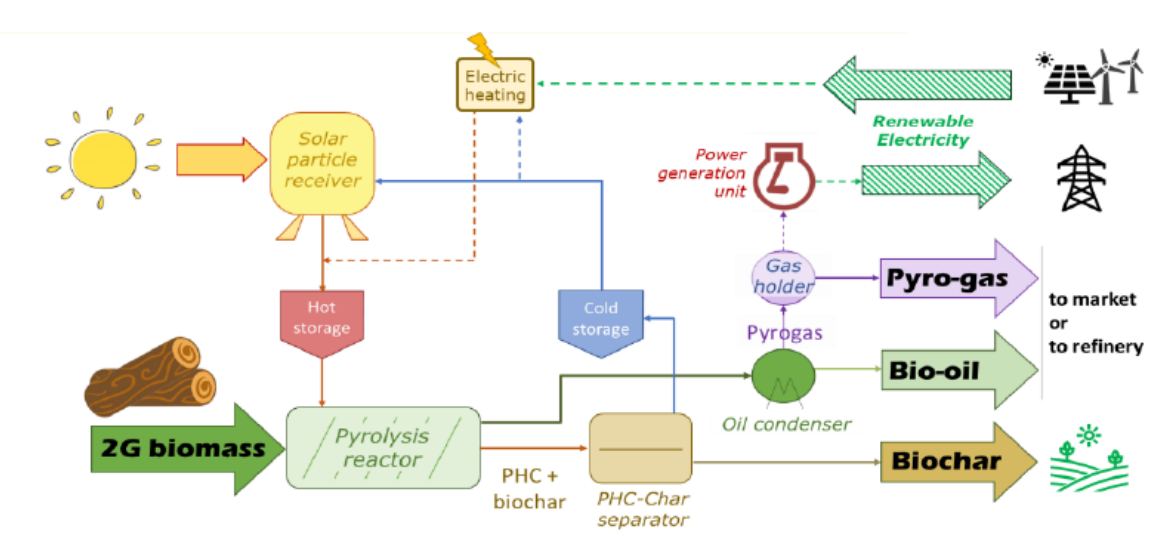


Figure 1.1: General concept of the solar Pyrolysis PYSOLO process [5].

.

1.2 Problem Statement

As global decarbonization efforts accelerate, the deployment of renewable energy in high-temperature industrial applications has become increasingly urgent. Concentrated Solar Power (CSP) offers a promising route to provide sustainable, high-temperature heat for thermochemical processes such as biomass pyrolysis, as demonstrated in recent pilot studies[7, 8]. However, achieving continuous, high-temperature, solar-driven operation remains a significant technical and environmental challenge.

Conventional pyrolysis plants often rely on combustion of biomass or process residues to supply heat. While renewable, this approach can lower carbon conversion efficiency and increase life-cycle emissions[9, 10]. Meanwhile, most CSP systems are primarily designed for electricity generation and are not optimized for direct integration with thermal reactors, which limits their application in biomass conversion[11].

Recent innovations, particularly hybrid systems combining CSP with particle heat carriers (PHCs), have shown potential to overcome intermittency and enable continuous, heat-driven chemical processes[8]. The PYSOLO system, for instance, integrates a tower-based CSP receiver with a rotary kiln heated by PHCs, targeting high carbon efficiency and the potential for net-negative emissions.

Despite these advancements, comprehensive environmental evaluations of such systems are scarce. Key uncertainties remain regarding:

- The environmental costs of manufacturing and maintaining large heliostat fields.
- The life-cycle performance of PHCs, including production, use, and disposal.
- Trade-offs between system efficiency, cost, and sustainability[11].

Given that PYSOLO's current design is supported primarily by simulations rather than operational data, a Life Cycle Assessment (LCA) is essential to:

- Identify environmental "hotspots" across the system's life cycle.
- Inform decisions on material selection, design optimization, and operating strategies.
- Evaluate whether solar-driven biomass pyrolysis can meaningfully contribute to decarbonization goals.

1.3 Objectives of the Thesis

To address the gaps identified in Section 1.2—particularly the need for sustainability evaluation of emerging high-temperature solar thermal technologies—this thesis conducts a comprehensive Life Cycle Assessment (LCA) of the solar subsystem in the PYSOLO project. The solar subsystem comprises the heliostat field and the rotary kiln solar reactor. Since the system is still under development and not yet operational, the analysis is based on engineering specifications, numerical simulations, and experimentally derived assumptions. The study follows the ISO 14040/44 framework and applies the ReCiPe 2016 Midpoint (H) method to quantify environmental impacts across multiple categories. The specific objectives are as follows.

Quantify the environmental impacts of the entire life cycle

This thesis provides a detailed look at the environmental impacts of the PYSOLO solar subsystem throughout its entire life cycle. Starting with the extraction of raw materials, it follows the process through the manufacturing of key components—such as the heliostat field, rotary kiln, and Particle Heat Carrier (PHC) materials—into the operation phase, and finally considers how these materials are managed at the end of their life, whether through recycling or disposal. Impacts are normalised to the delivery of 1 kWh of useful thermal energy at the kiln bed, with the total lifetime output fixed at 98,550 kWh. This figure corresponds to the laboratory-scale operation of the PYSOLO test facility, representing the cumulative energy output over its assumed service life.

Compare three operational scenarios with different PHCs

A key part of this study is comparing three different ways to operate the system, each using a different PHC material: silica sand, bauxite, or olivine. Because PHCs circulate continuously in the kiln, only their make-up mass due to attrition losses is considered as a material input. This treatment avoids overestimating material use while still capturing realistic sourcing and disposal burdens.

Evaluate environmental performance across multiple impact categories

For each PHC scenario, environmental performance is quantified using six key categories from ReCiPe Midpoint (H):

- Climate change (kg CO₂-eq)
- Energy resources: non-renewable, fossil (kg oil -eq)
- Material resources:metals/minerals (kg Cu-eq)
- Land use (m²a crop-eq)
- Water use (m³)
- **Human toxicity** (kg 1,4-DCB-eq)

These categories were chosen because they reflect both global decarbonisation targets and known sustainability trade-offs for CSP and material-intensive systems.

Identify environmental hotspots within the life cycle

The study also breaks down the environmental impact by each stage in the life cycle—material extraction, manufacturing, operation, and disposal—to identify which parts contribute the most to the total footprint. Knowing these 'hotspots' helps focus efforts on improving materials, design, and operation for better sustainability.

Provide baseline sustainability insights for future development

Finally, this work establishes the first detailed Life Cycle Assessment for the PYSOLO solar subsystem, creating a baseline for future development. This will provide valuable guidance for engineers, scientists, and decision-makers as they work to improve material choices, system designs, and operating practices, ultimately supporting the shift toward low-carbon, solar-powered thermal technologies.

1.4 Research Questions

This research addresses the following questions:

- 1. What are the life cycle environmental impacts of the heliostat field and rotary kiln receiver in the PYSOLO system, expressed per functional unit (1 kWh useful thermal energy)?
- 2. How do different PHC materials (silica sand, bauxite, olivine) influence sustainability performance, considering only their attrition make-up requirements?
- 3. Which life cycle stages (manufacturing, operation, or disposal) contribute most to the environmental footprint?
- 4. How sensitive are the results to assumed operational lifetimes, given that this study focuses on the laboratory-scale case of 98,550 kWh?
- 5. What design and material changes could improve the environmental profile of solar-powered pyrolysis systems?

1.5 Scope and Limitations

This thesis focuses exclusively on the solar subsystem of the PYSOLO project, specifically the heliostat field and the rotary kiln-based solar receiver. It does not cover downstream components of the pyrolysis process, such as the reactor chamber, bio-oil condensation, syngas handling, or storage systems. These elements are assumed to be constant across all scenarios and are excluded from the system boundary.

Given that the PYSOLO system is in development and lacks operational data, the assessment relies on simulated inputs, engineering design specifications, and literature-derived assumptions. Material quantities, transport distances, and energy demands are estimated using conservative modelling practices. For PHCs, only attrition replacement is included as a material input. Certain datasets—particularly for component manufacturing and end-of-life treatment—are approximated based on analogous technologies. These constraints are explicitly acknowledged and tested through sensitivity analysis to ensure transparency and robustness.

1.6 Thesis Structure

This thesis is organised into seven chapters, each building logically from background context to the final conclusions and recommendations:

Chapter 1 –Introduction

Presents the industrial decarbonisation challenge, the potential of concentrated solar power (CSP) for high-temperature processes, and the aims of the PYSOLO project. States the research questions, scope, and functional units used in the LCA.

Chapter 2 – Technological Background

Reviews relevant technologies, including CSP system types, solar tower configurations, rotary kiln operation, and Particle Heat Carrier (PHC) materials. Each subsection concludes with a short "Relevance to PYSOLO" link.

Chapter 3 – System Overview

Describes the experimental configuration of the PYSOLO solar subsystem, covering heliostat characteristics, receiver design, and kiln integration. Includes heliostat sizing calculations using site-specific DNI data and PHC material selection.

Chapter 4 - LCA Methodology

Defines the goal, scope, boundaries, functional unit, data sources, and impact assessment methods. Summarises modelling assumptions and their justification.

Chapter 5 – Results

Presents the environmental impact results for different PHC materials and heliostat sizing scenarios. Compares performance across multiple impact categories.

Chapter 6 – Discussion

Interprets the findings in relation to literature, highlights trade-offs, addresses limitations, and suggests improvement strategies for solar-driven pyrolysis systems.

Chapter 7 – Conclusions and Recommendations

Summarises key outcomes, provides final conclusions on the environmental feasibility of the proposed system, and offers recommendations for future research.

2 Technological Background

2.1 PYSOLO components

The PYSOLO system comprises the following key subsystems:

- **Heliostat Field**: Tracks the sun and concentrates direct normal irradiance (DNI) onto the receiver aperture at the Solar Tower. The layout of the field is carefully designed to reduce losses caused by the angle of sunlight (cosine losses) and shading between mirrors.
- Rotary Kiln Particle Receiver: It captures the concentrated solar energy and directly heats the Particle Heat Carriers (PHCs) as they move through the kiln in a cascading motion. This setup ensures more even heat transfer and eliminates the need for intermediate fluids.
- Thermal Energy Storage (TES):Hot PHCs are used to store sensible heat, allowing energy to be supplied to the pyrolysis process even when sunlight is low or unavailable.
- **Pyrolysis Reactor**: The biomass conversion takes place here, with the reactor being indirectly heated by the PHCs to maintain precise and stable reaction temperatures.
- **Particle–Char Separator**: This component separates the PHCs from the solid biochar produced during pyrolysis, enabling the particles to be reused in a closed-loop system.

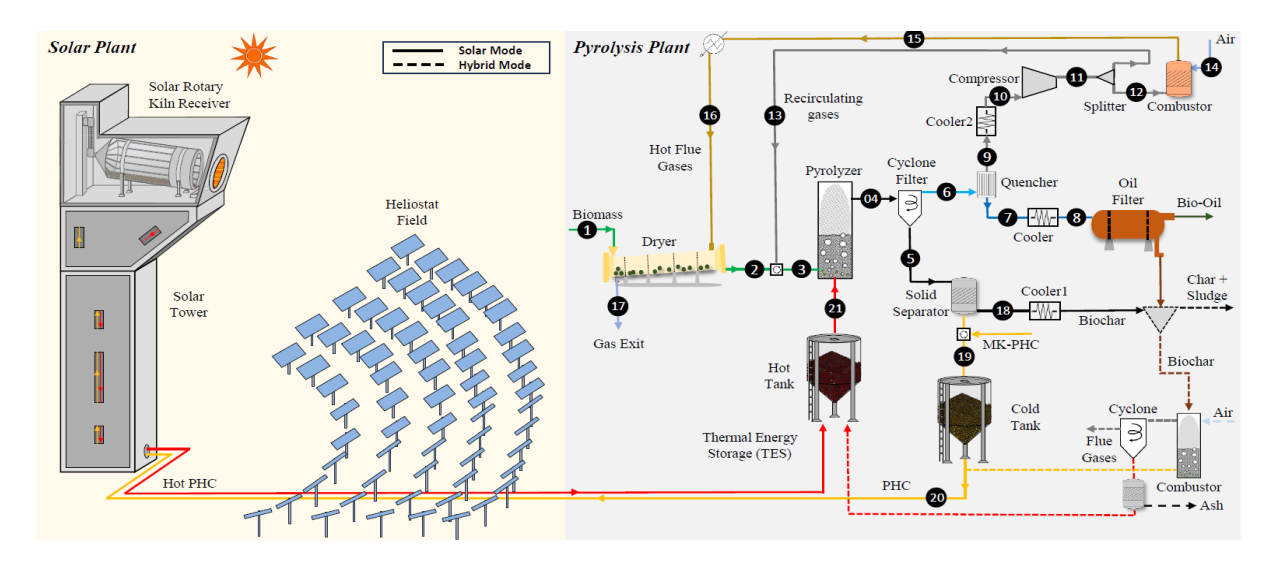


Figure 2.1: Simplified schematic of the CSP-based and hybrid pyrolysis plants, with dashed lines showing hybrid operation when solar heat is unavailable[5].

•

2.2 Concentrated Solar Power Technologies

Concentrated Solar Power (CSP) technologies convert solar radiation into thermal energy using optical concentrators. Unlike photovoltaic (PV) systems, CSP generates heat, that can be used directly in industrial processes or converted to electricity. The inclusion of thermal energy storage (TES) systems allows CSP to offer dispatchable power, making it a strong candidate for continuous, high-temperature applications.

2.2.1 Types of CSP Systems

The main CSP configurations that have reached pilot or demonstration scale are illustrated in Figure 2.2. Each differs in optical layout, receiver configuration, and operating temperature range:

- **Parabolic trough collectors (PTC):** Curved mirrors focus sunlight along a linear focal line onto a receiver tube containing a heat transfer fluid, typically reaching temperatures of 300–400 °C. PTC systems are the most widely deployed CSP technology and are well suited for medium-temperature applications [12].
- Linear Fresnel systems: Flat mirrors are arranged in rows to approximate a trough geometry. This design offers lower construction costs and simpler mechanics compared to PTCs but generally achieves similar medium-temperature ranges.
- Solar power towers (central receiver systems): A field of heliostats focuses sunlight onto a single elevated receiver. Operating temperatures can exceed 600–1000 °C, making these systems ideal for advanced industrial heat applications and high-temperature TES[13].
- **Dish-Stirling systems:** Parabolic dish mirrors concentrate sunlight onto a receiver connected to a Stirling engine, enabling direct conversion of heat to electricity with high theoretical efficiency. Despite strong performance potential, commercial deployment has been limited.

Romero and González-Aguilar (2014) emphasise that central receiver systems present the highest thermodynamic efficiency potential and the greatest suitability for thermal storage due to their high operating temperatures (p. 44). These characteristics make them particularly attractive for industrial heat applications beyond power generation[13].

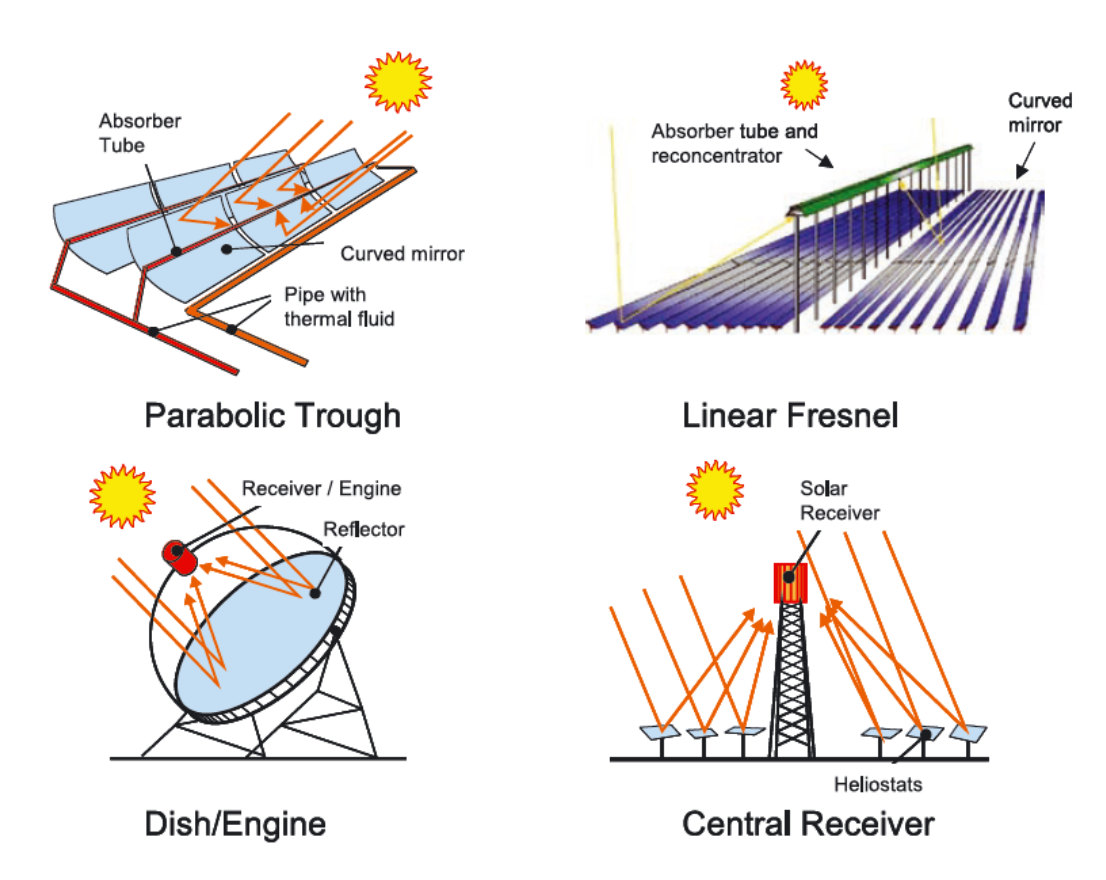


Figure 2.2: Diagrams illustrating the four CSP systems that have been scaled up to pilot and demonstration levels [13].

2.2.2 Thermal Energy Storage (TES) and Dispatchability

One of the key advantages of CSP over PV lies in its compatibility with TES, allowing the temporal decoupling of energy collection from use. This capability supports industrial processes requiring constant heat supply and enables electricity generation during periods without sunlight.

A Life Cycle Assessment (LCA) by Gasa et al. (2021) compared a solar tower plant with and without TES [14]. Their findings showed that integrating TES not only increases energy availability but also reduces life-cycle environmental impacts. Plants without TES exhibited higher reliance on grid electricity during low-solar periods, increasing operational-phase emissions.

The study also identified that the solar field and the Thermal Energy Storage (TES) and heat transfer fluid system are the primary contributors to the environmental footprint of Concentrated Solar Power (CSP) plants. Additionally, the choice of storage medium significantly influences environmental impacts; naturally mined molten salts tend to have lower environmental burdens compared to synthetically produced alternatives. These findings underscore the dual role of TES—not only in enhancing operational flexibility but also in reducing greenhouse gas (GHG) emissions throughout the plant's lifecycle.

2.2.3 Deployment Trends and Strategic Importance

Concentrated Solar Power (CSP) has become an increasingly important source of high-temperature, reliable renewable energy. Although solar photovoltaics (PV) have gained much more attention recently due to their lower upfront costs, CSP offers distinct advantages. It can achieve higher thermal efficiency and is particularly well-suited for supplying direct heat to industrial processes—especially when combined with thermal energy storage (TES).

By 2012, the global CSP capacity had surpassed 6 gigawatts, mainly installed in sunny desert regions with abundant sunlight[12]. More recent forecasts predict substantial growth in CSP across Europe and North Africa through 2050, with a particular emphasis on providing industrial heat[15]. Among various CSP designs, central receiver tower systems are viewed as the most promising, benefiting from decreasing costs and improved efficiency when paired with TES.

Today, CSP capacity continues to grow and is expected to play a key role in helping industries transition away from fossil fuels by delivering clean, dispatchable heat and power—even during periods without sunlight.

2.3 Rotary Kiln Receiver Design

Rotary kilns are robust, continuous reactors widely employed in sectors such as cement manufacturing, mineral processing, and waste treatment. Their scalability, mechanical durability, and capacity to achieve uniform thermal distribution make them particularly suitable for high-temperature particulate processing. In solar applications, these kilns have been adapted as direct particle receivers, in which granular heat carriers absorb concentrated solar radiation for subsequent thermal processes.

In the PYSOLO project, a solar-driven rotary kiln serves as the main reactor for biomass pyrolysis. The design builds upon concepts tested at the German Aerospace Center (DLR) and within the SOLPART project[16], which demonstrated high-temperature solar calcination under concentrated flux. While retaining the durability of conventional industrial designs, this kiln is adapted to efficiently heat particles using focused solar energy. It accommodates multiple Particle Heat Carrier (PHC) types and is optimized for continuous operation with high solar-to-thermal conversion efficiency Figure 2.3.

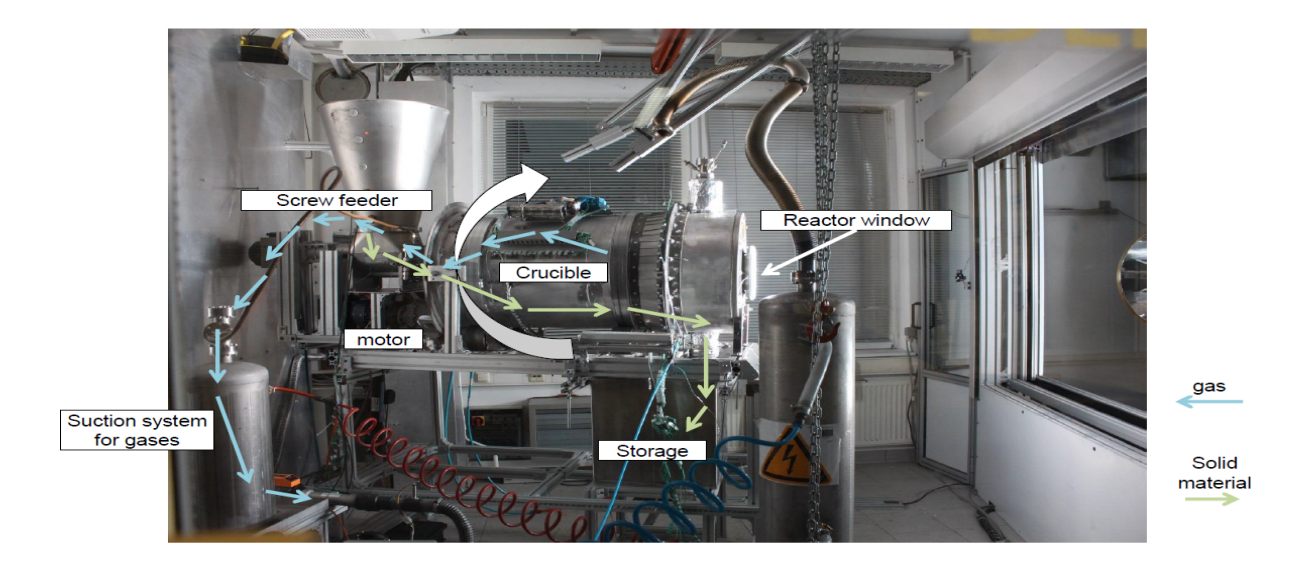


Figure 2.3: solar rotary kiln reactor at the DLR[17].

2.3.1 Concept and Operating Principle

The reactor consists of a cylindrical, cavity-type kiln set at a slight incline and rotating about its longitudinal axis. Concentrated solar radiation enters through a circular aperture at the front, directly heating both the refractory internal surfaces and the moving bed of particles. U-shaped lifters positioned along the inner wall lift and drop the particles in a cascading motion, ensuring thorough mixing and repeated contact with the heated surfaces. This configuration supports uniform heating and consistent residence times, even for particles with relatively low absorptance[18, 19].

To optimize heat transfer, the kiln operates in a rolling regime with Froude numbers between 10^{-4} and 10^{-2} [18, 20], creating a stratified flow pattern, as illustrated in Figure 2.4, a passive bed at the bottom and an active rolling layer at the top, maximizing exposure to thermal radiation.

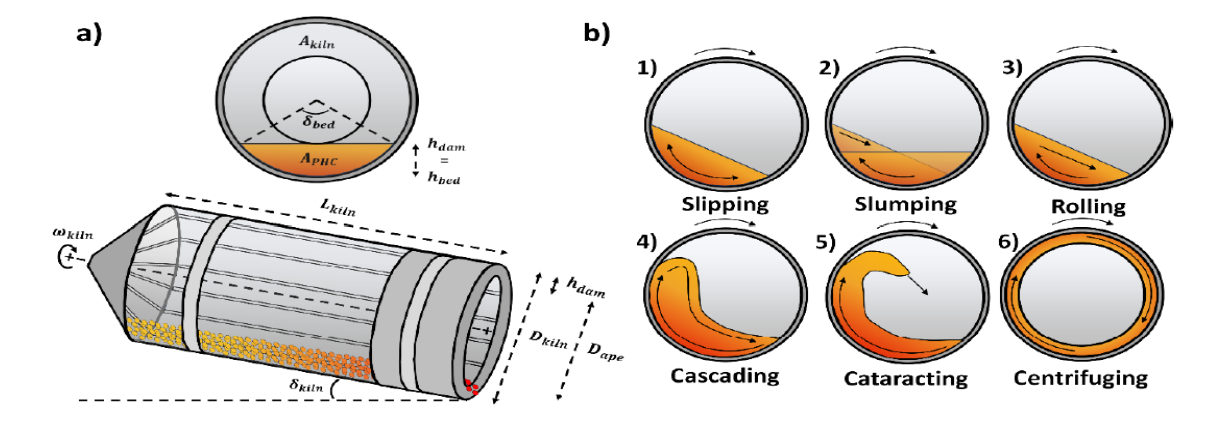


Figure 2.4: a) Key geometric aspects of rotary kiln design b) Particle flow patterns in rotating drums as Froude number increases [18, 20, 21].

2.3.2 Receiver Configuration

The receiver incorporates a rotary crucible housed within a cavity, with solar flux entering through the aperture. Particle feed is introduced at the upper end and advances by gravity toward the discharge end. Kiln inclination, rotation speed, and internal lifter geometry jointly determine residence time and mixing intensity, directly affecting temperature uniformity and throughputFigure 2.5.

This configuration is particularly effective for PHCs with moderate to low absorptance, as the continuous tumbling motion compensates for optical inefficiencies. The modular design also allows straightforward scaling from laboratory to pilot-scale systems[18, 19].

2.3.3 Materials and Mechanical Construction

For the PYSOLO project, a laboratory-scale rotary kiln receiver-reactor is currently under construction. The design and material selection are informed by numerical simulations, thermal and mechanical modeling, and prior experimental experience at the German Aerospace Center (DLR). The objective is to ensure reliable performance under concentrated solar flux while maintaining scalability for future reactor configurations. Material selection has prioritized thermal resistance, mechanical durability, and compatibility with high-intensity solar radiation[22]. The key materials and their functions are as follows:

- **S355 structural steel**: forms the external frame and support structures. This steel mainly consists of iron with approximately 0.20% carbon, 1.6% manganese, and minor amounts of silicon, phosphorus, and sulfur. It provides mechanical strength, weldability, and cost-effectiveness, making it suitable for kiln housing.
- **Inconel 600**: used for internal components exposed to the highest thermal loads, particularly in the crucible and receiver zone directly irradiated by concentrated flux. It is a nickel–chromium alloy (approximately 72% Ni, 14–17% Cr, 6–10% Fe), known for high oxidation resistance and mechanical stability above 800 °C, as confirmed by prior DLR tests [22].
- Stainless steel alloys (V4A, 1.4841): applied to rotating and interface components subjected to cyclic thermal and mechanical stresses. V4A (similar to AISI 316) contains approximately 16–18% Cr, 10–14% Ni, and 2–3% Mo; 1.4841 (AISI 314) has about 24–26% Cr and 19–22% Ni. Both offer excellent corrosion resistance, durability, and stability under repeated heating–cooling cycles.
- Thermal insulation:achieved using calcium silicate boards (CaSiO₃), Superwool blankets (alkaline earth silicate fibers, primarily SiO₂ and CaO), and vacuum-formed ceramic bricks (Al₂O₃–SiO₂ based). These materials minimize heat loss and resist thermal shock, maintaining consistent internal temperatures.
- Aluminum profiles and high-temperature sealing cords:used in external housing and interface seals to reduce leakage and ensure mechanical integrity. Aluminum is primarily Al with minor Mg, Si, and Fe, while sealing cords are composed of high-temperature resistant fibers such as glass, silica, or ceramic composites.

Fabrication employs standard industrial processes, including material cutting, rolling, machining, and welding, ensuring precise alignment and structural integrity. Although this setup functions as a laboratory-scale prototype, the materials and construction methods reflect best practices from previous high-flux rotary kiln projects [22, 23].

2.3.4 Thermal Performance and Operating Conditions

The PYSOLO rotary kiln is designed to operate at a net thermal input of 15 kW under steady-state conditions. For laboratory-scale tests at DLR, this input is sustained for approximately two hours per run, corresponding to the kiln's design point for biomass pyrolysis experiments[24]. The solar subsystem consists of five heliostats, each with an 8.2 m² reflective area. Under typical clear-sky conditions at Jülich (DNI 750–800 W/m², optical efficiency 60%), the heliostat field delivers about 20 kW gross power to the receiver—providing a margin above the 15 kW design requirement.

Key Kiln Operating Conditions

- Inlet particle temperature: approximately 400 °C
- Outlet particle temperature: approximately 800 °C
- Thermal efficiency: 70–80% (based on simulations and prior reactor data [18])

These conditions are derived from numerical simulations and previous high-temperature solar trials[18]. Long-term operational reliability is expected, though periodic maintenance will be required for bearings and sealing elements, and insulation performance will be monitored for degradation under cyclic heating.

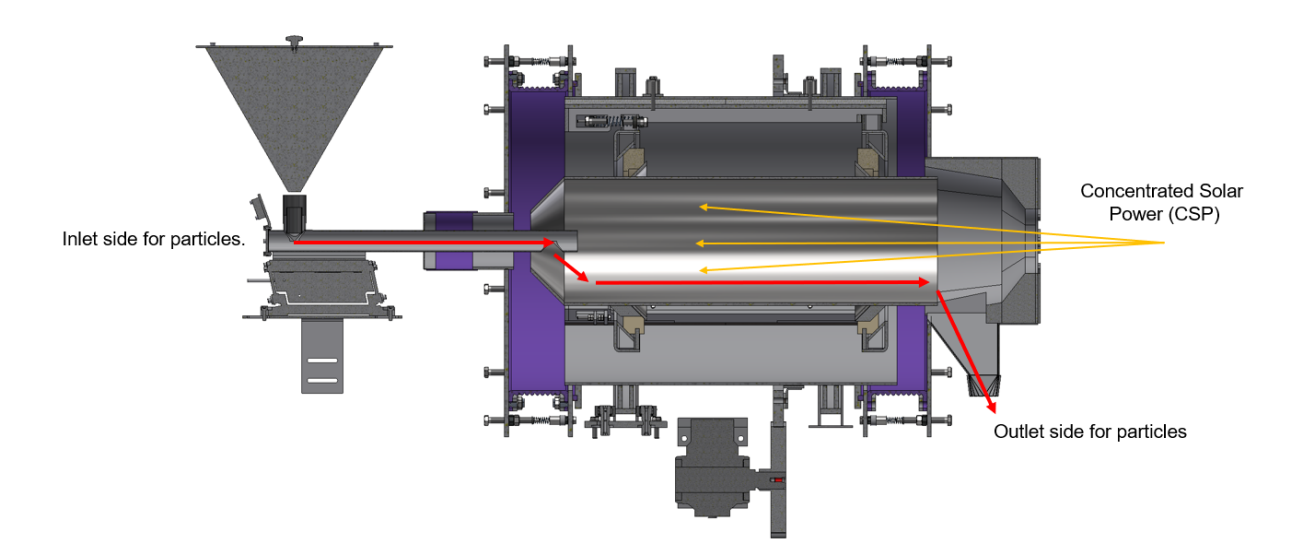


Figure 2.5: Simulation of the Rotary Kiln for the PYSOLO Project[5].

2.3.5 Simulation and Experimental Validation

The receiver design is supported by detailed CFD-DEM simulations performed in collaboration with Politecnico di Milano[18]. These simulations model granular flow, gas—solid heat exchange, and ray-traced solar flux distribution across the kiln walls. Simulation data inform both the thermal balance and geometry optimization.

Experimental validation is now underway at DLR's solar research center in Cologne[24], utilizing two key test facilities:

- DLR Solar Simulator: 10 xenon lamps capable of delivering up to 25 kw thermal power at the focal plane, enabling high-precision testing under controlled irradiationFigure 2.6;
- DLR Solar Furnace: A high-flux facility using real sunlight, offering dynamic environmental testing of the receiver in near-operational conditions.

These experimental campaigns will confirm the system's thermal behavior, validate the simulation models, and determine the optimal range of operating parameters for pyrolysis using solar-heated PHCs[5].



Figure 2.6: Xenon lamps used in the spotlight facility in Cologne for rotary kiln testing[24, 5].

2.4 Particle Heat Carriers (PHCs)

Particle Heat Carriers (PHCs) are granular solids designed to absorb, store, and transport thermal energy in high-temperature processes. In solar-driven rotary kiln systems, PHCs act as both the direct solar absorber and the heat transfer medium. This dual role enables continuous operation, as the particles carry energy from the concentrated solar flux zone to the reaction zone, such as the biomass pyrolysis chamber[18, 19].

The concept of direct particle heating has been demonstrated in projects such as SOLPART and CENTRec[25], where particles were directly exposed to concentrated solar irradiation. Eliminating the need for intermediate heat transfer fluids reduces system complexity, allows higher operating temperatures (often $> 800\,^{\circ}$ C), and minimises thermal losses[26].

2.4.1 Functional Requirements

The selection of PHCs requires careful consideration of thermal, optical, and mechanical criteria, which must be balanced to suit the intended process conditions. Key requirements include:

- High solar absorptance across the relevant spectrum to maximize conversion of incoming radiation into thermal energy.
- Low thermal emittance at operating temperature to reduce radiative heat losses.
- High specific heat capacity and thermal conductivity to enable efficient energy storage and rapid heat transfer.
- Mechanical robustness, including resistance to sintering, attrition, and thermal shock during cyclic heating.
- Chemical compatibility with process gases and feedstocks, such as the vapors generated during biomass pyrolysis.

These criteria are widely reported in the literature on candidate materials for concentrated solar power (CSP) particle receivers[18, 20], and have been validated through extended-duration solar experiments at institutions such as the German Aerospace Center (DLR).

2.4.2 Common Materials in Literature

Previous research has identified a range of particle types with suitable characteristics for PHC applications:

- **Bauxite and sintered alumina** valued for their high thermal stability, density, and resistance to chemical degradation.
- **Silica sand** inexpensive and widely available, though its absorptance is lower unless the surface is modified or coated.
- Olivine thermally stable and mechanically robust, with the added benefit of catalytic activity for tar reduction in biomass gasification[27].
- Silicon carbide (SiC) excellent thermal stability and absorptance, but cost and brittleness can limit large-scale deployment.

• **Metallic particles (e.g., steel shot)** — offer high thermal conductivity but are prone to oxidation at elevated temperatures unless protective measures are implemented.

Gallo et al. (2016) observed that, in rotary kiln receivers, particle shape and density affect not only heat-transfer performance but also the cascading motion of particles, influencing residence time and temperature uniformity.[19].

2.4.3 Particle Selection for PYSOLO

In the PYSOLO project, the selection of particle heat carriers (PHCs) has been based on a combination of literature benchmarks and experimental data obtained through collaborative work with Re-Cord[28], DLR[29], Politecnico di Torino[30], and Politecnico di Milano[31]. Mechanical, thermal, and optical characterization—performed as part of Deliverable D3.1 from PYSOLO project—was used to rank potential candidates and guide the final selection[32]. Three PHCs emerged as the most promising for the intended solar rotary kiln application:

- **Silica sand** Selected as a cost-effective baseline due to its wide availability and stable flowability under operational temperatures. Although its initial solar absorptance is lower than that of other candidates, results from D3.1 confirm that absorptance increases significantly after exposure to pyrolysis conditions, making it viable for solar applications.
- **Bauxite** Demonstrated the highest combined score in D3.1, with excellent flowability, high thermal stability at 950 °C, and consistently high solar absorptance. Its proven track record in the SOLPART project further validates its suitability for large-scale CSP-based pyrolysis.
- Olivine Exhibited strong mechanical resilience and favorable flowability, with the added advantage of catalytic tar-cracking activity that can enhance overall process performance. While its absorptance is moderate in fresh form, it improves markedly after thermal cycling and pyrolysis exposure.

The selection process considered the following key factors:

- Reference data from previous rotary kiln and particle receiver studies (Tescari et al., 2020; Amjed et al., 2024), which establish baseline thermal and mechanical performance metrics [18, 22].
- Compatibility with lifter-assisted rotary kiln geometries to ensure stable cascading motion and minimal particle attrition during continuous operation.
- Target operational outlet temperatures of 800 °C to optimize heat transfer while preserving particle integrity under repeated heating cycles.
- Scalability, cost, and supply chain robustness for potential pilot-scale deployment.

Ongoing laboratory trials at DLR are focused on precise optical and thermal measurements of the selected PHCs, including solar absorptance, thermal emittance, and specific heat capacity. These results will feed into detailed simulation models to refine operational parameters and predict material lifespan under high-temperature cyclic conditions [32].

2.5 Jülich Solar Tower Facility

Concentrated Solar Power (CSP) plants capable of delivering dispatchable, high-temperature heat are critical to projects such as PYSOLO, where a continuous and high-quality thermal supply is essential for stable biomass pyrolysis. In this thesis, the Jülich Solar Tower facility in North Rhine-Westphalia, Germany, is assumed as the CSP plant providing the renewable heat input for the rotary kiln particle receiver. Its extensive heliostat field, high-precision solar tracking, and flexible research infrastructure make it a suitable platform for advanced solar-thermal experimentationFigure 2.7.

.



Figure 2.7: Over 2,000 Mirrors in Front of Solar Towers in Jülich, Germany[33].

2.5.1 Overview of the Jülich Solar Tower Facility

The Jülich Solar Tower facility, located in North Rhine-Westphalia, Germany, represents one of the most important pilot-scale infrastructures for central receiver systems in Europe. Commissioned in 2009, the facility comprises a heliostat field of 2153 tracking mirrors, each with an aperture area of 8.2 m², amounting to a total reflective surface of over 17,600 m². Originally developed as a demonstration project for air-based CSP technologies, the field has since evolved into a testbed for innovative thermal applications, including solar fuels, high-temperature receivers, and particle-based energy systems[34].

The heliostat field is currently operated by Synhelion AG in close collaboration with the German Aerospace Center (DLR). Within the framework of the PYSOLO project, the facility serves as the source of solar heat for a rotary kiln-based pyrolysis process, which requires both high operating temperatures and consistent energy input. The site's proven operational record and adaptable configuration further enhance its suitability for hybrid and advanced solar-thermal

applications.

2.5.2 Retrofitting History and Field Performance at Jülich

The heliostat field at the Jülich Solar Research Facility has undergone significant technological evolution since its commissioning. The original heliostats, supplied by Ausra and installed by Kraftanlagen München (KAM), featured single large mirror panels adhered to steel frames [35]. Over time, these units exhibited widespread issues such as corrosion, adhesive failure, and mirror delamination, which necessitated full replacement of many units by 2015 [36].

In addition to mirror degradation, the actuation system presented substantial reliability challenges. Linear actuators originally adapted from satellite dish technology lacked the required torque precision and mechanical robustness for continuous solar tracking in CSP applications. Failures included gearbox damage, bent spindles, and calibration drift, leading to poor tracking accuracy and high maintenance costs.

To address these problems, a major retrofitting campaign began in 2020, replacing the original design with a modular heliostat configuration featuring four smaller, cantable mirror facets. This allowed selective replacement of damaged parts and improved both optical performance and maintainability. The upgraded mirrorsFigure 2.8 from Flabeg were installed alongside galvanized steel frames with bolt-on mounts, eliminating the earlier adhesive-only fixation method.

Simultaneously, the actuation and tracking systems were fully redesigned to meet the mechanical demands of dual-axis operation. Field performance data shows that these enhancements reduced average pointing errors from over 5 milliradians to approximately 2 milliradians, marking a substantial gain in tracking precision and operational stability [36].

These upgrades have made the Jülich field more suitable for high-precision solar thermal applications like those in the PYSOLO project, which require continuous and accurate solar flux for thermochemical processing.





Figure 2.8: Synhelion heliostats with linear actuators and new kinematics, each having four mirror facets (mirrors by Flabeg; frame and canting by KAM)[36].

2.5.3 Control System and Operational Management

In parallel with the mechanical and structural upgrades, substantial progress has also been made in the heliostat control system, which is critical for ensuring accurate solar flux delivery and safe operation in complex research configurations. Since 2020, the Jülich heliostat field has been operated using DLR's proprietary control platform, HeliOS (Heliostat Operating System), developed specifically for research-scale multi-tower CSP applications[36]. Unlike commercial systems that are typically optimized for single-receiver operations with high thermal dispatchability, HeliOS is designed for flexibility, accommodating simultaneous control of two solar towers and up to five independent receiver targets.

One of the core features of HeliOS is its parallel calibration capability, allowing for rapid and accurate alignment of heliostats across different sectors of the field. This is especially important at Jülich, where the close proximity of the towers, only 10 meters apart, requires highly controlled flux management to avoid optical interference and ensure operator safety. The system integrates real-time data logging via relational databases and provides automated feedback for aim point optimization, enabling dynamic adjustment based on receiver temperature, flux distribution, or weather conditions.

HeliOS also includes advanced safety protocols, such as automatic exclusion zones and emergency shutdown routines, which are essential in a research environment where experiments involving varying receiver types and flux intensities are routinely performed. Since its full deployment, the system has significantly reduced tracking error and contributed to the overall increase in field uptime and operational flexibility, aligning well with the demands of the PYSOLO project, which requires stable and continuous heat input for biomass pyrolysis processes[36].

2.5.4 Tower Infrastructure and Experimental Platforms

The Jülich Solar Research Facility features a dual-tower layout, as seen in Figure 2.9, which significantly enhances its research flexibility and relevance to projects such as PYSOLO. The main solar tower, originally constructed in 2009, serves as the primary receiver platform for high-flux solar thermal experiments. It is optimized for large-scale solar heat delivery and has been instrumental in testing air-based receivers, solar fuels, and high-temperature materials.

In 2020, a second structure, the Multifocus Tower, was commissioned to expand the facility's capabilities. This tower is designed specifically for modular experimentation and features three vertically stacked testing platforms, each configured for distinct solar thermal applications [37]:

- Top Platform: Dedicated to solid particle receiver systems, using ceramic heat carriers for high-temperature energy capture and thermal storage.
- Middle Platform: Equipped for solar thermochemical applications such as hydrogen production via water-splitting or redox-based cycles.
- Bottom Platform: Designed for molten salt experiments, integrating heat exchangers, thermal storage units, and circulation systems.

Each platform is capable of handling experimental setups weighing up to 100 tons and is exposed to concentrated solar flux intensities exceeding 1000 kw/m². The towers are spaced only 10 meters apart, enabling tight integration with the heliostat field and allowing shared use of heliostats for different configurations. This proximity supports simultaneous multi-receiver operation, rapid setup changes, and efficient utilization of the field's tracking infrastructure.

The compact and flexible tower arrangement is especially beneficial for the PYSOLO project, which requires stable and continuous heat delivery for rotary kiln-based biomass pyrolysis. Precise thermal control, rapid ramping, and uninterrupted flux are essential for maintaining consistent reaction conditions—capabilities made possible by the combination of tower design, heliostat field layout, and the advanced HeliOS control system.



Figure 2.9: The solar thermal tower power plant at DLR Jülich is shown on the left, while the Multifocus Tower, which has been utilized for testing advanced solar technologies since 2020, is on the right[37].

2.5.5 Advances in Heliostat Design and Material Properties

Earlier generations of heliostats in CSP systems commonly employed monolithic glass panels configured as sandwich structures and bonded to steel frames using industrial adhesives [38]. While straightforward to manufacture, these systems posed long-term durability issues such as adhesive degradation, mirror delamination, and challenges in maintenance and component replacement.

The current generation of heliostats used in the PYSOLO project, Figure 2.8, adopts a modular mirror design, reflecting a broader industry shift aimed at enhancing reliability and serviceability. Each heliostat comprises four individual mirror facets, which simplifies optical alignment, allows for selective replacement of damaged units, and streamlines field assembly [39, 40]. The mirror facets are manufactured by Flabeg and made from 4 mm thick low-iron solar glass, coated with a silver layer to ensure high solar reflectivity and environmental durability [41]. The structural frame is constructed from galvanized mild steel, and includes canting mechanisms that enable precise adjustment of each mirror facet during installation [39, 40]. This modular and materials-efficient design is particularly well-suited to mid-scale solar thermal systems like the one used in PYSOLO, where optical performance, low maintenance needs, and scalable deployment are critical. These design features also contribute positively to lifecycle assessments by reducing embodied carbon and improving end-of-life recovery potential.

3 System Overview

3.1 System Configuration

The PYSOLO solar subsystem is modeled using heliostats from the existing Jülich Solar Power Tower (Germany), retrofitted by Synhelion to experimentally couple concentrated solar power (CSP) technology with high-temperature thermochemical processes. The system integrates a rotary kiln particle receiver—designed to directly heat granular particle heat carriers (PHCs)—with a downstream biomass pyrolysis reactor. The heliostat field concentrates direct normal irradiance (DNI) onto the kiln aperture, where PHCs absorb and store thermal energy before transferring it to the pyrolysis unit[18, 39, 36, 40, 37, 23].

The laboratory-scale design point is 15 kW of thermal power at the kiln aperture under steady-state operation, sustained for approximately two hours per test. For the LCA, a functional unit (FU) of 1 kWh of useful heat delivered to the particle bed is used. This allows all energy and material flows—construction, operation, and end-of-life—to be expressed per FU.

3.1.1 Power from Individual Heliostats

Each Jülich heliostat has an effective reflective area of $8.2 \,\mathrm{m}^2$ and an optical efficiency of 60%. Under ideal clear-sky conditions (DNI = $900 \,\mathrm{W/m}^2$), the thermal power delivered by a single heliostat is:

$$P_{\text{per heliostat}} = 900 \,\text{W/m}^2 \times 8.2 \,\text{m}^2 \times 0.60 \approx 4.43 \,\text{kW}$$
 (3.1)

To achieve the 15 kW target at the aperture:

$$N_{\text{heliostats}} = \frac{15 \,\text{kW}}{4.43 \,\text{kW}} \approx 3.39 \to 4 \tag{3.2}$$

Thus, under optimal irradiation, four heliostats are theoretically sufficient.

However, long-term meteorological data for Jülich show that typical clear-sky midday DNI values range between 750–800 W/m²[42]. To maintain realistic and reliable operation, a baseline DNI of 750 W/m² is adopted for all calculations. This choice ensures that the system is not undersized under common operating conditions, rather than assuming ideal peak irradiance that occurs only occasionally.

At DNI = 800 W/m^2 :

$$P_{\text{per heliostat}} = 800 \,\text{W} \times 8.2 \,\text{m}^2 \times 0.60 \approx 3.94 \,\text{kW}$$
 (3.3)

$$N \approx \frac{15 \,\mathrm{kW}}{3.94 \,\mathrm{kW}} \approx 3.81 \to 4 \tag{3.4}$$

At DNI = 750 W/m^2 :

$$P_{\text{per heliostat}} = 750 \,\text{W} \times 8.2 \,\text{m}^2 \times 0.60 \approx 3.69 \,\text{kW} \tag{3.5}$$

$$N \approx \frac{15 \,\mathrm{kW}}{3.69 \,\mathrm{kW}} \approx 4.07 \to 5 \tag{3.6}$$

This shows that under typical German conditions, five heliostats are sufficient to maintain stable 15 kW operation, while still leaving a margin for variability.

3.1.2 Sensitivity to Less Favorable Conditions

When DNI decreases further or optical efficiency is lower, the number of heliostats required increases. For example:

At 700 W/m² and 60% optical efficiency:

$$P_{\text{per heliostat}} = 700 \,\text{W/m}^2 \times 8.2 \,\text{m}^2 \times 0.60 \approx 3.44 \,\text{kW}$$
 (3.7)

This requires:

$$N \approx \frac{15 \,\mathrm{kW}}{3.44 \,\mathrm{kW}} \approx 4.36 \to 5 \tag{3.8}$$

At 800 W/m² and 50% efficiency:

$$P_{\text{per heliostat}} = 800 \,\text{W/m}^2 \times 8.2 \,\text{m}^2 \times 0.50 \approx 3.28 \,\text{kW}$$
 (3.9)

Requiring:

$$N \approx \frac{15 \,\mathrm{kW}}{3.28 \,\mathrm{kW}} \approx 4.57 \to 5 \tag{3.10}$$

At 700 W/m² and 50% efficiency:

$$P_{\text{per heliostat}} = 700 \,\text{W/m}^2 \times 8.2 \,\text{m}^2 \times 0.50 \approx 2.87 \,\text{kW}$$
 (3.11)

Requiring:

$$N \approx \frac{15 \,\text{kW}}{2.87 \,\text{kW}} \approx 5.23 \to 6 \tag{3.12}$$

Thus, the baseline of five heliostats provides a practical balance between reliability and cost while accommodating typical variations in solar input.

3.1.3 System Operational Lifetime and Energy Delivery

Although the system setup shows how the system performs at any given moment, evaluating its overall impact over time requires looking at the entire lifespan. So, the operational scenario is defined based on the total energy the kiln delivers throughout its entire service life.

For laboratory-scale operation, the kiln operates at its design point of 15 kW at the receiver aperture. Each experimental run lasts approximately 2 hours, with 292 operational days per year. Assuming a service life of 15 years, the cumulative useful thermal energy delivered to the particle bed is:

• **Laboratory-scale operation**: The kiln operates at its design point of 15 kW net thermal input for approximately two hours per experimental run. Assuming 292 operational days per year and a service life of 15 years, the cumulative useful thermal energy delivered to the particle bed amounts to approximately 98,550 kWh (hereafter referred to as *net functional units*, NFUs).

$$t_{life} = 292 \, days/yr \times 2 \, hours/day \times 15 \, years = 8,760 \, hours$$

$$P_{useful} = 15 \, kW \times \eta_{kiln} = 15 \, kW \times 0.75 = 11.25 \, kW$$

$$NFU_{lab} = P_{useful} \times t_{life} = 11.25 \, kW \times 8,760 \, hours = 98,550 \, kWh$$

$$(3.13)$$

This total, expressed as 98,550 kWh NFU, forms the reference basis for all subsequent inventory modelling and impact assessment. All results are normalized to the functional unit (FU), which corresponds to 1 kWh of useful thermal energy delivered to the kiln bed.

All subsequent inventory modelling is normalized to the **functional unit** (FU), defined as 1 kWh of useful thermal energy delivered to the particle bed inside the kiln. This definition ensures that construction, operation, and end-of-life burdens are consistently allocated and that alternative scenarios remain directly comparable.

3.1.4 Heat Delivered to the Kiln

The thermal energy at the receiver aperture is not fully transferred to the particle bed; the actual useful energy depends on the kiln efficiency, η_{kiln} :

$$Q_{\text{useful}} = Q_{\text{aperture}} \times \eta_{\text{kiln}} \tag{3.14}$$

The functional unit (FU) of this study is defined as 1 kWh of useful thermal energy delivered to the particle bed inside the rotary kiln. This is the actual amount of heat available for the downstream pyrolysis process.

However, because the kiln is not perfectly efficient, more energy must be supplied at the aperture to achieve this useful output. Assuming a kiln efficiency of 75%, the aperture input required per FU is:

$$Q_{\text{useful}} = Q_{\text{aperture}} \times 0.75 \tag{3.15}$$

$$Q_{\text{aperture per FU}} = \frac{1 \text{ kWh}}{0.75} \approx 1.333 \text{ kWh}$$
 (3.16)

In other words, for every kilowatt-hour of heat delivered to the particle bed, roughly 1.333 kWh needs to enter through the kiln aperture.

This approach allows all flows of materials and energy—whether in construction, operation, or end-of-life—to be expressed per 1 kWh of useful energy delivered to the particle bed, which is particularly useful for comparing the different PHC scenarios.

3.1.5 Solar Power Requirements

Not all of the sunlight collected by the heliostats reaches the aperture due to optical losses (e.g., reflection, tracking errors, shading).

Considering an optical efficiency of $\eta_{opt} = 60\%$, the incident solar energy required at the heliostat mirrors for the delivery of 1 FU (1 kWh of useful thermal energy) is:

$$E_{\text{incident per FU}} = \frac{Q_{\text{aperture per FU}}}{\eta_{\text{opt}}} \approx \frac{1.333 \text{ kWh}}{0.60} \approx 2.22 \text{ kWh per FU}$$
 (3.17)

This means that Each FU corresponds to 2.22 kWh of DNI incident on the heliostat mirrors (before optical losses to the aperture).

At a baseline Direct Normal Irradiance (DNI) of 750 W/m², each heliostat with a mirror area of 8.2 m² collects:

$$P_{\text{mirror}} = 750 \text{ W/m}^2 \times 8.2 \text{ m}^2 \approx 6.15 \text{ kW}$$
 (3.18)

For 1 FU, only a fraction of this per-heliostat power is required. To ensure operational flexibility and a safety margin, five heliostats are combined:

$$5 \times 6.15 \text{ kW} \approx 30.75 \text{ kW}$$
 (3.19)

Accounting for optical efficiency:

$$P_{\text{delivered}} = 30.75 \text{ kW} \times 0.60 \approx 18.45 \text{ kW}$$
 (3.20)

This delivered power exceeds the 15 kW thermal requirement, providing operational flexibility and accommodating variations in DNI, heliostat modulation, and other strategies. Under higher insolation conditions (DNI = 900 W/m^2), each heliostat receives:

$$P_{\text{mirror}} = 900 \text{ W/m}^2 \times 8.2 \text{ m}^2 \approx 7.38 \text{ kW}$$
 (3.21)

Total power from five heliostats:

$$5 \times 7.38 \text{ kW} \approx 36.9 \text{ kW} \tag{3.22}$$

After optical losses:

$$P_{\text{delivered}} \approx 36.9 \text{ kW} \times 0.60 \approx 22.1 \text{ kW}$$
 (3.23)

3.1.6 Scaling to Lifetime

The performance estimates described above correspond to the system's instantaneous operation, but for life cycle assessment (LCA) purposes, they must be scaled to the full system lifetime. In this study, the heliostat field and rotary kiln are assumed to operate for 15 years, with an availability of 80%, corresponding to approximately 292 operating days per year.

The total system lifetime useful energy, defined as the Net Functional Unit (NFU), is calculated as:

$$NFU_{lab} = 15 \text{ kW} \times 0.75 \times 292 \text{ days/year} \times 2 \text{ h/day} \times 15 \text{ years} \approx 98,550 \text{ kWh}$$
 (3.24)

Each Functional Unit (FU) corresponds to 1 kWh of useful thermal energy delivered to the particle bed. Scaling the instantaneous energy flows to the cumulative NFU gives the following lifetime energy requirements, accounting for kiln efficiency ($\eta_{kiln} = 75\%$) and heliostat optical efficiency ($\eta_{optical} = 60\%$):

Useful heat delivered to the particle bed:

$$E_{\text{useful}} = \text{NFU}_{\text{lab}} = 98,550 \,\text{kWh} \tag{3.25}$$

Thermal energy required at the kiln aperture:

$$E_{\text{aperture}} = \frac{E_{\text{useful}}}{\eta_{\text{kiln}}} = \frac{98,550}{0.75} \approx 131,400 \,\text{kWh}$$
 (3.26)

Solar energy incident at heliostat mirrors:

$$E_{\text{incident}} = \frac{E_{\text{aperture}}}{\eta_{\text{ontical}}} = \frac{131,400}{0.60} \approx 219,000 \,\text{kWh}$$
 (3.27)

On a per-FU basis (1 kWh useful heat), the energy requirements are:

$$Q_{\text{aperture, per FU}} = \frac{1 \,\text{kWh}}{\eta_{\text{kiln}}} \approx 1.333 \,\text{kWh/FU}$$
 (3.28)

$$Q_{\text{collected, per FU}} = Q_{\text{aperture, per FU}} \times \frac{1}{\eta_{\text{optical}}} \approx 2.22 \,\text{kWh/FU}$$
 (3.29)

Table 3.1: Summary of laboratory-scale lifetime values.

Flow	Lifetime total	Per FU
Useful thermal energy delivered to the	98,550 kWh	1 kWh/FU
particle bed		
Thermal energy entering at the kiln	131,400 kWh	1.333 kWh/FU
aperture		
Incident solar energy collected at	219,000 kWh	2.22 kWh/FU
heliostat mirrors		

These cumulative totals provide the quantitative foundation for linking the system's technical performance to the environmental burdens assessed in the LCA. They are used to scale all material, energy, and emissions flows consistently, ensuring that both lifetime totals and per-FU impacts are correctly captured.

3.2 PHC Scenarios

The PYSOLO solar subsystem is analyzed under three operational scenarios, each using a different Particle Heat Carrier (PHC): silica sand, bauxite, and olivine. The performance and environmental impact of each scenario are quantified by calculating the energy and material requirements per functional unit (FU) and over the system lifetime.

The particle mass required per FU is determined from the sensible heat needed to raise the particle bed from 400°C to 800°C, based on the following equation:

$$m = \frac{Q_{\text{useful per FU}}}{c_p \times \Delta T} \tag{3.30}$$

where:

- m = particle mass per FU (kg)
- $Q_{\text{useful per FU}} = 1 \text{ kWh} \approx 3.6 \text{ MJ} = 3.6 \times 10^3 \text{ kJ}$
- c_p = specific heat capacity of the particle material (kJ·kg⁻¹·K⁻¹)
- $\Delta T = 800 \,^{\circ}\text{C} 400 \,^{\circ}\text{C} = 400 \,^{\circ}\text{C} = 400 \,^{\circ}\text{K}$

Assumptions

- Baseline kiln efficiency = 75%, so the FU is defined at the particle bed as 1 kWh useful heat.
- Steady-state operation with uniform bed heating.
- Specific heat capacities at 800°C (datasheets):

Table 3.2: Specific Heat Capacities of Materials.

Material	$c_p (\mathbf{k} \mathbf{J} \cdot \mathbf{k} \mathbf{g}^{-1} \cdot \mathbf{K}^{-1})$
Silica sand	0.95
Bauxite	1.05
Olivine	1.25

Mass Calculations Per-FU

$$m_{\rm sand} = \frac{3.6 \times 10^3}{0.95 \times 400} \approx 9.47 \text{ kg/FU}$$
 (3.31)

$$m_{\text{bauxite}} = \frac{3.6 \times 10^3}{1.05 \times 400} \approx 8.57 \text{ kg/FU}$$
 (3.32)

$$m_{\text{olivine}} = \frac{3.6 \times 10^3}{1.25 \times 400} \approx 7.20 \text{ kg/FU}$$
 (3.33)

Initial Circulating Inventory

Each laboratory run lasts 2 hours, during which the kiln delivers 11.25 kW of useful heat, corresponding to a total of:

$$Q_{\text{run}} = 11.25 \times 2 = 22.5 \,\text{kWh} \tag{3.34}$$

Since each FU is 1 kWh, this means each run delivers 22.5 FUs.

The circulating particle inventory must therefore be sufficient to supply 22.5 FUs in a single run:

$$M = m_{\text{per FU}} \times 22.5 \tag{3.35}$$

where:

• Sand:

$$9.47 \times 22.5 \approx 213.16$$
kg

• Bauxite:

$$8.57 \times 22.5 \approx 192.86 \text{kg}$$

• Olivine:

$$7.20 \times 22.5 = 162.00 \,\mathrm{kg}$$

These values represent the one-time initial fill of the kiln with PHCs and are not repeatedly counted in the life cycle model.

Cumulative Recirculated Mass

Over the projected 15 years of laboratory-scale operation (292 operating days per year at 80% availability of a year, with 2 hours of daily operation), the kiln is expected to deliver a total of 98,550 functional units (FUs), corresponding to 98,550 kWh of useful heat.

The total particle mass cycled through the kiln can be obtained by multiplying the material demand per FU by the number of FUs delivered over the system lifetime.

Lifetime total =
$$m_{\text{particle}} \times 98,550$$
 (3.36)

Silica sand:
$$9.47 \times 98,550 \approx 933,269 \text{kg} \approx 933.27 \text{t}$$
 (3.37)

Bauxite:
$$8.57 \times 98,550 \approx 844,573 \,\mathrm{kg} \approx 844.57 \,\mathrm{t}$$
 (3.38)

Olivine:
$$7.20 \times 98,550 \approx 709,560 \text{ kg} \approx 709.56t$$
 (3.39)

It is important to note that these values represent the cumulative throughput of the particles as they are repeatedly circulated and heated within the kiln. They do not correspond to fresh material demand, since the bulk particle inventory is reused continuously and only minor replacement is required due to attrition losses.

Lifetime Make-up (Attrition)

In the PYSOLO system, Particle Heat Carriers (PHCs) such as sand, bauxite, or olivine circulate continuously within the rotary kiln and are reused rather than consumed. Consequently, the environmental impacts associated with the full particle inventory are only accounted for once, at the time of system filling. If the entire inventory were counted for each functional unit (FU), this would substantially overestimate material use and the corresponding environmental burdens.

Over time, a small fraction of the particles is lost due to attrition, which includes mechanical wear, surface erosion, and fracture during handling and transport within the system. To reflect this in the life cycle assessment, only the make-up mass required to replace these losses is considered as an input.

Attrition is modeled as a constant annual fraction of the circulating inventory. The total make-up mass over the laboratory-scale operational lifetime (15 years) is calculated as:

Lifetime make-up =
$$M \times a \times Y$$
 (3.40)

where:

M = circulating inventory (kg)

a = annual attrition rate (fraction per year)

Y = operational lifetime (years, 15 for the lab case)

This gives the total mass of fresh particles that must be supplied over the system's lifetime.

To integrate this into OpenLCA, the per-FU make-up are calculated, which represents the amount of replacement material associated with each 1 kWh of useful thermal energy delivered.

Make-up per FU =
$$\frac{\text{Lifetime make-up}}{\text{NFU}_{lab}} = \frac{M \times a \times Y}{98,550}$$
 (3.41)

In this study, NFU_{lab} = $98,550\,\mathrm{kWh}$ represents the total useful thermal energy delivered over the 15-year laboratory-scale operation. Dividing the total make-up mass by this value yields a material input expressed per functional unit, which can be directly implemented in OpenLCA. This approach ensures that the environmental impacts associated with particle replacement are accurately allocated on a per-kilowatt-hour basis, while preventing the repeated counting of the circulating PHC inventory that is continuously reused throughout operation.

 $a (yr^{-1})$ Lifetime make-up Per-FU make-up Material M (kg) (kg) (kg/FU) Sand $3.24 \times 10^{-}$ 213.16 0.01 31.97 1.47×10^{-4} Bauxite 192.86 0.005 14.46 7.40×10^{-5} Olivine 162.00 0.003 7.29

Table 3.3: Inventory Values for Circulating Particles.

Notes: These values reflect only the replacement material required to compensate for attrition. The large circulating throughput is not re-counted, ensuring a realistic representation of material demand.

This approach provides a realistic representation of material demand, allowing for accurate assessment and comparison of different PHC scenarios without inflating the environmental burdens associated with internal particle recirculation.

Material	$c_p \left(\mathbf{kJ \cdot kg^{-1} \cdot K^{-1}} \right)$	Mass per FU (kg)	Lifetime total (kg)	Per-FU make-up (kg/FU)
Sand	0.95	9.47	933,269	3.24×10^{-4}
Bauxite	1.05	8.57	844,573	1.47×10^{-4}
Olivine	1.25	7.20	709,560	7.40×10^{-5}

Table 3.4: Summary Table — Material Requirements Per Functional Unit.

Notes: All results are reported per functional unit (1 kWh useful heat) delivered to the particle bed. Lifetime burdens are calculated for 15 years of laboratory-scale operation, assuming 292 operating days per year (80% availability).

4 LCA Methodology

4.1 Goal and Scope

The goal of this life cycle assessment (LCA) is to quantify the environmental impacts associated with the construction, operation, and end-of-life stages of the PYSOLO solar-driven thermal energy delivery system. The assessment encompasses all phases from raw material extraction through decommissioning, with a specific focus on the heliostat field, rotary kiln receiver, and supporting infrastructure. Both direct operational impacts and upstream and downstream burdens are captured.

Results are reported per a clearly defined functional unit (FU) to ensure comparability and reproducibility. In addition to quantifying environmental burdens, the study evaluates which particle heat carrier (PHC) scenario—silica sand, bauxite, or olivine—yields the lowest lifecycle impact under consistent system boundaries. The assessment follows the ISO 14040/44 framework for attributional LCA and adopts a cradle-to-grave perspective.

4.2 Functional Unit

For this assessment, the functional unit (FU) is defined as 1 kWh of useful thermal energy delivered to the particle bed in the rotary kiln. This FU represents the actual energy available for downstream processes and enables normalization of all material, energy, and emission flows per unit of delivered useful heat.

All system components—including the heliostat field, rotary kiln receiver, and particle heat carriers (PHCs)—are included within the FU. This ensures that construction, operation, and end-of-life impacts are consistently allocated across the system and across different PHC scenarios.

The system is assumed to operate at 80% availability, corresponding to 292 operating days per year. Over a 15-year laboratory-scale service life, this amounts to 4,380 operating days. During each operating day, the kiln runs for two hours at a useful thermal output of 11.25 kilowatts. This results in a daily energy delivery of 22.5 kilowatt-hours of useful heat. Since the functional unit (FU) is defined as one kilowatt-hour of useful thermal energy, each operating day corresponds to 22.5 FUs.

Over the 15-year lifetime, the kiln therefore delivers a total of 98,550 FUs, equivalent to 98,550 kilowatt-hours of useful heat. Construction and end-of-life burdens are modeled as one-time activities and distributed evenly across all 98,550 FUs. Operation and maintenance activities are modeled cumulatively over the system lifetime and likewise normalized per FU.

Each FU represents one kilowatt-hour of useful thermal energy delivered to the particle bed. To provide this, approximately 2.22 kilowatt-hours of incident solar energy must reach the heliostat mirrors, reflecting a kiln efficiency of 75 percent and an optical efficiency of 60 percent.

Defining the FU in this way ensures that the life cycle assessment accounts only for the thermal energy actually delivered by the system, while allowing fair comparison between different particle heat carrier (PHC) scenarios and with other thermal energy technologies. The total lifetime delivery of 98,550 kilowatt-hours thus forms the reference basis for all subsequent modeling and impact assessment.

4.3 Life Cycle Phases

The life cycle of the PYSOLO solar subsystem is divided into three main phases:

- **Construction**: This phase includes the manufacture, transport, and installation of heliostats, the rotary kiln receiver, structural supports, and auxiliary systems. Construction is modeled as a one-time activity, with all associated impacts distributed evenly across the total number of functional units (FUs).
- Operation and Maintenance (O&M): Routine servicing, spare parts replacement, and auxiliary electricity consumption over the 15-year laboratory-scale operational period are included in this phase. Impacts are modeled as cumulative totals and allocated per FU to accurately reflect their contribution to the life cycle.
- End-of-Life (EoL): Activities related to dismantling, recycling, and disposal of system components are included. Like construction, these impacts are modeled as one-time events and evenly distributed across all FUs.

These three phases together constitute the full system life cycle, forming the basis for all perkWh intensity results reported in the environmental impact assessment.

4.4 Software and Databases

The LCA modeling was performed using OpenLCA, selected for its flexibility in handling custom process chains and its compatibility with widely used life cycle inventory databases.

• Ecoinvent v3.10 (cut-off approach) was the main data source, ensuring conservative accounting of recycled materials.

This combination provides a comprehensive and robust dataset for modeling the environmental impacts of the PYSOLO system.

4.4.1 Allocation procedures

No allocation was applied in this study. For background processes that produce more than one output, the default Ecoinvent "cut-off by classification" approach was used. This ensures consistency with widely used life-cycle inventories and avoids introducing additional allocation assumptions.

4.4.2 Cut-off rules

Flows that contributed less than 1% of the total mass or energy of a process were left out of the system model. These small inputs are not expected to change the overall results of the study.

4.4.3 Data quality

Foreground data, such as particle circulation and kiln operation, came from laboratory and pilot-scale experiments, which adds some uncertainty. Background data for materials, energy, and waste management were taken from the Ecoinvent database, giving good consistency but not always perfectly matching the specific location or technology of the system.

4.5 System Boundaries

In life cycle assessment, the system boundary defines which processes and stages are included in the evaluation. It sets the limits for raw material extraction, manufacturing, transportation, use phase, and end-of-life treatment, including relevant upstream and downstream activities. Clearly defined boundaries are critical for ensuring transparency, reproducibility, and accurate assessment of the system's environmental profile.

For this study, the system boundary covers the solar subsystem of the PYSOLO project and includes the following processes and components(Figure 4.1).

- Raw material extraction for major components.
- Manufacturing of heliostats, the rotary kiln receiver, structural supports, and auxiliary equipment.
- Transportation of components to the experimental site.
- System operation, including solar energy input, auxiliary electricity use, and O&M activities.
- End-of-life treatment, including dismantling, recycling, and disposal.

Processes outside this boundary are excluded, including downstream impacts beyond the delivery of useful thermal energy to the rotary kiln, as well as unrelated infrastructure. The chosen boundary ensures a focused assessment of the environmental impacts associated with the solar-driven thermal subsystem.

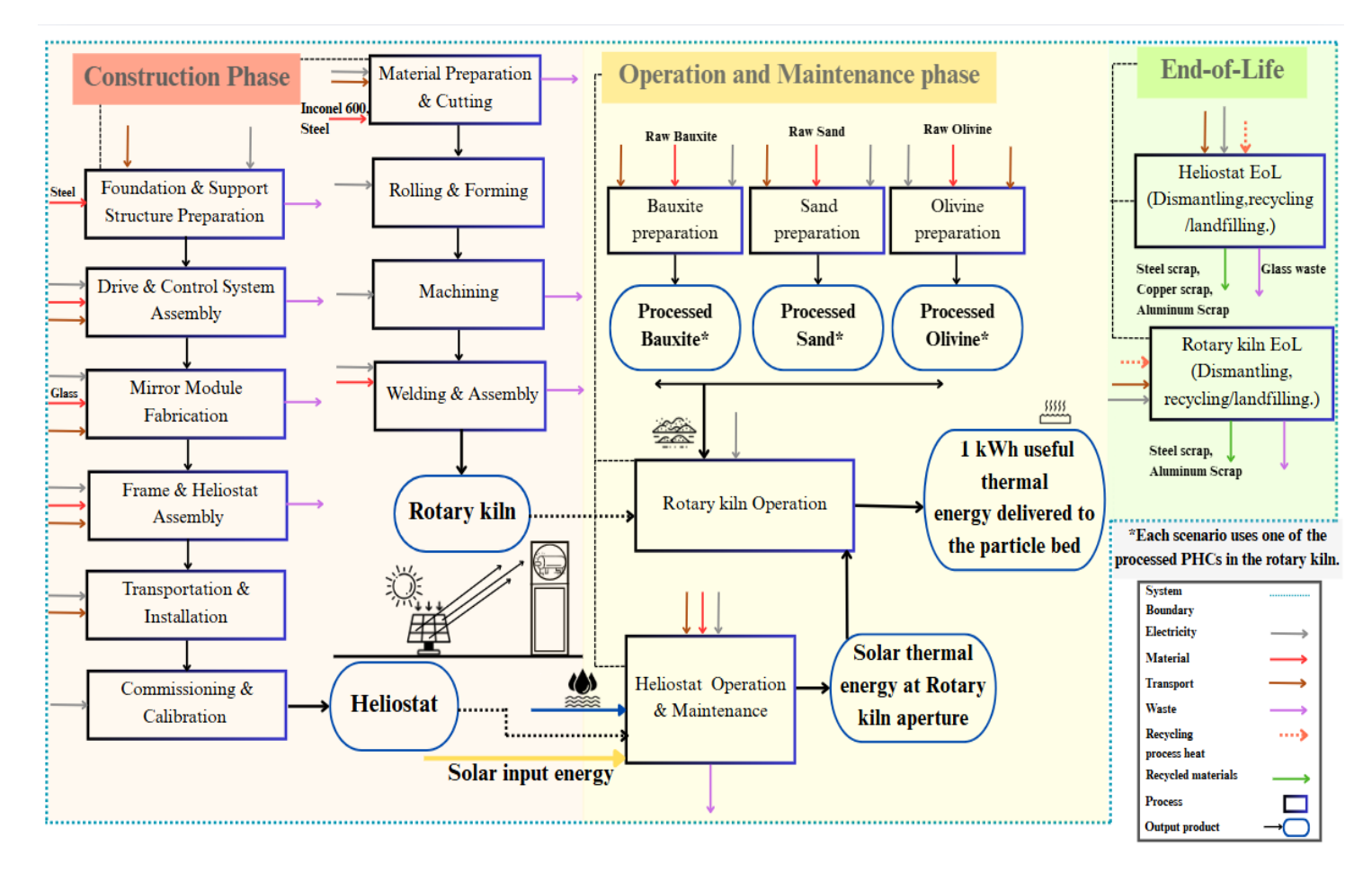


Figure 4.1: System boundary of the solar subsystem in the PYSOLO project, showing key materials, manufacturing, transport, operation, and end-of-life; downstream impacts beyond thermal energy delivery are excluded.

4.6 Life Cycle Inventory (LCI)

The life cycle inventory (LCI) compiles all material and energy inputs associated with the construction, operation, and end-of-life of the solar thermal system. As described in Chapter 3, calculations of material and energy flows were performed on both a per functional unit (FU) basis and for the entire 15-year lifetime of the system (98,550 FUs). These totals are now translated into structured inventory tables suitable for LCA modeling in OpenLCA.

All inventory flows in OpenLCA a modeled on a 15-year system lifetime. Construction and end-of-life activities were entered as one-time flows for the whole system; operation and maintenance flows were entered as cumulative totals over 15 years; and particle make-up was entered as the total replacement mass required over 15 years. After performing LCIA for the lifetime system, results were normalized to the functional unit by dividing lifetime impacts by the total number of functional units delivered over the lifetime NFU $_{lab} = 98,550 \, kWh$, yielding impacts reported per 1 kWh useful thermal energy delivered.

The ReCiPe 2016 Midpoint (Hierarchical) method was selected for the impact assessment for several reasons. First, it provides a wide set of midpoint indicators that are widely used in energy-system LCAs, allowing clear analysis of specific environmental impacts such as climate

change, acidification, particulate matter, human toxicity, and resource depletion. Midpoint indicators are particularly useful for process-level studies because they avoid the extra uncertainty and high aggregation that comes with endpoint indicators, making the results easier to interpret for design decisions[14, 43].

Second, ReCiPe's characterization factors are well-documented and available in most LCA software, which makes the results reproducible and comparable with other recent studies on concentrated solar power (CSP). Compared to other common methods like CML or the Product Environmental Footprint (PEF/EF 3.1), ReCiPe covers a broader range of midpoint indicators relevant to both construction (materials, metals) and operation (emissions, toxicity), and it is widely used in recent CSP literature.

However, no single method is perfect. ReCiPe has limitations in capturing localized impacts, such as site-specific water scarcity or land transformation.

4.6.1 Heliostat construction

The material calculations for the heliostats in the Jülich solar power plant were adapted using the Synhelion DAWN heliostat design Figure 2.8 as a reference for current industrial implementation. Initial reference values were taken from the SunRing heliostat model documented by NREL, which features a 26.96 m² aperture and a total mass of approximately 390 kg, including glass mirrors, steel structures, drives, electronics, foundation materials, and fasteners[39]. Scaling factors based on per-square-meter aperture and facet geometry were applied to align these reference values with the DAWN configuration and operational data from the plant.

The DAWN heliostats differ from the SunRing model by employing four separate mirror facets instead of a single monolithic panel, providing a total reflective surface area of $8.2 \,\mathrm{m}^2$ per heliostat[36, 41]. The mirrors are manufactured from 4 mm low-iron solar glass, contributing a volume of $0.0328 \,\mathrm{m}^3$ and a mass of approximately 82 kg per heliostat (410 kg for a batch of five). Supporting elements are constructed from low-alloy steel. Based on scaled SunRing data and DAWN geometry, the steel allocation per heliostat is approximately 44 kg for foundation pylons, 25 kg for the mirror frame and canting structures, 8 kg for drive components, 3 kg for fasteners and brackets, and 4 kg for the motor housing, totaling 84 kg per unit (420 kg for five heliostats).

Each mirror is oriented using two electric actuators per heliostat—one for azimuth rotation and one for elevation rotation[34]. Each actuator contains a small electric motor (10 kg) and associated mechanical components, including housings, bushings, lubricating oil, and fasteners. Each motor comprises roughly 2.5 kg of copper windings, 4 kg of electrical steel laminations, 3 kg of aluminium housing, 0.5 kg of Nylon-6, and 0.01 kg of lubricating oil. Motor fabrication requires approximately 250 MJ (69.4 kWh) of electricity per motor, resulting in typical machining and assembly losses of 0.05 kg of copper, 0.12 kg of steel, 0.06 kg of aluminium, 0.025 kg of Nylon-6, and 0.0005 kg of oil. Two actuators per heliostat result in a total motor energy demand of 500 MJ (138.8 kWh) per unit.

Beyond the motors themselves, system-level assembly for a five-heliostat batch includes additional components: 3 kg of copper cabling, 1.5 kg of PVC insulation, 2 kg of printed wiring boards, 1.5 kg of passive electronic components, 2.5 kg of Nylon-6 bushings and covers, 10 kg

of steel gearbox parts, 2 kg of aluminium casings, 0.5 kg of lubricating oil, and 30 kg of steel actuator supports and housings. Integration activities—such as PCB soldering, wiring, housing assembly, and functional testing—consume approximately 70 MJ (19.4kWh) for the batch, or 14 MJ (3.9kWh) per heliostat.

The construction of each heliostat was divided into six main steps: foundation and support structure preparation, drive and control system assembly, mirror module fabrication, frame and heliostat assembly, transportation and installation, and commissioning and calibration.

Each step was modeled individually in OpenLCA using data from environmental product declarations (EPDs), industrial reports, and relevant literature. Mass flows, energy requirements, transport distances, and waste fractions were incorporated to provide a detailed and realistic representation of heliostat construction impacts, consistent with European industrial practices.

I. Foundation and Support Structure Preparation

The foundation and support structure for each Synhelion DAWN heliostat was modeled using 0.08 m³ of reinforced concrete per unit, corresponding to 192 kg per heliostat or 960 kg for the five-unit batch. Low-alloyed steel for pylons and support structures was estimated at 44 kg per heliostat, totaling 220 kg for five units.

1. Energy

Electricity demand for this stage was calculated by summing the contributions from rebar fabrication, concrete pumping, and concrete vibration.

- **Rebar fabrication**: 220 kg of steel processed at 15.34 kWh/t [44] ⇒ 3.37 kWh for 220 kg of steel.
- Concrete pumping: 0.4 m³ per 5 heliostat at 3.89 kWh/m³ [45] ⇒ 1.56 kWh per 5 heliostat.
- Concrete vibration: Literature reports 4.66 MJ for five minutes of operation [46]. Assuming this value applies to 0.4 m³, the required energy is:

 ⇒ 1.30 kWh.

Total electricity per heliostat: $3.37 + 1.56 + 1.30 \approx 6.23$ kWh, or 31.15 kWh for the five-heliostat batch.

2. Transport

Transport requirements were calculated based on the delivery distances and material masses:

- Concrete: locally mixed at Jülich, 0.96 t \times 20 km \Rightarrow 19.2 t·km.
- Steel: fabricated at Kraftanlagen München, $0.22 \text{ t} \times 150 \text{ km} \Rightarrow 33 \text{ t·km}$.

Total transport: 52 t·km.

3. Waste

Waste flows were included according to typical European construction practices:

• Concrete waste: 3% of the total concrete (29 kg) is assumed due to over-ordering, spillage, and handling losses, consistent with industry data where baseline wastage rates for in-situ concrete range from 2.5% (good practice) to 5% (baseline) [47].

• **Steel scrap:** 3% of total steel (6.6 kg) from cutting and trimming during fabrication and installation, in line with observed construction practices [48].

The outputs of this stage are the prepared concrete foundations and steel support structures for the five heliostats, ready for assembly of the drive and mirror modules.

II. Drive & Control System Assembly

Each Synhelion DAWN heliostat is equipped with two electric actuators: one for azimuth (horizontal rotation) and one for elevation (vertical rotation). Each actuator contains a small electric motor (10 kg) along with minor mechanical components, including housings, bushings, lubricating oil, and fasteners. The motor is the core energy-converting component, while the actuator represents the complete assembly transmitting motion to the mirror.

I. Motor Composition per Actuator:

Each heliostat in the Jülich solar field is equipped with two electric actuators—one controlling azimuth and the other controlling elevation—resulting in a total of 10 motors for a batch of five heliostats. Each actuator's motor is composed of multiple materials: copper windings (2.5 kg), electrical steel laminates (4 kg), an aluminium housing (3 kg), Nylon-6 components (0.5 kg), and a small quantity of lubricating oil (0.01 kg).

1. Energy

The fabrication and assembly of each motor require approximately 250 MJ (69.4 kWh) of electricity. This estimate includes upstream processing of raw materials, motor manufacturing, assembly, and motor-level testing, based on literature values for small industrial motors[49, 50, 51].

2. Transport

Transport of the motor components from European suppliers contributes roughly 3 t·km per motor.

3. Waste

Material losses during fabrication are relatively minor. Typical waste streams per motor include about 0.05 kg of copper, 0.12 kg of steel, 0.06 kg of aluminium, 0.025 kg of Nylon-6, and 0.0005 kg of lubricating oil. These losses represent machining offcuts, trimming, and handling inefficiencies, consistent with standard industrial practices.

A summary of motor composition, energy use, transport, and waste for the actuator fabrication stage is provided in the Table4.1.

Input Component	Total Mass (kg)	Description	Notes
Copper, cathode	2.5 kg	Copper (windings)	Small electric motor contains
			15–25% copper by mass
Steel, low-alloyed	4 kg	Electrical steel (laminates)	40-50% by mass in small motors
Aluminum, wrought alloy	3 kg	Aluminum housing	20-30% by mass in typical motor
			design
Nylon 6	0.5 kg	Plastics (insulation, fans)	5% of motor mass
Lubricating oil	0.01 kg	Lubricating oil (minor)	< 0.1% of total motor mass
Electricity, medium voltage	69.44 kWh (250 MJ)	Motor fabrication energy	Based on MIT study, approx. 25
			MJ/kg
Transport transport, freight,	3 t.km	-	Transport distances are approxi-
lorry 16-32 metric ton,			mately 500 km for copper wind-
EURO6			ings, around 200 km for steel cores;
			about 300 km for aluminum hous-
			ings; approximately 150 km for
			Nylon 6; and roughly 100 km for
			lubricating oil.

Table 4.1: Electric motor, small, assembled (heliostat actuator type).

Output Components	Total Mass (kg)	Description	Notes		
Electric motor, small, as-	1 item	Completed heliostat actuator			
sembled		motor			
Scrap copper	0.05 kg	Winding trimming	2% loss of copper		
Scrap steel	0.12 kg	Offcuts from lamination 2–3% of steel			
Waste aluminum	0.06 kg	Machining/extrusion scrap	2-3% of aluminum		
Waste mineral oil	0.0005 kg	Spill/filling losses	3–6% of oil		
Waste plastic, mixture	0.025 kg	Injection moulding scrap	(Nylon 6 scrap) 3–5% of nylon		

II. System-Level Assembly for 5 Heliostats (10 Actuators Total):

The system-level assembly for a batch of five heliostats, which includes ten actuators, covers the mechanical and electronic integration needed to operate the motors. Components installed at this stage include copper cabling (3 kg), PVC insulation (1.5 kg), printed wiring boards (2 kg), passive electronic components (1.5 kg), Nylon-6 bushings and covers (2.5 kg), and steel actuator supports and housings (30 kg). The gearboxes themselves contain 10 kg of steel, 2 kg of aluminium, and 0.5 kg of lubricating oil.

1. Energy

Assembly activities such as PCB soldering, wiring, housing integration, and functional testing consume about 70 MJ of energy for the entire batch, or roughly 14 MJ per motor. This represents the additional energy needed beyond the motor fabrication itself and ensures that the system-level assembly is accounted for without double-counting motor-level energy.

2. Transport

Transport of components adds another contribution to the life cycle. Copper cabling and electronics are transported approximately 400 km from Device Logic in the Frankfurt region to Jülich, accounting for 5.2 t·km, while steel supports and housings are shipped 550 km from Kraftanlagen München, adding 22 t·km. The total transport for this stage is therefore 27.2 t·km.

3. Waste

Waste generated during assembly is small but included in the modeling. Typical losses include approximately 0.06 kg of copper (about 2% of cabling and windings), 1.2 kg of steel (around 3% of structural steel), 0.07 kg of electronics (1–2% of PCBs and passive components), 0.2 kg of plastic (roughly 5% of Nylon-6 and PVC from molding losses), 0.025 kg of lubricating oil (less than 0.1% of the total), and 0.04 kg of aluminum (about 2% machining losses). These

losses reflect machining offcuts, trimming, soldering rejects, minor spillage, and small assembly errors, all handled according to standard European recycling and disposal practices.

III. Mirror Module Fabrication

The heliostat mirror assemblies consist of low-iron glass with a silvered back coating, mounted on steel frames. Each heliostat employs four facets with a total reflective area of 8.2 m², giving 41 m² across the five units considered here. With 4 mm glass thickness and a density of 2,500 kg/m³, the total mirror glass mass is 410 kg. A thin reflective silver layer (0.15 g/m) contributes 6.15 g for all mirrors. The support structures require 125 kg of low-alloyed steel and 2 kg of PVC for fastening and minor framing components.

1. Energy

Energy demand is based on the Guardian Glass EPD for wet-coated glass, which specifies 21.91 MJ/m² (6.086 kWh/m²) for silvering and curing (A3 stage)[52]. Applied to the 41 m² total mirror area, this yields 249.5 kWh. Cutting losses are accounted for using a conservative estimate of 0.3 kWh/m², based on CNC score-and-break cutting tables (Bottero 352BCS; Biesse Genius CT-Next), giving an additional 12.3 kWh[53, 54]. The total processing energy is therefore 263.3 kWh, corresponding to 0.64 kWh/kg of mirror glass.

2. Transport

Transport burdens are calculated for delivery of mirror glass, silver, and structural backing materials from Flabeg (Germany)[41] to Jülich (300km). With a shipment mass of 0.54 t, this equals 161 t·km of freight transport.

3. Waste

Material efficiency is constrained by processing losses. Cutting and breakage of glass is assumed at 3% (12 kg) in line with DOE heliostat fabrication data and European flat glass LCAs. Steel cutting scrap is set at 3% (3.75 kg). For PVC supports, approximately 5% offcuts (0.1 kg) are considered. These wastes are managed conventionally, steel scrap is recycled, while minor plastics and glass wastes are disposed of or downcycled, with glass cullet potentially remelted where infrastructure allows.

The output of this process is five fully fabricated mirror modules, representing 410 kg of functional silvered glass mounted in 125 kg of supporting steel structure, ready for heliostat assembly.

IV. Frame & Heliostat Assembly

The frame and heliostat assembly stage comprises final integration of the mirror modules, steel support structures, drive assemblies, and auxiliary components. Activities include welding of minor structural joints, bolting of subassemblies, routing and soldering of cabling, lubrication of moving parts, and installation of actuators.

1. Energy

Electricity demand is dominated by welding operations. Literature reports arc welding electricity use between 4–7 kWh per kg of deposited weld metal[55]. Assuming 0.4 kg of weld metal per heliostat, or 2 kg across the batch of five units, results in 8–14 kWh of electricity. Additional energy stems from bolting, wiring, soldering, and tool use, estimated at 1–2 kWh per heliostat, or 5–10 kWh in total. Lubrication of gearboxes and joints contributes negligible consumption (0.5 kWh). The combined electricity use therefore falls in the range 13.5–24.5 kWh, making the conservative assumption of 25 kWh for five heliostats (5 kWh per unit) consistent with both industrial data and previous CSP component LCAs.

2. Transport

Material inputs include 15 kg of steel fasteners and brackets, 1 kg of nylon bushings, and 2.5 kg of lubricating oil for gear assemblies. Subassemblies such as supports, drives, and mirrors, which are produced in earlier stages, are moved internally to the final assembly zone. For a standard shipment of approximately 0.8 tons over a distance of 20 kilometers, this amounts to roughly 16 ton-kilometers of lorry transportation.

3. Waste

Waste streams arise from offcuts and handling losses. Steel trimming losses are estimated at 3% (0.45 kg), nylon bushings at 5% (0.05 kg), and mineral oil at 5% (0.125 kg). These waste streams are managed in accordance with European regulations: steel scrap is recycled or land-filled, plastics are incinerated, and waste oil is burned as hazardous waste.

The result of this stage is a set of five complete heliostats, each featuring a welded and bolted steel frame, reflective mirror modules, drive and actuator assemblies, and lubricated moving parts, fully prepared for transport and installation on site.

V. Transportation & Installation

Five fully assembled heliostats (approximately 174.32 kg each after accounting for losses, total 0.871 t) are transported from the fabrication site to the solar field. Assuming a delivery distance of 100 km using a EURO6 lorry (16–32 t capacity), this results in 87.16 t·km of freight transport.

For installation, a small electric crane or mobile hoist is used to lift and position each heliostat. Crane electricity demand was estimated using an engineering power × time approach. Typical small hoists and site cranes draw 5–15 kW during lifting, with active hoist durations of 20–60 seconds per lift. This corresponds to 0.03–0.25 kWh per lift. With 2–3 lifts per heliostat and 5 heliostats in total, the installation requires approximately 0.4–2.3 kWh, with a midpoint of 1.2 kWh reported in the LCA. These estimates are consistent with crane energy studies [56, 57] and manufacturer data for small electric cranes [58].

VI. Commissioning & Calibration

Following installation, each heliostat undergoes a one-time commissioning and calibration procedure to ensure correct motor alignment, tracking functionality, and control system reliability. This is considered part of the installation stage, not regular operation.

The electricity demand is estimated as:

- **Motor calibration:** approximately 1.5 kWh per actuator. With 2 actuators per heliostat and 5 heliostats, this equals 15 kWh.
- Controls, testing, and recalibration: approximately 2–3 kWh per heliostat, giving an additional 22.5 kWh.

The total commissioning load is therefore **37.5 kWh** for all 5 heliostats. This value represents a one-time startup requirement, not ongoing operational energy.

Table 4.2 provides a detailed overview of the materials, energy inputs, and transport processes involved in manufacturing the Synhelion DAWN heliostats currently operating at the Jülich solar tower. It covers the main construction materials—concrete, steel, aluminium, copper,

plastics, glass, lubricants, and electronic components—as well as the detailed composition of the electric motor subassemblies. The table also reports associated waste fractions, capturing typical industrial losses such as cutting offcuts, machining residues, handling inefficiencies, and assembly spillages.

The values presented are assumed in this thesis, based on scaling from reference designs and literature-based estimates, due to the lack of detailed site-specific data. As such, the quantities may not exactly reflect actual material or energy use but provide a conservative and transparent basis for life cycle assessment modeling.

Table 4.2: Materials, Energy Inputs, Transport, and Waste in Heliostat Manufacturing (5 units, Synhelion DAWN design, Jülich).

Material / Flow	Process Step	Input Amount	Unit	Waste / Losses	Waste %	Notes / References
Concrete (30 MPa)	Foundation & Support Structure	960	kg	29.0	3.0%	Foundations; waste due to over- ordering/spillage
Steel, low-alloyed	Foundation & Support Structure	220	kg	6.6	3.0%	Pylons/supports; cutting/rebar losses
Electricity, medium voltage	Foundation & Support Structure	31.15	kWh	_	-	Cutting/welding steel and concrete prepration energy
Freight, lorry 16–32 t (EU6)	Foundation & Support Structure	52	t∙km	_	-	Steel + concrete delivery
Output:Support Structures	Foundation & Support Structure	5	item	_	_	Prepared concrete bases + steel supports.
Aluminium, wrought alloy	Drive& Control System	2	kg	0.04	2.0%	Gearbox-Casing material, if separate from motor body; Machining losses
Steel, low-alloyed	Drive & Control System	40	kg	1.2	3.0%	Motor mounts, actuator supports, frames and Gearbox Components-Small gear housings and mechanical mounts; Machining scrap
Copper, cathode	Drive & Control System	3	kg	0.06	2.0%	Cabling & Electronics-Wiring for motors and control systems; Wiring offcuts
Nylon 6	Drive & Control System	2.5	kg	0.125	5.0%	Cabling & Electronics-Bushings and fasteners; Electronics casing

Continued on next page

Table 4.2 continued

Material / Flow	Process Step	Input Amount	Unit	Waste Losses	Waste %	Notes / References
PVC (susp. polymerized)	Drive & Control System	1.5	kg	0.075	5.0%	Cabling & Electronics-Cable insulation and supports; Cabling insulation scrap
Lubricating oil	Drive & Control System (gearbox)	0.5	kg	0.025	5.0%	Gearbox-Lubricating oil (gear lubrication; Handling/filling losses
Printed wiring boards (Pb-free)	Drive & Control System	2.0	kg	0.04	2.0%	Cabling & Electronics-PCBs for heliostat controllers; Reject/rework
Electronic components, passive	Drive & Control System	1.5	kg	0.03	2.0%	Cabling & Electronics-Sensors, chips, and control elements; Small reject fraction
Electric motors, assembled	Drive & Control System	10	items	_	_	2 per heliostat; materials counted in Table4.1
Electricity, medium voltage	Drive & Control System	19.4	kWh	_	_	Assembly energy
Freight, lorry 16–32 t (EU6)	Drive & Control system	27.2	t∙km	_	_	Electronics + casings transport
Output: Drive Assemblies	Drive & Control system	5	item	_	_	Complete motor-drive systems with controls
Steel, low-alloyed	Mirror Module Fabrication	125	kg	3.75	3.0%	Mirror frame and canting structure; Frame waste
Flat glass, uncoated	Mirror Module Fabrication	410	kg	12.0	3.0%	Mirror surfaces for 5 heliostats; Cutting/breakage
Silver	Mirror Module Fabrication	0.00615	kg	_	_	Reflective layer,0.15 g/m 2 × 41 m 2 . Source: DOE/NREL and Flabeg typical solar mirrors

Table 4.2 continued

Material / Flow	Process Step	Input Amount	Unit	Waste / Losses	Waste %	Notes / References
PVC (susp. polymerized)	Mirror Module Fabrication	2.0	kg	0.1	5.0%	Frames and supports; Moulding losses
Electricity, medium voltage-DE	Mirror Module Fabrication	263.3	kWh	_	_	Glass cutting, silvering
Freight, lorry 16–32 t (EU6)	Mirror Module Fabrication	161	t·km	_	-	Delivery of glass and backing materials, Glass supply (Flabeg)
Output: Mirror Modules	Mirror Module Fabrication	5	item	_	-	Fully assembled mirror panels
Support Structures	Frame & Heliostat Assembly	5	item	_	_	Prepared concrete bases + steel supports.
Drive Assemblies	Frame & Heliostat Assembly	5	item	_	-	Complete motor-drive systems with controls
Mirror Modules	Frame & Heliostat Assembly	5	item	_	_	Fully assembled mirror panels
Steel, low-alloyed	Frame & Heliostat Assembly	15	kg	0.45	3.0%	Fasteners & Adhesives-Additional frame and bracket parts; Offcuts
Nylon 6	Frame & Heliostat Assembly	1.0	kg	0.05	5.0%	Frame Assembly(joint bushings); Bushings/insulation
Lubricating oil	Frame & Heliostat Assembly	2.5	kg	0.125	5.0%	Gear lubrication during assembly; Spillage
Electricity, medium voltage-DE	Frame & Heliostat Assembly	25.0	kWh	_	_	Welding/bolting energy

Table 4.2 continued

		1аоте 4.2	2 001101110				
Material / Flow	Process Step	Input	Unit	Waste	/		Notes / References
		Amount		Losses		%	
Freight, lorry 16–32 t (EU6)	Frame & Heliostat Assembly	16	t∙km	_		_	Delivery of heliostats
Output: Assembled Heliostats	Frame & Heliostat Assembly	5	item	_		_	Complete heliostats ready for transport
Output: Assembled Heliostats	Transportation & Installation	5	item	_		_	Complete heliostats ready for transport
Electricity, medium voltage-DE	Transportation & Installation	1.2	kWh	_		_	cranes and positioning energy
Freight, lorry 16–32 t (EU6)	Transportation & Installation	87.16	t∙km	_		_	Delivery of heliostats to solar field
Output: Installed Heliostats	Transportation & Installation	5	item	_		-	Heliostats mounted and aligned on site
Output: Installed Heliostats	Commissioning & Calibration	5	item	_		_	Heliostats mounted and aligned on site
Electricity, medium voltage-DE	Commissioning & Calibration	37.5	kWh	_		_	Running motors for calibration and testing
Output: Heliostats	Commissioning & Calibration	5	item	_		_	Fully operational heliostats, calibrated and functional

Transportation in Heliostat Construction

Transportation plays an important role in the life cycle of heliostats, as materials and components need to be moved from suppliers to fabrication sites and then to the installation location. In this study, transportation is considered at two levels. First, the movement of raw materials and components to fabrication and assembly sites, which is included within each process step. Second, the transport of fully assembled heliostats from the assembly location to the installation site is accounted for separately, using the total weight and an average distance of 100 km. This approach avoids double-counting while capturing both upstream and downstream transport impacts in the life cycle assessment.

The following table provides detailed information on the transportation distances, process steps, and source locations for various materials and components involved in the heliostat manufacturing process.

Table 4.3: Transport Details of Materials and Components in Heliostat Manufacturing.

Material / Component	Process Step	Transport Distance	Source Location
Concrete	Foundation & Sup- port	20 km	Local batching, Jülich
	Structure		
Steel (structural)	Foundation & Sup- port	550 km	Kraftanlagen München, Ger-
	Structure		many
Cabling and Electronics	Drive & Control Sys-	400 km	Device Logic, Frankfurt area,
	tem		Germany
Steel Supports and Housing	Drive & Control Sys-	550 km	Kraftanlagen München, Ger-
	tem		many
Small Electric Motors	Drive & Control Sys-	300 km	Regional European suppliers
	tem		
Aluminium	Mirror and Frame As-	300 km	Nearby EU plants
	sembly		
Nylon 6	Mirror and Frame As-	150 km	Chemical plants, Germany /
	sembly		Belgium
Lubricating Oil	Mirror and Frame As-	100 km	Local refinery
	sembly		
Flat Glass (mirrors)	Mirror and Frame As-	300 km	FLABEG Automotive, Furth
	sembly		im Wald, Germany
Subassemblies	Frame and Heliostat	20 km	From fabrication steps to final
	Assembly		assembly site
Fully Assembled Heliostats	Transport to Solar Field	100 km	Assembly site to installation
			site, Jülich

4.6.2 Heliostat Operation and Maintenance

The total primary energy input from solar sources required over the 15-year operational lifetime of the heliostat system is assumed to be approximately 219,000 kWh. As detailed in Section 3 (System Overview), this calculation incorporates an assumed optical efficiency of 60%, meaning that only 60% of incident solar radiation is effectively converted into thermal energy at the kiln. The useful thermal energy delivered to the kiln over 15 years is assumed to be 98,550 kWh. Adjusting for the kiln's thermal efficiency of 75% increases this to an aperture energy requirement of about 131,400 kWh. When further adjusted for heliostat field optical efficiency, the total incident solar energy aligns with the previously calculated 219,000 kWh.

Maintenance requirements over the system lifetime are estimated and include the replacement and repair of mechanical, electronic, and structural components. Passive electronic components (e.g., sensors, control units) are assumed to require 4.5 kg of replacement materials, based on a 30% replacement rate applied twice (years 7 and 14) to the baseline on-site stock of 7.5 kg across the five heliostats. Lubrication oil usage is projected at 1.5 kg over 15 years, assuming 0.02 kg per heliostat annually for the five operating units. Nylon 6 components used in bushings and fittings are expected to total 0.75 kg, accounting for periodic UV- and heat-related degradation. Steel structures, including actuator parts, are assumed to require approximately 53.3 kg of low-alloy steel, accounting for scheduled replacements and corrosion-related repairs.

Water consumption for mirror cleaning is estimated at 900 kg over 15 years, assuming monthly cleaning with 1 liter per heliostat. Transport logistics for maintenance materials are assumed at 273 tonne-kilometers (t·km), based on expected material volumes and supplier distances.

The system's electrical energy consumption, primarily from heliostat motor tracking, is assumed at 1,095 kWh over 15 years (five heliostats, each consuming 0.05 kWh per day across 292 operational days annually).

Planned component replacements are also assumed for mirror glass ((replaced in two events, 20.5 kg at year 7 and 20.5 kg at year 14, approximately 10% of the mirror mass) and electrical wiring (2 kg every decade). Over the full operational lifetime, the resulting waste streams are projected to include 53.3 kg of steel scrap, 41 kg of waste glass, 2.75 kg of plastic waste (including nylon and wiring insulation), 1.5 kg of used mineral oil, 900 kg of wastewater from cleaning, and 6 kg of electronic waste.

Table 4.4 summarizes the assumed energy inputs, material requirements, and waste outputs associated with heliostat operation and maintenance over the 15-year system lifetime.

Table 4.4: Comprehensive breakdown of material and energy transfers, maintenance procedures, and waste outputs associated with the heliostat operation system throughout a 15-year lifespan.

Material / Energy	Process Step	Allocated Amount	Notes		
Energy, primary, from solar energy	÷ •		Total solar input over 15 years, accounting for optical and kiln efficiencies. Incident solar required (assuming optical $\eta = 0.60$) = 219,000 kWh.		
Electronic component, passive, unspecified	Maintenance / replacement	4.5 kg	Waste electric and electronic equipment; baseline electronics mass = 1.5 kg per heliostat $\times 5 \text{ heliostats} = 7.5 \text{ kg}$; replaced 30% every 7 years (Year 7 and Year 14). Total replaced = 4.5 kg .		
Lubrication oil	Actuator maintenance	1.5 kg	Waste mineral oil; approximately 0.02 kg per heliostat per year over 15 years.		
Nylon 6	Bushings & fittings replacement	0.75 kg	Waste plastic, due to aging under UV and thermal stress.		
Steel low alloyed	Actuator & structural components	53.3 kg	Steel scrap from replacements and repairs over 15 years.		
water, deionised, from tap water, at user	Mirror cleaning	900 kg	Estimated from monthly cleaning, approximately 1 L per heliostat.		
transport, freight, lorry 16-32 metric ton, EURO6	Material delivery	273 t·km	Transportation of replacement materials over 15 years.		
Electricity, medium voltage-DE	Tracking motors operation	1,095 kWh	0.05 kWh/day per heliostat, 292 days/year, 5 heliostats, over 15 years.		
flat glass, uncoated	Mirror replacement	41 kg	Waste glass; replaced in two events (20.5 kg at Year 7 and Year 14).		
polyvinylchloride, suspension polymerised	Wiring replacement	2 kg	Plastic waste; replaced every 10 years (20% of wiring mass).		
Energy entering the aperture (lifetime)	Output	131,400 kWh	Useful thermal energy delivered to particle bed (lifetime). Aperture input required (assuming kiln $\eta = 0.75$) = 131,400 kWh.		
Waste plastic, mixture	Waste output	2.75 kg	From wiring insulation and packaging(Nylon 6+ PVC)		
Waste mineral oil	Waste output	7.5 kg	Oil from replaced lubrication over 15 years.		
Wastewater, average	Waste output	900 kg	From mirror cleaning activities.		
Waste electric and electronic equipment	Waste output	6 kg	E-waste from electronics replacements.		
Steel scrap	Waste output	53.3 kg	Steel scrap from replaced steel actuators and frame parts.		
Waste glass	Waste output	41 kg	Waste from broken or replaced mirror glass.		

4.6.3 Heliostat End-of-Life

Once heliostats reach end-of-life, they are dismantled and their material fractions are separated into recyclable and non-recyclable streams.

Metals

From the heliostat structure, 440 kg of steel is recovered, of which 90% (396 kg) is recycled[59]. Recycling is assumed to occur in a German Electric Arc Furnace (EAF), requiring approximately 380 kWh per tonne of steel, with best practice at 360 kWh per tonne [60]. Scaling to 0.396 t, this corresponds to approximately 144 kWh (518 MJ) of electricity demand, with a sensitivity range of 136–151 kWh. For comparison, if total energy inputs (electricity + fuels) are considered, the BREF benchmark of 690 kWh per tonne yields approximately 273.2 kWh (983.6 MJ) for 396 kg. The recovered steel (396 kg) is modeled as a credit, displacing primary steel production, while 44 kg (10%) is landfilled.

The heliostat aluminium mass is estimated at 32 kg, of which 95% (30.4 kg) is remelted, consistent with European recycling rates for structural aluminium[61, 62]. The energy demand is approximately 10.4 MJ/kg (2.89 kWh/kg), resulting in 316 MJ (87.8 kWh) for the recycled scrap. The remaining 1.6 kg of aluminium is landfilled.

For 28 kg of copper, the end-of-life recycling rate is 40%, so approximately 11.2 kg is recycled, with 16.8 kg landfilled. Recycling is modeled with an electricity demand of 1.44 kWh/kg, yielding approximately 16.13 kWh (58 MJ) for electrolytic refining[63, 64, 65].

Non-recyclable materials and waste flows

Electronic components (3.15 kg, i.e., 90% of 3.5 kg total) are sent to WEEE treatment. Mirror glass, amounting to 410 kg, is considered non-recyclable due to its silver backing and is sent to inert landfill.

Plastics (PVC and nylon, 12 kg total) are incinerated using a custom flow (*plastic incineration*) created for this inventory. The plastics have a lower heating value (LHV) of 28 MJ/kg, resulting in a total LHV:

Total LHV =
$$12 \text{kg} \times 28 \text{MJ/kg} = 336 \text{MJ}$$
 (4.1)

Energy recovery and auxiliary inputs (per 12 kg):

- Heat recovered (credit): 35% of LHV = $0.35 \times 336 = 117.6$ MJ ≈ 32.67 kWh, credited to heat (district/industrial).
- Electricity generated (credit): 15% of LHV = $0.15 \times 336 = 50.4$ MJ ≈ 14 kWh, credited to the electricity market (medium voltage, Germany).
- Auxiliary electricity (burden): approximately 5 kWh \approx 17.82 MJ, used for fans, pumps, controls, shredding; scaled as $0.2517 \, \text{kWh/kg} + 0.161 \, \text{kWh/kg}$.
- External heat input (burden): $0.18 \text{ kWh} \approx 0.648 \text{ MJ}$, corresponding to $54 \text{ MJ/t} \approx 0.054 \text{ MJ/kg} \times 12 \text{ kg}$.

Residues and emissions (per 12 kg):

- **Bottom/fly ash:** approximately 10% of input mass \rightarrow 1.2kg.
- CO (fossil): 0.00198 kg (derived as $0.165 \times 0.012 \text{ kg}$).
- NO_x: $0.0066 \text{ kg (from } 0.550 \times 0.012 \text{ kg)}$.
- HCl: 0.000336 kg (from 0.028×0.012 kg).
- **HF:** $0.000066 \text{ kg (from } 0.0055 \times 0.012 \text{ kg)}.$

Energy recovery fractions and auxiliary inputs are based on Gracia-Gutierrez et al., "Environmental and economic assessment of plastic waste recycling," citing CEWEP averages for electricity share (15% of LHV). The ash ratio (100 kg/t) is from "Chemical Recycling of Mixed Plastic Wastes by Pyrolysis – Pilot Scale Investigations".[66].

Concrete: The concrete foundations contribute 960 kg of inert waste, assumed to be disposed of entirely in inert landfills (192 kg per heliostat $\times 5$ units).

Site dismantling consumes 5 kWh of electricity for crane operation, cutting, and sorting. Transport to recycling/disposal facilities is modeled as 100 t·km of freight by 16–32 t EURO6 lorries.

The material flows at the end-of-life of heliostat systems, including inputs, recycled fractions, and waste outputs, are summarized in the table below. (Table 4.5).

Table 4.5: Material flows at end-of-life for heliostat systems, including inputs, recycling, and waste outputs.

Flow	Amount	Unit	Type	Description / Justification
Inputs				
Electricity,	273.2	kWh	Input	Energy demand for recycling 396 kg of steel in an
medium voltage				Electric Arc Furnace (EAF).
(Steel recycling)				(MJ: 983.6 MJ; based on 690 kWh/t benchmark)
Heat, natural gas	87.8	kWh	Input	Energy required to remelt 30.4 kg of aluminium
(Al recycling)				scrap.
				(MJ: 316.2 MJ; based on 10.4 MJ/kg)
Electricity,	16.13	kWh	Input	Electricity required to recycle 11.2 kg of copper
medium voltage				scrap.
(Cu refining)				(MJ: 58 MJ; based on 5.2 MJ per 0.4 kg)
Dismantling	5	kWh	Input	On-site dismantling activities (crane, cutting,
electricity				sorting).
Transport, lorry	100	t∙km	Input	Transport of recovered and waste materials to
16-32 t				recycling or disposal facilities.
Recycled Materi-				
als (Dismantled				
heliostat)				
Steel scrap	396	kg	Output	90% of steel (440 kg) recovered and credited
				against primary steel production.
Aluminium scrap	30.4	kg	Output	95% of aluminium (32 kg) recovered, credited
				against primary aluminium production.
Copper scrap	11.2	kg	Output	40% of copper (28 kg) recovered, credited against
				primary copper production.
Wastes				
Waste	3.15	kg	Output	90% of 3.5 kg electronics treated as WEEE.
electric/electronic				
equipment				
Waste glass	410	kg	Output	Mirror glass (100%) sent to inert landfill due to
				silver coating.
Waste plastic (PVC	12	kg	Output	Incinerated or landfilled.
+ Nylon)				(LHV: 196 MJ; energy recovery: 35% heat [68.6
				MJ], 15% electricity [29.4 MJ])
Waste mineral oil	3.1	kg	Output	Treated as hazardous waste incineration.
Waste aluminium	1.6	kg	Output	Sent to landfill.
(non-recovered)				
Waste copper	16.8	kg	Output	Sent to landfill.
(non-recovered)				
Waste steel	44	kg	Output	Sent to landfill.
(non-recovered)				
Waste concrete	960	kg	Output	Concrete foundation disposed of in inert landfill.

4.6.4 Rotary kiln Construction

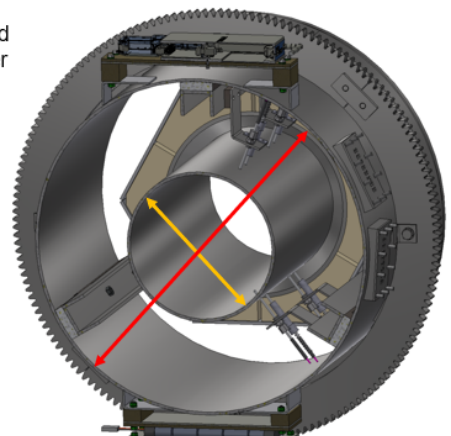
A laboratory-scale rotary kiln receiver-reactor is currently being built at the German Aerospace Center (DLR). Its design is informed by numerical simulations, thermal and mechanical modeling, and lessons learned from previous experimental campaigns. The objective is to achieve reliable operation under concentrated solar flux while maintaining the potential for scale-up to larger reactor configurations. Material selection has therefore focused on thermal resistance, mechanical strength, and compatibility with intense solar irradiation(Figure 4.2).



Crucible (orange): Constructed from Inconel 600, it has an inner diameter of 240 mm, an outer diameter of 250 mm, and a length of 725 mm.

Housing / Shell (red): Made of S355 steel, with an inner diameter of 550 mm, an outer diameter of 560 mm, and a length of 625 mm.

The Space between crucible and housing is filled with SUPERWOOL insulation blankets



The crucible extends 100 mm beyond the housing on the particle outlet side (refer to figure 2.5).

Figure 4.2: Cutaway view illustrating the rotary components 2.5.

Rotary Kiln Component Masses

The total mass of the laboratory-scale rotary kiln was estimated at approximately 113.14 kg, based on detailed geometric modeling and material density calculations. Each component was dimensioned according to its functional role in the reactor design, and its mass was obtained by multiplying calculated volumes with material densities, followed by conservative adjustments to account for fasteners, connectors, and construction tolerances. The results are summarized below.

• **Inconel 600 Crucible:** Modeled as a hollow cylinder with inner diameter 0.24 m, outer diameter 0.25 m, and length 0.725 m. With a wall thickness of 5 mm, the volume is 0.0028 m³. Using a density of 8,430 kg/m³, the mass is calculated as:

$$m = 8,430 \text{ kg/m}^3 \times 0.0028 \text{ m}^3 = 23.6 \text{ kg}$$

• Outer Housing: Formed from S355 low-alloy steel, modeled as a hollow cylinder with inner radius 0.275 m, outer radius 0.28 m, and length 0.625 m, resulting in a volume of 0.00545 m³. With a density of 7,850 kg/m³, the mass is:

$$m = 7,850 \text{ kg/m}^3 \times 0.00545 \text{ m}^3 = 43 \text{ kg}$$

• **Insulation** (**Superwool Fiber Blanket**): Assumed annular volume of approximately 0.1178 m³ with a low-density value of 64 kg/m³, leading to a mass of:

$$m = 64 \text{ kg/m}^3 \times 0.1178 \text{ m}^3 \approx 7.54 \text{ kg}$$

Higher densities would increase this value; however, the low-density option was selected for a conservative baseline.

- Vacuum-formed Insulation Bricks: Effective volume assumed between 0.03–0.05 m³; at a density of 300 kg/m³, the mass is approximately 12.5 kg.
- Internal Support Structure: Consisting of three stainless steel rings and four axial rods from V4A steel, with combined volume 0.00139 m³. At a density of 7,900 kg/m³, this corresponds to:

$$m = 7,900 \text{ kg/m}^3 \times 0.00139 \text{ m}^3 \approx 11 \text{ kg}$$

- **Sealing (Ceramic Fiber Rope):** Total length 4 m, with a specific mass of 0.5–1.0 kg/m; the total estimate is approximately 3 kg.
- External Support Frame: Modeled using 40×40 mm aluminum square tubing with 2 mm wall thickness and 3 m length, volume 0.000912 m³. At a density of 2,700 kg/m³, the mass is:

$$m = 2,700 \text{ kg/m}^3 \times 0.000912 \text{ m}^3 \approx 2.5 \text{ kg}$$

Including connectors, fasteners, and base plates, the mass was conservatively estimated at 12.5 kg.

Summing all components yields a total kiln mass of approximately **113.14 kg**, aligning with independent estimates ranging from 107 to 119 kg. This detailed balance of materials—high-performance alloys, structural steel, lightweight aluminum, and advanced insulation—ensures the kiln's mechanical robustness and thermal stability during operation.

The construction process is divided into four stages: material preparation and cutting, rolling and forming, machining, and welding and assembly. Each stage involves specific energy requirements and material losses, which have been quantified in this study to provide a complete and accurate life cycle inventory of the rotary kiln.

1. Material Preparation and Cutting

The preparation of raw materials for the rotary kiln prototype involves machining, cutting, and shaping of metallic and ceramic components, as well as trimming of insulation materials. These operations contribute to both the energy demand and material waste of the kiln life cycle. In order to quantify these impacts, material-specific cutting intensities were assigned based on literature values, complemented by proxy estimates where direct data were not available.

1. Energy

For metallic components (S355 steel, stainless steel V4A/1.4841, Inconel 600, and aluminium), machining energy intensities were derived from Pervaiz et al. [67], who report typical ranges

of 0.34–4.3 MJ/kg (0.09–1.2 kWh/kg) for steel, 0.32–4.0 MJ/kg (0.09–1.1 kWh/kg) for aluminium, and 0.56–7.0 MJ/kg for cast iron across various industrial case studies. These values were applied uniformly to the steel- and nickel-based alloys of the kiln, with the upper range considered representative for more demanding alloys such as Inconel.

For ceramic vacuum insulation bricks, literature on machining of technical ceramics reports very high energy intensities for laser and EDM cutting, in the order of 10–50 MJ/kg (2.8–14 kWh/kg) [68, 69]. Since the bricks used in the kiln are cut mechanically rather than with high-precision methods, the intensity was conservatively scaled down by a factor of five, resulting in an estimated range of 2–10 MJ/kg (0.6–2.8 kWh/kg).

For fibrous insulation materials (Superwool blanket and ceramic sealing rope), no direct values were identified in the literature. In line with ISO 14044 and EC ILCD Handbook recommendations for proxy data, a fraction of the material's embodied energy was adopted as a conservative estimate. By analogy with textile and glass wool processing, cutting energy was assumed to represent approximately 1–5% of embodied energy, yielding a range of 0.1–0.5 MJ/kg (0.03–0.14 kWh/kg).

Multiplying these specific values with the respective material masses of the kiln yielded component-level energy requirements. For example, machining the 43 kg S355 steel housing corresponds to 14.6–184.9 MJ (4.1–51.4 kWh), while cutting the 12.5 kg ceramic vacuum bricks requires approximately 25–125 MJ (6.9–34.7 kWh). The fibrous insulation contributes negligibly by comparison (< 4 MJ in total). Summing across all materials, the cutting stage consumes between 56 MJ and 514 MJ, corresponding to approximately 16–143 kWh.

2. Waste

In addition to electricity consumption, machining also results in material waste. Based on Ecoinvent v3.10 datasets [70], metallic machining losses were assumed at 2–5% of the processed mass, while ceramics and insulation materials were assigned a 3% cutting or handling loss. Across all kiln components, this results in approximately 3.9 kg of waste material generated in the cutting stage.

Overall, the material preparation and cutting of the 113.14 kg kiln components are thus estimated to require between 16 and 143 kWh,considering a midpoint of 79.5 kWh of electricity and to generate approximately 3.9 kg of waste. The large variation is mainly due to uncertainties in machining intensity for high-alloy metals and ceramics.

3. Transportation

To account for upstream logistics, transportation was modeled as lorry freight (16–32 t, EURO6) over regional distances. Suppliers were assumed within Germany, reflecting typical industrial distribution patterns and aiming to avoid unrealistic global supply chains.

The total transport amounts to approximately 9.2 tonne-kilometers (t·km). Table 4.6 details the assumed sourcing distances.

Component	Supplier (assumed)	Distance (km)	Mass (t)	Transport (t·km)			
S355 Steel	UnionStahl, Duisburg	50	0.043	2.15			
Stainless Steel	Metallstore24.de	100	0.011	1.1			
Inconel 600	Kalikund Steel, German distributor	120	0.024	2.83			
Aluminium	Speira, Germany	80	0.013	1.0			
Superwool Blanket	Isotec Isolierungen	90	0.0075	0.68			
Vacuum Bricks	Isotec Isolierungen	90	0.0125	1.13			
Ceramic Rope	CeraMaterials	100	0.003	0.3			
Total	_	_	0.113	9.2			
Sources [71, 72, 73, 74, 75]							

Table 4.6: Material transport assumptions (to DLR Cologne).

2. Rolling and Forming

After the initial cutting and preparation, several kiln components are bent and formed to obtain their cylindrical or structural shapes. Since this is a laboratory-scale build, the work is carried out using small presses and manual tools rather than industrial hot-rolling mills or automated stamping lines. Consequently, the energy demand is considerably lower than what is typically reported for large-scale sheet-metal production.

Given the lack of specific industrial data for forming prototype-scale kiln parts, a conservative estimate of 0.02 kWh/kg was applied. This figure aligns with values reported for small-scale operations such as manual bending and light press work (0.018–0.025 kWh/kg), as summarized in the Forming Handbook ([76]) and supported by steel plate rolling data in Ecoinvent. For comparison, industrial sheet-forming and deep-drawing processes average around 0.21 kWh/kg, roughly an order of magnitude higher, but not representative of the laboratory context at DLR. Using the specific energy of 0.02 kWh/kg and the total component mass of 113.14 kg, the estimated demand for the rolling and forming stage is:

Energy =
$$0.02 \text{ kWh/kg} \times 113.14 \text{ kg} = 2.26 \text{ kWh}$$

This covers the shaping of the main structural parts, including the cylindrical steel housing and aluminum frame sections, before they proceed to machining and assembly.

In summary, forming contributes only a small fraction of the total energy use compared to cutting, which reflects both the limited scale of the prototype and the relatively light mechanical work needed to shape its parts.

3. Machining

After rolling and forming, the kiln components undergo machining to achieve their final geometries, tolerances, and surface finishes. This stage primarily involves CNC milling, turning, and drilling of metallic parts, with minor adjustments to insulation components to ensure precise fitting. Since most of the rotary kiln mass consists of steels and nickel alloys, machining energy intensities for steel cutting (0.34–4.3 MJ/kg) were applied, supplemented by values for aluminum and ceramic/fibrous materials where relevant [67, 77].

Based on these ranges, the total machining electricity demand was estimated to be between 31.6 and 446 MJ (8.8–124 kWh). Taking the midpoint yields approximately 66.4 kWh, aligning well with reported values for mixed-metal laboratory assemblies of comparable scale. Consequently, a practical estimate of 66–70 kWh was adopted as representative for the DLR kiln.

In addition to energy consumption, machining produces material losses in the form of swarf and fine cutting residues. For this system, approximately 1.8 kg of mixed-metal waste is generated, including stainless steel, Inconel, and aluminum chips, along with minor ceramic and fiber insulation residues. These waste streams were modeled using standard Ecoinvent flows for metal swarf (unsorted) and insulation waste, ensuring that material recycling and disposal pathways are appropriately represented in the life cycle inventory. The machining stage is one of the more energy-intensive steps in the kiln's construction sequence but is also critical for ensuring the precision and mechanical robustness of the final assembly.

4. Welding and Assembly

The final stage of construction consists of welding and mechanical fastening to assemble the machined parts into a complete rotary kiln system. These joining processes provide the structural strength required to withstand concentrated solar flux and prepare the unit for laboratory operation.

Welding energy was estimated using small-batch industrial data from the IEA Industrial Welding Dataset, supported by Ecoinvent flows. A specific intensity of 0.028 kWh/kg was applied, representative of MIG/arc welding processes at this scale [78]. For the total kiln mass of 113.14 kg, this results in an electricity demand of about 3.16 kWh, covering arc welding, grinding, and auxiliary hand-tool use.

In addition to electricity, small amounts of consumables were included. Welding rods were represented by 0.6 kg of drawn steel wire, serving as a proxy due to their similar production energy and form. Mechanical fastening was modeled as 0.3 kg of low-alloyed steel bolts, nuts, and washers, corresponding to roughly 10–15 joints. This value is conservative, as some connections are welded directly or reused from standard laboratory hardware.

The process also generates minor solid residues such as slag, spatter, and sparks, approximated as 0.2 kg of welding waste. While negligible compared to the kiln's total mass, these residues were included for completeness in the life-cycle inventory.

At the end of this stage, the prototype is fully assembled: a laboratory-scale rotary kiln receiver—reactor integrating all structural, thermal, and support components into a single operational unit.

The Table 4.7 summarizes the material composition of the rotary kiln, highlighting the main construction components and their corresponding masses.

Table 4.7: Detailed Material, Process Inputs, Waste, and Outputs for Rotary Kiln Construction and Assembly (using Ecoinvent flows).

Stage	Flow/Dataset (Ecoinvent v3.100)	Input /Output	Amount	Description/Notes	Waste/Losses	waste amoun and %
(1) Material Pr	reparation & Cutting					
	steel production, elec- tric, low-alloyed	Input	43 kg	Housing / shell structure	$\begin{array}{c} \text{scrap steel} \rightarrow \text{in-} \\ \text{ert material land-} \\ \text{fill} \end{array}$	2.15 kg (5%)
	market for steel, chromium steel 18/8, hot rolled	Input	11 kg	Internal supports (V4A, heat-resistant)	scrap steel→ in- ert material land- fill	0.55 kg (5%)
	market for iron-nickel- chromium alloy	Input	23.6 kg	Crucible (Inconel 600) Proxy: no Inconel dataset, approximated with market for iron-nickel- chromium alloy	metal waste, unsorted	1.18 kg (5%)
	market for aluminium, wrought alloy	Input	12.5 kg	External frame, brackets	$\begin{array}{c} \text{scrap aluminium} \\ \rightarrow \text{ municipal incineration} \end{array}$	0.63 kg (5%)
	market for glass wool mat	Input	7.54 kg	Fiber insulation Proxy: used glass wool as substitute for Superwool blanket	waste mineral wool, collection for final disposal	0.23 kg (3%)
	market for refractory, basic, packed	Input	12.5 kg	Vacuum insulation bricks Proxy: Ca-Si bricks approx- imated by "basic refractory, packed"	inert waste, inert material landfill	0.38 kg (3%)
	market for glass wool mat	Input	3.0 kg	Ceramic sealing rope Proxy: ceramic rope substituted with glass wool mat	waste mineral wool, collection for final disposal	0.09 kg (3%)
	market for electricity, medium voltage	Process	79.5 kWh	Cutting processes	-	_
	transport, freight, lorry 16–32 t, EURO6	Process	9.2 t⋅km	Regional material delivery (200 km)	_	_
	Cut and prepped components	Output	1 unit	Ready for forming	_	_
(2) Rolling & F						
	Cut and prepped components	-	1 unit	From cutting stage	_	_
	market for electricity, medium voltage		2.26 kWh	Small-scale rolling/forming	_	_
(2) 3.5 1	Rolled components	Output	1 unit	Bent and formed parts	_	_
(3) Machining	D 11 1	T .	1 '4	D // 11 1 / 1 C		
	Rolled components	Input	1 unit	Bent/rolled parts ready for machining	_	_
	market for electricity, medium voltage	Process	66.4 kWh	CNC machining	-	_
	Machined components	Output	1 unit	Final-sized parts	_	_
	metal waste, swarf (unsorted)	Waste	1.8 kg	Machining residues	_	-
(4) Welding &						
	Machined components	Input	1 unit	Prepared for assembly	_	_
	wire drawing, steel	Input	0.6 kg	Welding rod	Proxy: welding wire approxi- mated with "steel wire"	0.02 kg (3%)
	market for steel, low- alloyed (fasteners proxy)	Input	0.3 kg	Bolts, nuts, washers	Proxy: no fas- tener dataset, ap- proximated with low-alloy steel	-
	market for electricity, medium voltage	Process	2.3 kWh	Welding, grinding, hand-tool use	-	-
	Assembled Rotary Kiln	Output	1 unit	Fully integrated rotary kiln	_	_
	metal waste (slag, sparks)	Waste	0.2 kg	Minor welding residues	_	-

4.6.5 Rotary kiln Operation

n the PYSOLO project, the rotary kiln is operated using particle heat carriers (PHCs), which are continuously circulated through the kiln and heated by concentrated solar radiation reflected from heliostats. The main purpose is to transfer solar energy into the particles, which then deliver usable thermal energy to the process. In this setup, the kiln functions as the core energy conversion unit, transforming intermittent solar flux into a stable stream of thermal energy via the PHCs.

For the Life Cycle Assessment (LCA), the functional unit (FU) is defined as 1 kWh of useful thermal energy delivered to the particle bed in the rotary kiln. This FU represents the net heat available for downstream processes (such as pyrolysis) and serves as the basis for normalizing all material, energy, and emission flows.

4.6.6 Process Representation and Custom PHC Flows

The Ecoinvent v3.10 database does not provide specific waste flows for "spent PHC" materials, such as kiln-cycled olivine, sand, or non-refined bauxite grains. To accurately reflect the mass inventory and replacement dynamics of these primary raw materials (PHCs) in the kiln process, processed PHC and initial PHC stock processes are created.

1. Processed PHCs processes

The three solid heat carrier candidates investigated in this study—bauxite, olivine, and silica sand—follow distinct supply and processing chains before reaching the DLR research facilities in Cologne. To ensure realism, sourcing was aligned with actual industrial suppliers and their documented operations. Since raw minerals cannot be directly applied, custom PHC flows were modeled to represent processed and sieved materials with suitable particle sizes (Table 4.8). The required PHC mass per functional unit (FU) was calculated in the PHC Scenarios section. Each pathway considers from the location of processing (drying, crushing, sieving), and the delivery of conditioned particles to Cologne. It is assumed that the suppliers are responsible for carrying out the processing steps.

Electricity demand for processing

Across all materials, a specific electricity demand of 1.9 kWh per tonne (0.0019 kWh per kilogram) was applied for preprocessing (drying, crushing, sieving). This value reflects motor-driven operations such as crushers, sieves, and auxiliary fans. The chosen figure is supported by literature values.

- USGS reports 1–2 kWh/t for crushing,
- ACEEE (2013) indicates approximately 2.1 kWh/t for combined crushing, screening, and conveying,
- Broader surveys (UK Aggregate Energy Guide) suggest 3–28 kWh/t depending on inclusion of washing and pumping.

Since the PYSOLO system employs dry operations, the lower-bound value of 1.9 kWh/t was selected as a conservative yet realistic baseline. [79, 80, 81].

Silica Sand

Material sourcing:

Silica sand is the most locally available PHC option. Quarzwerke GmbH operates a facility in Frechen, North Rhine-Westphalia, approximately 20 km from Cologne. The sand mined at this site is high-purity quartz, suitable for PHC applications[82].

Processing:

Once extracted, the sand undergoes drying, crushing, and sieving. These processes require 1.9 kWh per tonne, equivalent to 0.0019 kWh per kilogram of processed material. This electricity covers motor-driven operations such as crushers, sieves, and auxiliary fan systems. After processing, a custom PHC flow is defined per 1 kg of sand, representing the mass of material delivered to the rotary kiln.

Transport:

The processed sand is transported by truck over 20 km to DLR Cologne. For the 1 kg PHC unit, this corresponds to 0.020 t·km per kg. The transport flow reflects the use of a 16–32 t EURO6 truck, appropriate for short domestic deliveries.

Bauxite

Material sourcing:

Bauxite is not mined in Germany. For this study, the reference source is EKC AG in Würzburg, Germany, which is considered responsible for processing the raw bauxite into particle heat carrier (PHC)-grade material [83].

Processing:

Bauxite is dried, crushed, and sieved, requiring 1.9kWh per tonne (0.0019 kWh/kg). The processed bauxite is represented by a custom PHC flow per 1 kg, which includes the embodied impacts of the supplier's operations.

Transport:

Only the transport from EKC AG in Würzburg to DLR Cologne is considered. For 1 kg of PHC:

• Würzburg → Cologne: 0.30 t·km (truck, EURO6)

Upstream transport from the mine to the supplier is excluded, as it is assumed to be part of the supplier's responsibility.

Olivine

Material sourcing:

Olivine is supplied by EKC AG in Würzburg, Germany, which is responsible for providing

PHC-grade particles. The material is assumed to have been pre-processed (crushed, sieved, and dried) by the supplier[83].

Processing:

Processing electricity is identical to the other PHCs: 1.9 kWh/t, or 0.0019 kWh/kg. The PHC-grade olivine is represented as a custom 1 kg flow for the LCA, including all processing impacts at the supplier.

Transport:

Only the transport from EKC AG in Würzburg to DLR Cologne is considered. For 1 kg of PHC:

• Würzburg → Cologne: 0.30 t·km (truck, EURO6)

Upstream transport from the mine is excluded, assuming it is handled within the supplier's operations.

2. Initial PHCs stock processes

The total circulating inventory of Particle Heat Carriers (PHCs) over their operational lifespan is modeled as an Initial stock process for each type of particle. This Initial stock process produces one unit of the corresponding custom PHC flow, which is utilized as an input for the rotary kiln operation. This modeling approach is essential as it separates the one-time embodied impacts of the inventory from the ongoing operational impacts associated with the functional unit (FU).

Due to the absence of explicit flows for "waste olivine" or "waste bauxite (non-Bayer)" in the Ecoinvent v3.10 database, the spent or attrited PHC output is mapped to the "waste mixed aggregates" flow available in the database. This mapping is justified by the fact that the sand, olivine, and non-refined bauxite grains lost through wear and attrition behave as inert granular mineral fragments rather than chemically transformed industrial residues. As such, "waste mixed aggregates" serves as the closest available inert mineral waste category in database and is commonly used as a proxy for granular mineral residues like sand, gravel, and crushed stone when no more specific waste stream exists (Table 4.9).

Rotary Kiln Operation: Numerical Inputs and Electricity Demand

The operation of the rotary kiln in the PYSOLO system is modeled by combining solar thermal input, electricity demand for rotation and control, and the circulation of particle heat carriers (PHCs) with their associated attrition and waste flows. Over its lifetime, the kiln receives approximately 131,400 kWh of concentrated solar energy, corrected for heliostat and receiver efficiencies, which results in 98,550 kWh of useful thermal output. This useful energy serves as the basis for normalization to the functional unit of 1 kWh.

The electricity required to rotate the kiln and power its control system is comparatively minor due to the small scale of the laboratory device: with a mass of roughly 113 kg and a rotation speed of 2–3 rpm, the mechanical load is modest, and specifications for comparable kilns indicate motor powers of 40–50 W, while sensors, programmable logic controllers (PLCs), and interfaces consume an additional 5–35 W. On this basis, the lifetime electricity demand is estimated in the range of 13–44 kWh, representing about 0.3–1% of the total solar thermal input. A

midpoint value of 30 kWh is adopted, equivalent to 0.00685 kWh per 1 kWh of useful thermal output[22, 84, 85].

In the kiln model, the particle heat carriers (PHCs) are represented in two distinct steps. First, the initial circulating inventory is defined as a one-time stock, modeled in separate processes for each material: 213.16 kg of sand, 192.86 kg of bauxite, and 162.00 kg of olivine. These stocks are linked to the kiln operation as unit inputs, representing the recirculating particle bed that remains in use throughout the system's lifetime. Because the particles are continuously reused, these bulk inventories are only included once at the beginning of the system and are not repeatedly counted over the entire operating period.

To account for material losses, additional make-up flows are added to the rotary kiln operation. Over the 15-year reference period, these amount to 31.97 kg of sand, 14.46 kg of bauxite, and 7.29 kg of olivine. These inputs represent the fresh material required to compensate for attrition and maintain the circulating bed. The same quantities are reported as outputs and linked to the ecoinvent flow "waste mixed aggregates," which is used here as a conservative proxy for inert mineral disposal. This approach ensures that both the need for replacement and the corresponding end-of-life treatment of degraded particles are consistently represented within the system boundaries.

In OpenLCA, the initial circulating inventories are implemented as one-time processes (sand: 213.16 kg; bauxite: 192.86 kg; olivine: 162.00 kg). Attrition is modeled as recurring inputs to the kiln operation, equivalent to 31.97 kg of sand (0.000324 kg/FU), 14.46 kg of bauxite (0.000147 kg/FU), and 7.29 kg of olivine (0.000074 kg/FU) over the lifetime. For clarity, the cumulative particle throughput (e.g., 933,269 kg of sand) is reported separately, but it is not modeled as additional inputs, as these flows represent recirculation rather than new material demand.

Table 4.8: Processed Particle Heat Carriers (PHCs) – Custom Flows.

Raw Input (Ecoinvent)	Supporting Inputs	Output (Custom Flow)	Notes
Bauxite, bauxite mine operation — bauxite — Cutoff, S - GLO	 Electricity, medium voltage {GLO}: 0.0019 kWh Market for transport, freight, lorry 16–32 t, EURO6 {RoW}: 0.30 t·km 	Bauxite, processed for PHC use [custom] – 1.0 kg	Represents bauxite that has been mined, dried, crushed, and sieved for use in the rotary kiln. Transport considered from supplier to site.
Olivine, in ground	 Electricity, medium voltage {GLO}: 0.0019 kWh Market for transport, freight, lorry 16–32 t, EURO6 {RoW}: 0.30 t·km 	Olivine, processed for PHC use [custom] – 1.0 kg	Represents olivine after preprocessing (drying, crushing, sieving). Transport considered from supplier to site.
Silica sand , market for silica sand, cut-off, S - GLO	 Electricity, medium voltage {GLO}: 0.0019 kWh Market for transport, freight, lorry 16–32 t, EURO6 {DE}: 0.020 t·km 	Sand, processed for PHC use [custom] – 1.0 kg	Represents sand that has been conditioned for PHC application in the rotary kiln. Transport is a short domestic truck leg.

Table 4.9: Initial Stock Processes for Processed Particle Heat Carriers (PHCs) — Custom Flows.

Initial-stock process name	Inputs (custom PHC flow)	Inventory mass in process (kg)	Output (to rotary kiln operation)	Notes
Initial-stock — Sand	Sand, processed for PHC use [custom]	213.16 kg	1 unit (Initial-stock — Sand)	This process represents the one-time embodied inventory to establish the circulating sand bed, including upstream mining, supplier preprocessing (0.0019 kWh/kg), and transport from supplier to DLR Cologne. Impacts are counted once, separate from recurring operational flows.
Initial-stock — Bauxite	Bauxite, processed for PHC use [custom]	192.86 kg	1 unit (Initial-stock — Bauxite)	Represents the one-time embodied inventory required to establish the circulating bauxite bed. The process should include upstream impacts for 192.86 kg (processing + transport).
Initial-stock — Olivine	Olivine, processed for PHC use [custom]	162.0 kg	1 unit (Initial-stock — Olivine)	Represents the one-time embodied inventory required to establish the circulating olivine bed. The process should include upstream impacts for 162.0 kg (processing + transport).

Table 4.10 presents the operation data per lifetime totals for the three PHC scenarios.

Table 4.10: Rotary kiln operation (lifetime totals; per PHC scenario; normalized to FU in results).

Flow / item	Bauxite	Olivine	Sand	Notes
Solar thermal energy input (lifetime)	131,400 kWh	131,400 kWh	131,400 kWh	Corrected for heliostat & receiver efficiencies.
Useful thermal output (lifetime)	98,550 kWh	98,550 kWh	98,550 kWh	Normalized to FU = 1 kWh useful thermal energy in results.
Assembled Rotary kiln(input)	1 unit	1 unit	1 unit	Final complete kiln product.
Rotary motor & control electricity (lifetime)	30 kWh	30 kWh	30 kWh	Adopted midpoint (13–44 kWh range); = 0.000304 / FU.
PHC initial-stock input (to kiln operation)	Initial-stock — Bauxite (1 unit; represents 192.86 kg)	Initial-stock — Olivine (1 unit; 162.0 kg)	Initial-stock — Sand (1 unit; 213.16 kg)	Initial-stock processes (one-time embodied inventory) are entered as 1 unit inputs in the kiln operation.
Lifetime make-up inputs (attrition — total over 15 yr)	14.46 kg	7.29 kg	31.97 kg	Entered as repeated make-up inputs (custom PHC flow per kg); each replenishment carries upstream impacts.
Waste output (waste mixed aggregates)	14.46 kg	7.29 kg	31.97 kg	Same mass as lifetime make-up; mapped to waste mixed aggregates (ecoinvent v3.10) as conservative inert-mineral proxy.

4.6.7 Rotary kiln End-of-Life

At the end of its 15-year lifespan, the rotary kiln is dismantled into recyclable metals, inert insulation, and non-recyclable mineral wool. Construction machining losses is excluded, as it was accounted for in the manufacturing stage.

Metals

The metallic fractions consist of 43 kg of S355 structural steel, 11 kg of stainless steel V4A (1.4841), 12.5 kg of aluminum, and 23.6 kg of Inconel 600. High recovery rates are assumed, reflecting European industrial practice: 90% for steel and stainless steel[59, 60, 72, 86], 95% for aluminum[61, 62], and 85% for Inconel. This results in the recovery of 38.7 kg of steel, 9.9 kg of stainless steel, 11.9 kg of aluminum, and 20.1 kg of Inconel, while the remainder is lost as slag, residues, or dismantling inefficiencies.

Recycling is modeled via process-specific routes:

- 1. **Steel** is recycled via Electric Arc Furnace (EAF) technology, with an energy consumption of approximately 380 kWh per tonne. Scaling to 38.7 kg yields approximately 14.7 kWh[60].
- 2. **Stainless steel** requires EAF with Argon Oxygen Decarburization (AOD) refining, consuming about 0.694 kWh/kg, giving approximately 6.9 kWh for 9.9 kg. The combined ferrous recycling demand totals approximately 21.6 kWh (78 MJ). Including fuels, the total energy input rises to roughly 103 MJ[87].
- 3. **Inconel 600** recycling is conservatively modeled using literature data for nickel-based alloys, with an energy requirement of approximately 13 MJ/kg. Recycling 20.1 kg requires about 261 MJ (72.4 kWh), with sensitivity bounds of 10–20 MJ/kg[88].
- 4. **Aluminum** scrap is remelted, consuming roughly 10.4 MJ/kg. For 11.9 kg, this corresponds to about 124 MJ (34.5 kWh), with variability in the range of 5–15 MJ/kg, resulting in a sensitivity range of 60–179 MJ[61, 62].

Insulation and Residual Waste

The kiln's insulation materials do not enter the recycling stream. Specifically, 12.5 kg of calcium silicate bricks and 10.5 kg of ceramic fiber insulation (including blanket and sealing rope) are classified as non-recyclable and sent to inert or mineral waste disposal. Additional metallic residues, approximately 5.3 kg, arise from fasteners, welding slag, and dismantling losses.

Dismantling and Transport

he 113 kg kiln is dismantled manually using hand tools and a light hoist. Energy demand is estimated at around 0.017 kWh per kilogram, giving a total of roughly 2.0 kWh (7.2 MJ). This value falls within the documented range for light manual dismantling (0.015–0.025 kWh/kg). Following dismantling, all material fractions are transported about 150 km to recycling or disposal sites. For a kiln mass of 0.113 t, this equates to approximately 17 t·km of lorry transport (EURO6). (Table 4.11)

Table 4.11: End-of-Life Flows for Rotary Kiln.

Flow Name (Ecoinvent / Custom)	Amount	Туре	Description / Assumptions
electricity, medium voltage (market for electricity, medium voltage Cutoff,S-DE)	28.6 kWh	Input	Power for cutting and processing steel and stainless steel. Includes recycling of 38.7 kg S355 steel and 9.9 kg stainless steel V4A (90% recycling). Based on Electric Arc Furnace (EAF) with 103 MJ total energy demand (28.6 kWh). Sensitivity: 19.4–25.1 kWh.
electricity, medium voltage (market for electricity, medium voltage Cutoff,S-DE)	72.4 kWh	Input	Energy for Inconel 600 recycling. 23.6 kg with 85% recovery (20.06 kg). Recycling energy proxy: 13 MJ/kg \rightarrow 261 MJ (72.4 kWh). Sensitivity: 10–20 MJ/kg (201–401 MJ total).
heat, district or industrial, natural gas (market for heat $ Cutoff, S-EuropewithoutSv $	34.5 kWh vitzerland)	Input	Energy for aluminum remelting. 12.5 kg Al with 95% recovery (11.9 kg). Energy demand 10.4 MJ/kg \rightarrow 124 MJ (34.5 kWh). Sensitivity: 5–15 MJ/kg (16.7–49.7 kWh).
transport, lorry 16–32t, EURO6-GLO	17 t·km	Input	Transport to dismantling site. 113 kg (0.113 t) transported 150 km.
electricity, medium voltage (market for electricity, medium voltage $\ Cutoff, S-DE\ $	2.0 kWh	Input	Electricity for dismantling, cutting, and sorting. Assumed 0.017 kWh/kg for 115 kg equipment. Based on Fraunhofer ISE (2020).
Output			
inert waste, for final disposal (market for inert waste $\ Cutoff, S-RoW\ $)	12.5 kg	Output	From calcium silicate insulation bricks (non-recyclable).
waste mineral wool (market for waste mineral wool $ Cutoff, S-EuropewithoutSw $	10.54 kg vitzerland)	Output	From ceramic fiber blanket (7.54 kg) and ceramic sealing rope (3.0 kg). Not recyclable.
Dismantled Rotary kiln (cus	tom flow)		
	81.3 kg	Output	Consolidated recycled metals from dismantled kiln: • Steel scrap: 38.7 kg (90% recovery from 43 kg S355) • Aluminum scrap: 12.0 kg (95% recovery from 12.5 kg) • Stainless steel scrap: 10.0 kg (90% recovery from 11 kg V4A) • Inconel scrap: 20.6 kg (85% recovery from 23.6 kg Inconel 600).
Metal waste (custom flow)			
	5.3 kg	Output	Consolidated non-recycled metallic residues: • Welding rod input: 0.6 kg • Fasteners: 0.3 kg • Slag residue: 0.2 kg • Inconel unrecovered fraction: 3.0 kg (15% loss from 23.6 kg) • Disassembly/cutting losses: 1.2 kg. Total: 5.3 kg.
Steel waste (waste flow)			
	5.3 kg	Output	Steel losses: $43 \text{ kg} - 38.7 \text{ kg} = 4.3 \text{ kg} + 1.0 \text{ kg}$ disassembly losses = 5.3 kg.
Aluminum waste (waste flow	y)		
	0.5 kg	Output	Losses: $12.5 \text{ kg} - 12.0 \text{ kg} = 0.5 \text{ kg}$.

5 Results

5.1 Impact Analysis

The environmental evaluation of the solar-driven rotary kiln system was carried out through a Life Cycle Impact Assessment (LCIA), in accordance with ISO 14040/44 standards. LCIA translates the inventory of material and energy flows into potential environmental impacts, enabling comparison of different processes and design choices. Six midpoint impact categories were selected to represent the main environmental concerns:

- Climate change (kg CO₂-eq)
- Energy resources: non-renewable, fossil (kg oil-eq)
- Material resources:metals/minerals (kg Cu-eq)
- Land use (m²a crop-eq)
- Water use (m³)
- Human toxicity (kg 1,4-DCB-eq)

The LCIA results were first calculated for the entire system lifetime, corresponding to the delivery of 98,550 kWh of useful thermal energy. The results were then normalized per functional unit of 1 kWh of useful heat delivered, allowing meaningful comparisons across systems(See Tables 5.1 and 5.2).

Across all PHC scenarios (Bauxite, Sand, Olivine), the largest contributions were observed in human toxicity and climate change, with minor but measurable impacts in energy, materials, land, and water.

Table 5.1: Pre-Normalization Environmental Impact Assessment of Various Processes.

Processes	Climate change (kg CO ₂ -eq)	Energy resources: non-renewable, fossil (kg oil-eq)	Material resources: metals/minerals (kg Cu-eq)	Land use (m ² a crop-eq)	Water use (m ³)	Human toxicity (kg 1,4-DCB-eq)
Heliostat construction	2842.04	674.63	116.19	94.39	20.06	14968.45
Heliostat operation	1257.18	291.07	39.41	37.89	8.59	2130.71
Rotary construction	591.47	141.33	77.60	13.15	15.83	2290.62
Only Rotary with Bauxite	31.31	8.80	8.98	0.78	0.18	4.93
Only Rotary with Sand	24.15	6.70	0.26	0.67	0.08	3.58
Only Rotary with Olivine	22.89	6.39	0.26	0.65	0.08	3.58
Heliostat EoL	194.46	55.01	1.22	5.21	0.60	29.09
Rotary EoL	54.89	14.91	0.35	1.10	0.22	6.99
Entire system including EoL (with Bauxite)	4971.36	1185.75	243.75	152.53	45.48	19430.80
Entire system including EoL (with Sand)	4965.15	1183.35	234.86	152.27	45.36	19428.10
Entire system including EoL (with Olivine)	4962.93	1183.34	235.03	152.40	45.38	19429.44

Processes	Climate change (kg CO2-eq)	Energy resources: fossil (kg oil-eq)	Material resources: metals/minerals (kg Cu-eq)	Land use (m ² a crop-eq)	Water use (m ³)	Human toxicity (kg 1,4-DCB-eq)
Heliostat construction	0.02884	0.00685	0.00118	0.00096	0.00020	0.15189
Heliostat operation	0.01276	0.00295	0.00040	0.00038	8.72e-05	0.02162
Rotary construction	0.00600	0.00143	0.00079	0.00013	0.00016	0.02324
Only Rotary with Bauxite	0.000032	8.93e-05	9.11e-05	7.93e-06	1.82e-06	5.00e-05
Only Rotary with Sand	0.000245	6.80e-05	2.64e-05	6.79e-06	7.63e-07	3.63e-05
Only Rotary with Olivine	0.000232	6.49e-05	2.68e-05	6.58e-06	7.64e-07	3.63e-05
Helio EoL	0.00197	0.000558	1.23e-05	5.29e-05	6.11e-06	0.000295
Rotary EoL	0.000556	1.51e-04	3.53e-06	1.12e-05	2.21e-06	7.09e-05
Entire system incl. EoL (with Bauxite)	0.05044	0.01203	0.00247	0.00155	0.00046	0.19717
Entire system incl. EoL (with Sand)	0.05038	0.01201	0.00238	0.00155	0.00046	0.19715
Entire system incl. EoL (with Olivine)	0.05035	0.01200	0.00238	0.00155	0.00046	0.19714

Table 5.2: Normalized Results of Environmental Impact Assessment.

5.1.1 Total Impacts before Normalization

The total life cycle impacts for the different PHC scenarios—bauxite, sand, and olivine—reveal that human toxicity and climate change are the dominant categories. The human toxicity impacts are particularly pronounced, with the system producing approximately 19,430 kg 1,4-DCB-Eq over its lifetime. This is nearly an order of magnitude higher than the other impact categories, indicating that the potential harm to human health from the extraction and processing of metals and electronic components is a critical concern. Climate change impacts are also substantial, ranging from 4,963 to 4,971 kg CO₂-Eq, depending on the PHC material selected.

Other categories contribute smaller but still relevant burdens. Non-renewable fossil energy use ranges from 1,183 to 1,186 kg oil-eq, while metals and minerals depletion lies between 235 and 244 kg Cu-eq. Land use is consistent across scenarios, at approximately 152.3–152.5 m²a crop-eq, and water use is around 45.4 m³. These values reflect the combined environmental load of constructing, operating, and decommissioning the heliostat field and rotary kiln system(Table 5.1).

5.1.2 Normalized Results per Functional Unit

When expressed per unit of useful heat, the normalized impacts provide a clearer perspective on the efficiency and environmental intensity of the system. Non-renewable fossil energy demand amounts to 0.012~kg oil-eq/kWh,climate change impacts amount to approximately 0.0504~kg CO₂-eq per kWh of useful heat, while metals and minerals depletion ranges from 0.00238~to 0.00247~kg Cu-eq/kWh. Land use and water use remain relatively low, at $0.00155~m^2a$ cropeq/kWh and $0.00046~m^3/kWh$, respectively.

The human toxicity category remains the most striking, reaching 0.197 kg 1,4-DCB-Eq/kWh. This highlights that the environmental profile of the system is heavily influenced by the toxicological impacts associated with mining and processing metals, as well as the production of electronics and other components. The high human toxicity per functional unit underscores the importance of material selection, component efficiency, and supply chain management in reducing potential harm to human health(Table 5.2).

5.1.3 Comparison Across PHC Materials

The differences between the three PHC options—bauxite, sand, and olivine—are relatively small when considering the total environmental impacts. The largest variation is observed in the metals and minerals depletion category, where bauxite exhibits a slightly higher burden than sand and olivine. For all other impact categories, the results are nearly identical, suggesting that the choice of PHC material has a limited effect on the overall system performance, except for minor differences in material-intensive categories (see Figure 5.1).

Overall, these results indicate that the environmental profile of the solar-driven rotary kiln system is dominated by human toxicity and climate change, with smaller but non-negligible contributions from energy, land, water, and resource depletion. The normalized results per functional unit emphasize that, on a per-kWh basis, human toxicity remains the critical impact, highlighting the need for strategies focused on reducing metal-intensive components, optimizing assembly, and sourcing low-impact electricity to minimize the environmental burden of the system.

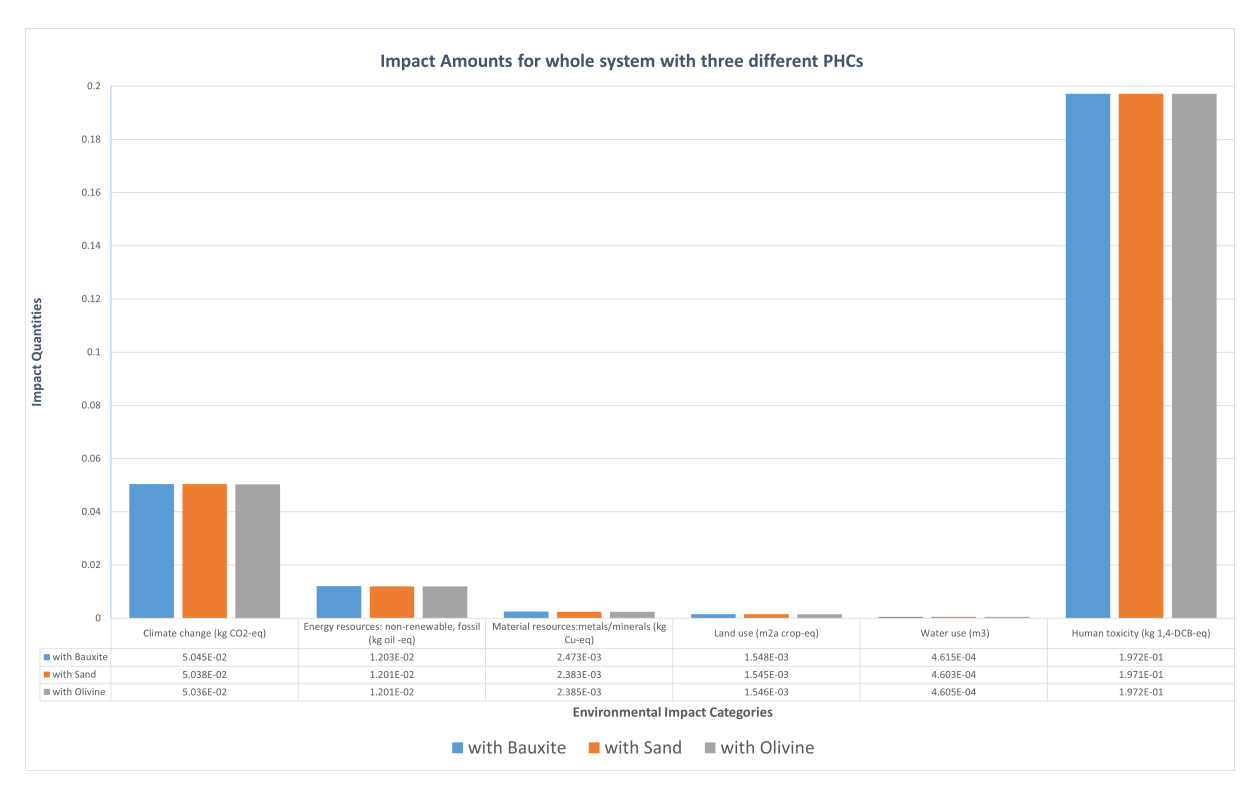


Figure 5.1: Impact Amounts for Different PHCs.

5.2 Contribution Analysis of Subsystem

5.2.1 Contribution Analysis of the Whole System with Bauxite as the Particle

The contribution analysis of the heliostat system with bauxite as the particle highlights that the construction phases dominate environmental impacts across the examined categories. Heliostat

construction emerges as the single most significant contributor, accounting for approximately 57% of the total climate change impact, 48% of material resource depletion, and 77% of human toxicity. This underscores that the upstream production and assembly of the heliostat components are the primary drivers of these environmental burdens.

Heliostat operation follows as the second most important contributor, with 25% of climate change, 16% of material resources, and a minor contribution to human toxicity. Rotary construction contributes substantially to material resources (32%) and human toxicity (12%), but has a lower influence on climate change (approximately 12%).

The operational phase of the rotary subsystem contributes negligibly across all categories, ranging from 1% for climate change to 4% for material resources, reflecting its low energy and material demands during operation. End-of-life phases of both heliostat and rotary subsystems are minor contributors, with heliostat end-of-life representing roughly 4% of climate change impacts and less than 1% for material and human toxicity categories, while rotary end-of-life contributes only around 1% for climate change and near-zero impacts in other categories.

To support visual interpretation, three pie charts were created illustrating the proportional contributions of the subsystems for climate change, human toxicity, and material resource depletion. These visualizations reinforce the quantitative analysis, clearly showing that the construction of the heliostat subsystem dominates environmental impacts, while operational and end-of-life phases play comparatively minor roles(Figures 5.2, 5.3, 5.4).

Overall, the data indicate that mitigation strategies should focus on material efficiency, sustainable sourcing, and energy optimization during the heliostat construction phase to achieve the most significant reductions in environmental impacts.

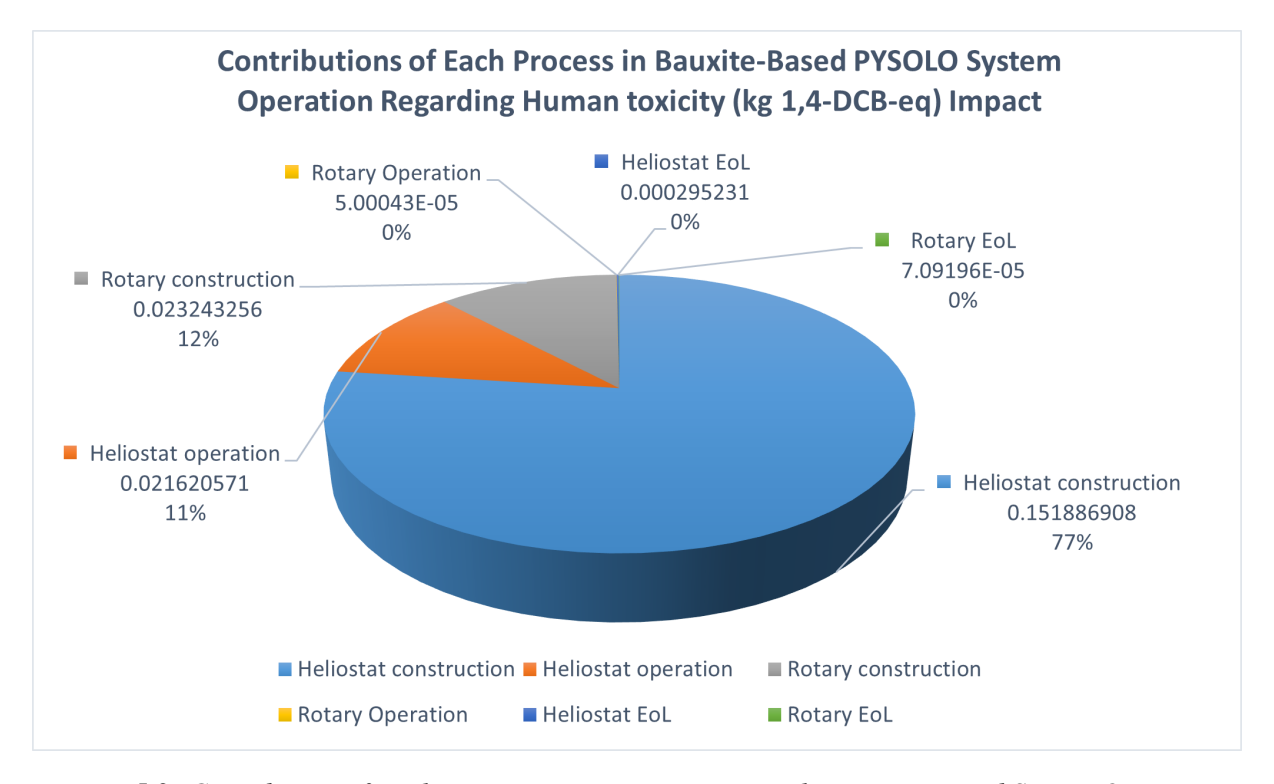


Figure 5.2: Contribution of Each Process to Human Toxicity in the Bauxite-Based System Operation.

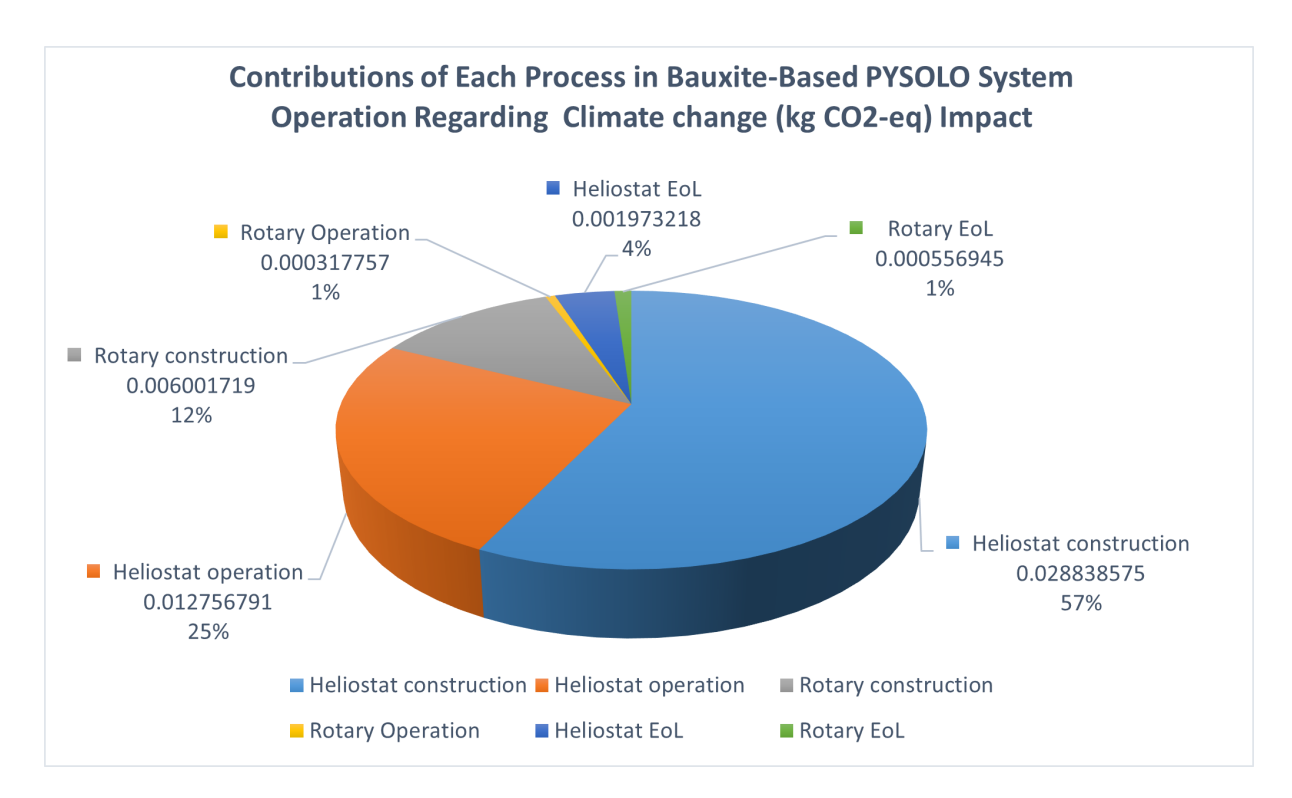


Figure 5.3: Contribution of Each Process to Climate Change in the Bauxite-Based System Operation.

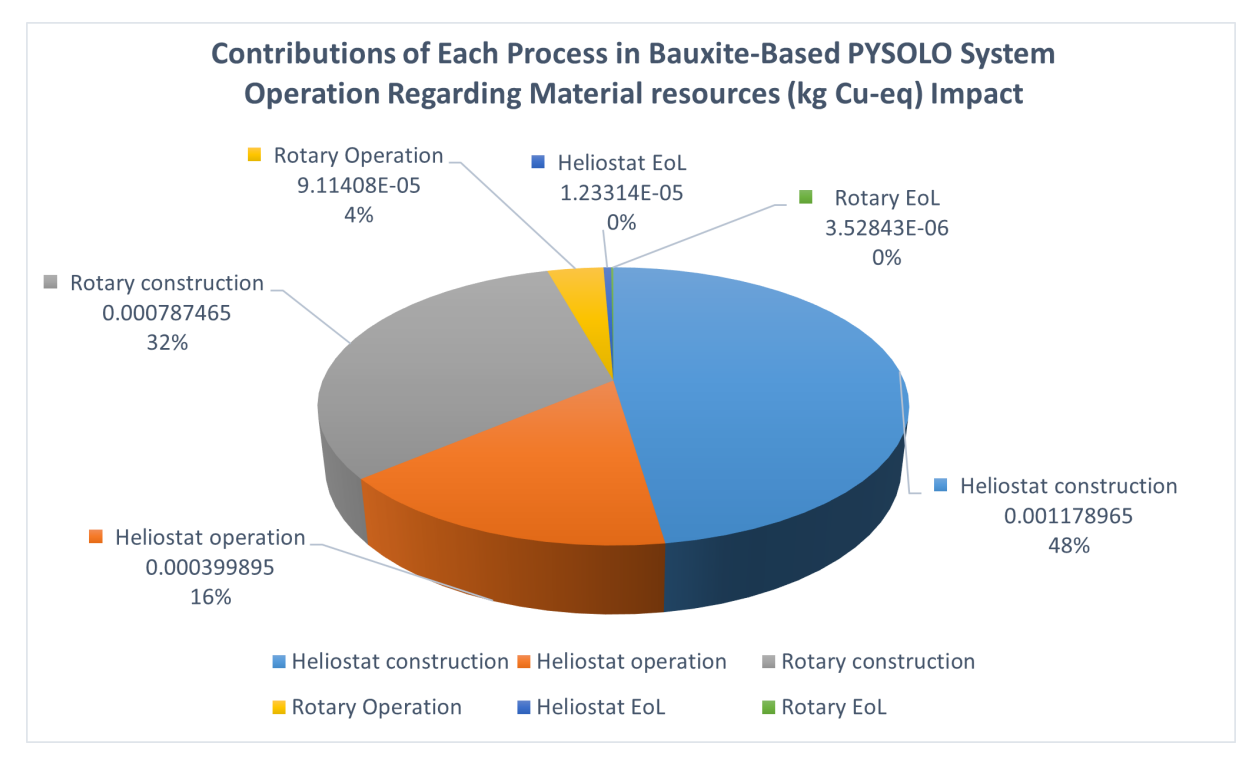


Figure 5.4: Contribution of Each Process to Material Resources in the Bauxite-Based System Operation.

5.2.2 Contribution Analysis of the Whole System with Sand as the Particle

When sand is used as the particulate material, the overall pattern of contributions from different subsystems remains similar to the bauxite case, but with some slight shifts worth noting. The largest share of environmental impact still originates from heliostat construction, which accounts for approximately 57% of climate change, 77% of human toxicity, and 62% of land use. This confirms that building the heliostat structures remains the most resource- and energy-intensive stage of the system.

A notable difference in the sand scenario is the land use footprint, which, although still relatively small in absolute terms, is slightly higher compared to the bauxite case. This indicates that even materials often considered low-impact, such as sand, can exert measurable environmental pressure when used in large volumes.

The second most significant stage is heliostat operation, contributing around 25% to climate change impacts, 11% to human toxicity, and 25% to land use. These results reflect the ongoing energy demand associated with system operation, which accumulates over time. Rotary construction also plays a non-negligible role, contributing about 12% to climate change, 12% to human toxicity, and 9% to land use. In contrast, the operation of the rotary subsystem itself has only a minimal impact, remaining well below 1% across all categories.

Finally, the end-of-life phases contribute only marginally. Heliostat end-of-life accounts for roughly 4% of climate change and 3% of land use, with its contribution to human toxicity being negligible. Rotary end-of-life contributes even less, with impacts staying consistently under 1% across all categories.

To visually illustrate these findings, three pie charts were prepared for climate change, human toxicity, and land use. These visualizations demonstrate that, although using sand does not drastically alter the overall contribution structure compared to bauxite, its impact is most evident in land use. This suggests that strategies aimed at reducing environmental impacts should continue to prioritize heliostat construction. However, it is also important to recognize that even "low-impact" materials like sand can generate measurable pressures, particularly regarding land occupation(Figures 5.5, 5.6, 5.7.

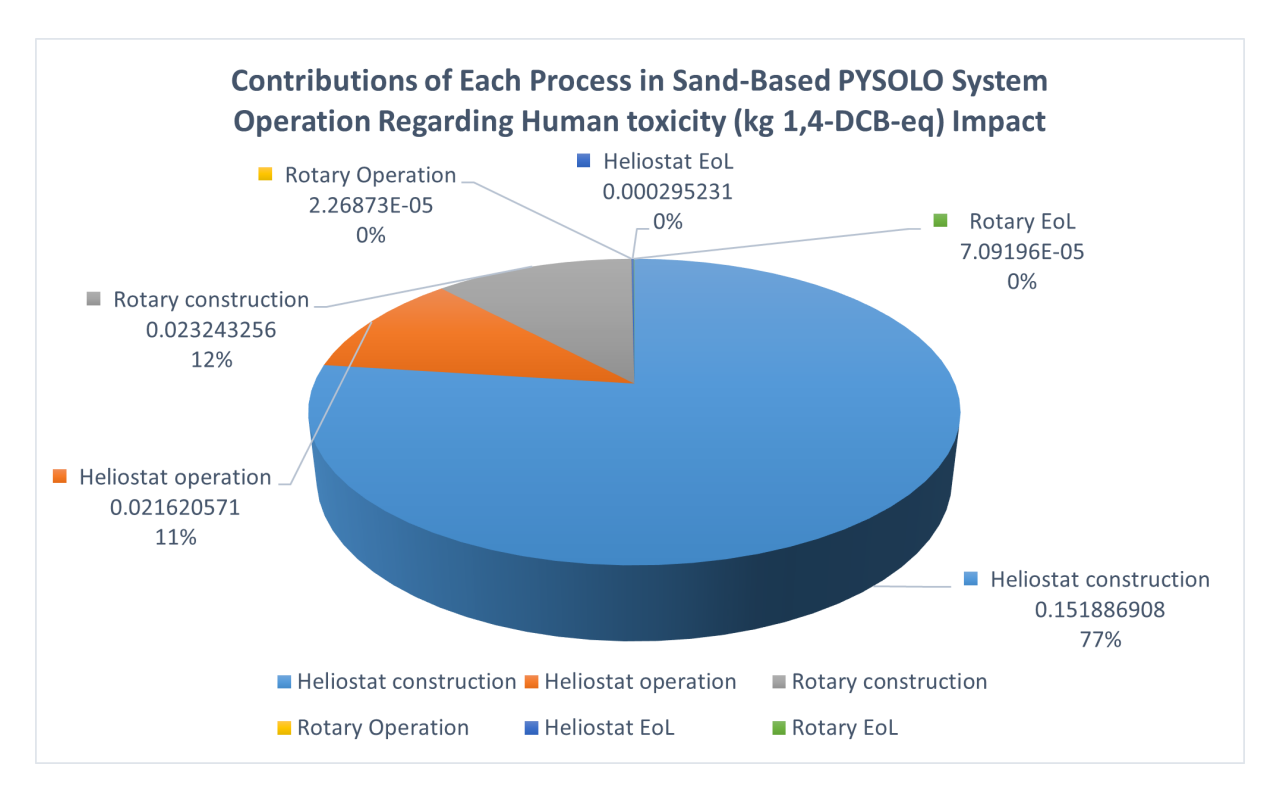


Figure 5.5: Contribution of Each Process to Human Toxicity in the Sand-Based System Operation.

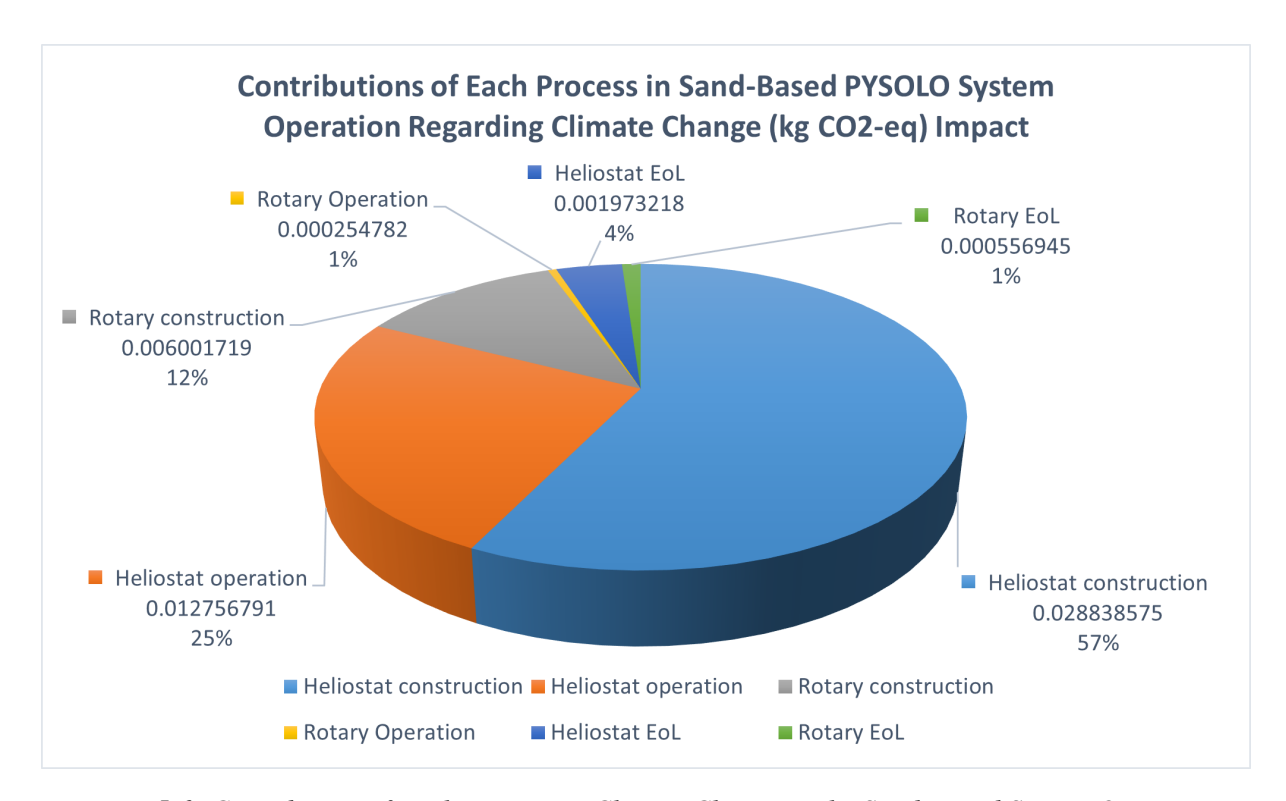


Figure 5.6: Contribution of Each Process to Climate Change in the Sand-Based System Operation.

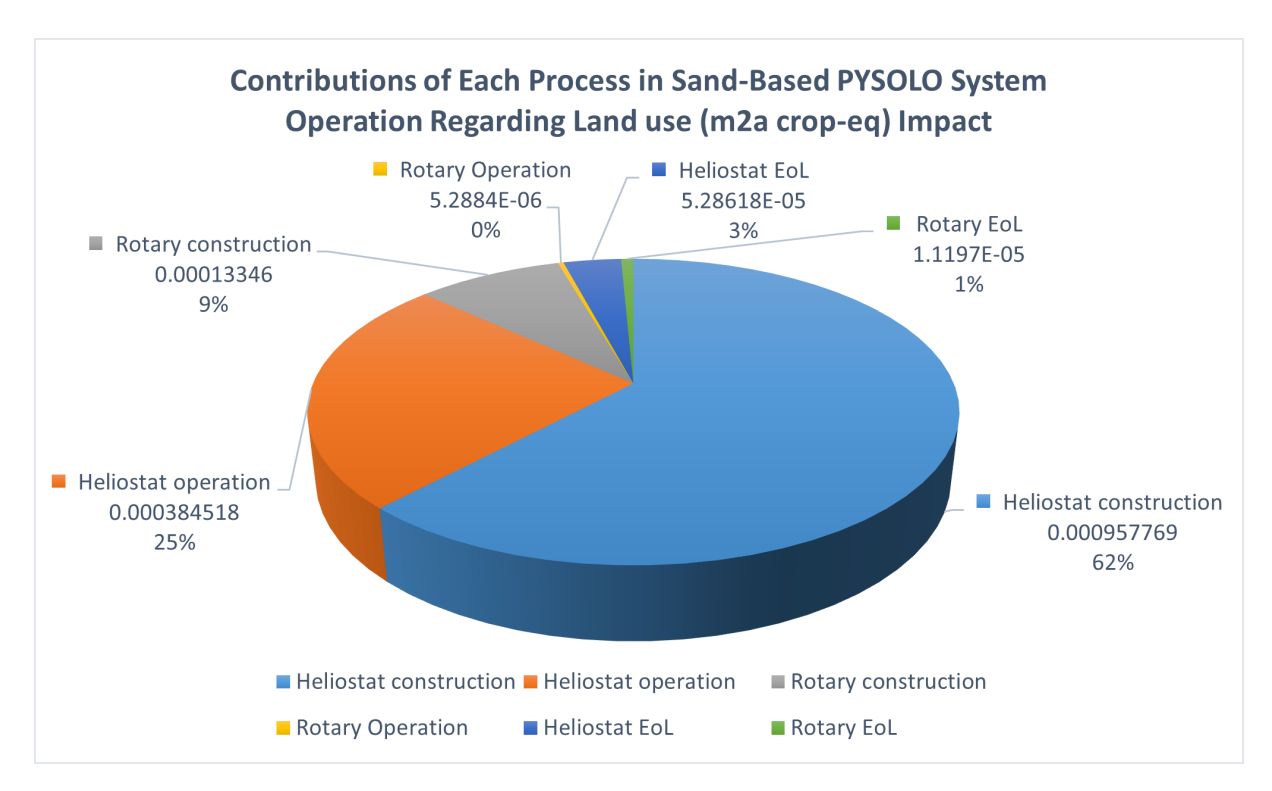


Figure 5.7: Contribution of Each Process to Land use in the Sand-Based System Operation.

5.2.3 Contribution Analysis of the Whole System with Olivine as the Particle

When olivine is considered as the particulate material, the contribution analysis again reveals a very similar distribution of environmental burdens to those observed in the bauxite and sand scenarios. The construction of the heliostat dominates the results, contributing approximately 57% of the total climate change impact and up to 77% of the human toxicity impact. This confirms the consistent finding across all three particulate types: the heliostat construction stage is the most critical subsystem driving overall environmental performance.

The operation of the heliostat follows, accounting for around 25% of climate change impacts and 11% of human toxicity. Rotary construction also emerges as a notable contributor, adding about 12% to both categories, indicating that although smaller in scale than the heliostat, the rotary system still carries a measurable footprint. In contrast, the direct operation of the rotary system contributes negligibly, with values below 1% for climate change and essentially zero for human toxicity.

End-of-life phases for both heliostat and rotary subsystems again play only a minor role, with heliostat end-of-life accounting for approximately 4% of climate change impacts and near-zero in human toxicity, while rotary end-of-life contributes roughly 1% to climate change and remains negligible otherwise.

To illustrate these findings, two pie charts were generated for the climate change and human toxicity categories. They confirm that the heliostat construction phase overwhelmingly dominates both categories, with other subsystems playing comparatively smaller roles(see Figures 5.8, 5.9). Overall, the olivine scenario reinforces the broader conclusion that the choice of particulate material has little effect on the proportional contribution of subsystems. Instead, efforts to improve the sustainability of the system should remain focused on reducing the material and energy demands of heliostat construction, as this stage consistently shapes the environmental performance across all impact categories.

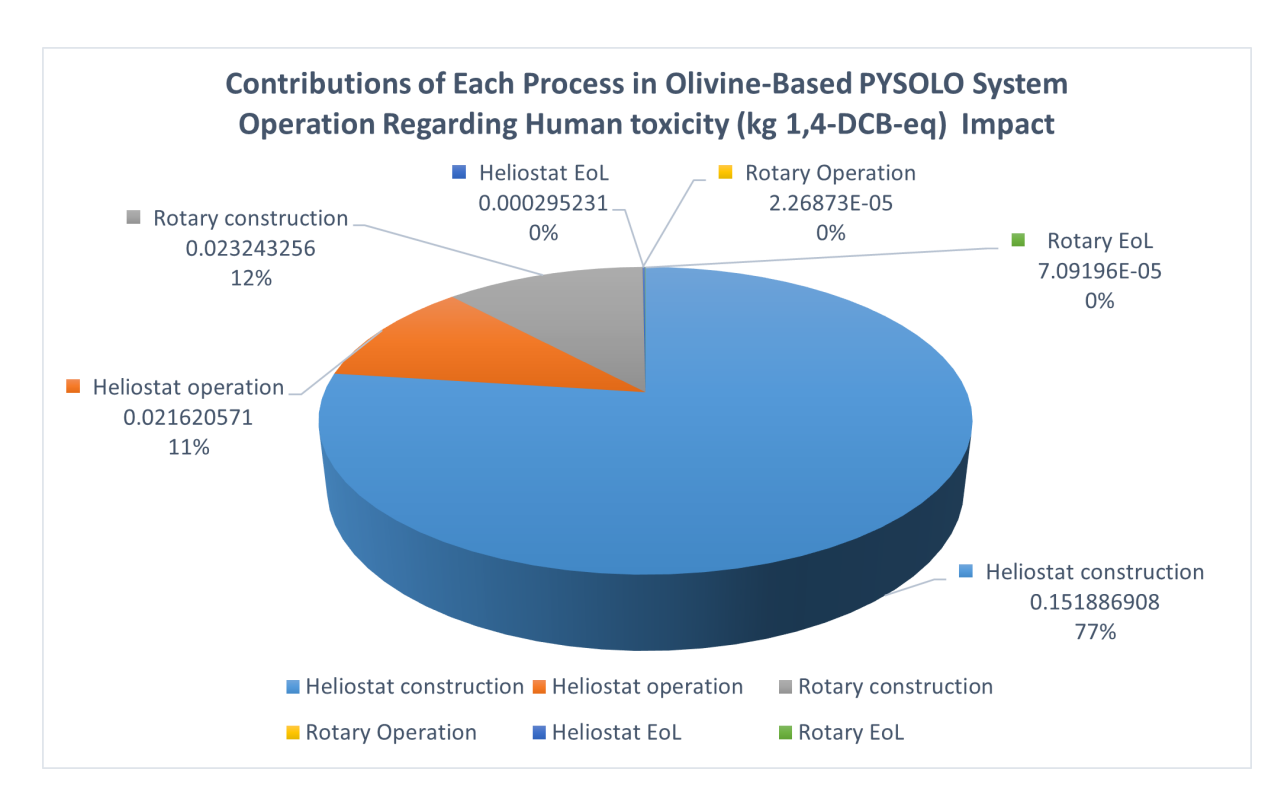


Figure 5.8: Contribution of Each Process to Human Toxicity in the Olivine-Based System Operation.

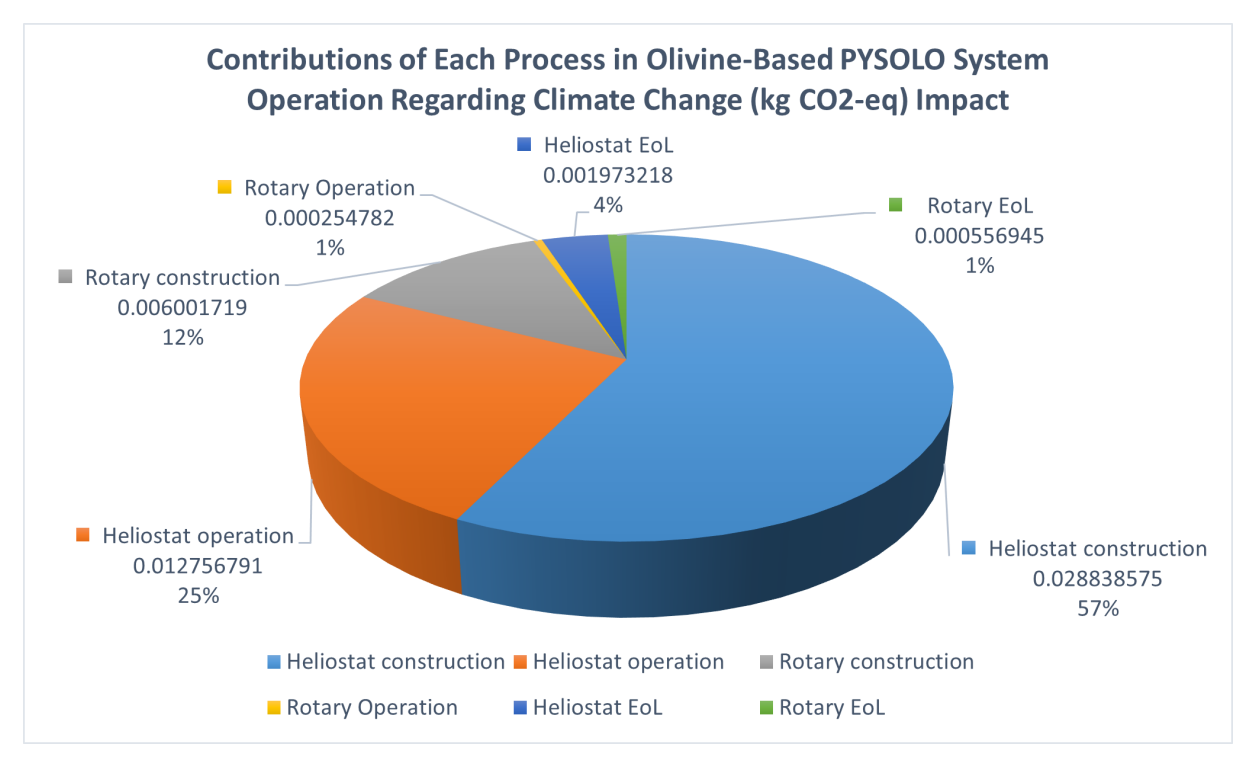


Figure 5.9: Contribution of Each Process to Climate Change in the Olivine-Based System Operation.

5.3 Process and Flow Contribution Analysis in the Entire System

Climate Change (kg CO₂-eq)

In the climate change category, the normalized total impact contributions were examined for the three modeled scenarios: Whole system with Bauxite, Whole system with Sand, and Whole system with Olivine. The analysis focused on the eleven most influential processes, selected because they account for the majority of greenhouse gas (GHG) emissions across the product system and were used to construct the diagram showin in Figure 5.10. It is important to note that other flows were also included in the inventory, but their individual contributions were relatively low and did not substantially affect the overall profile.

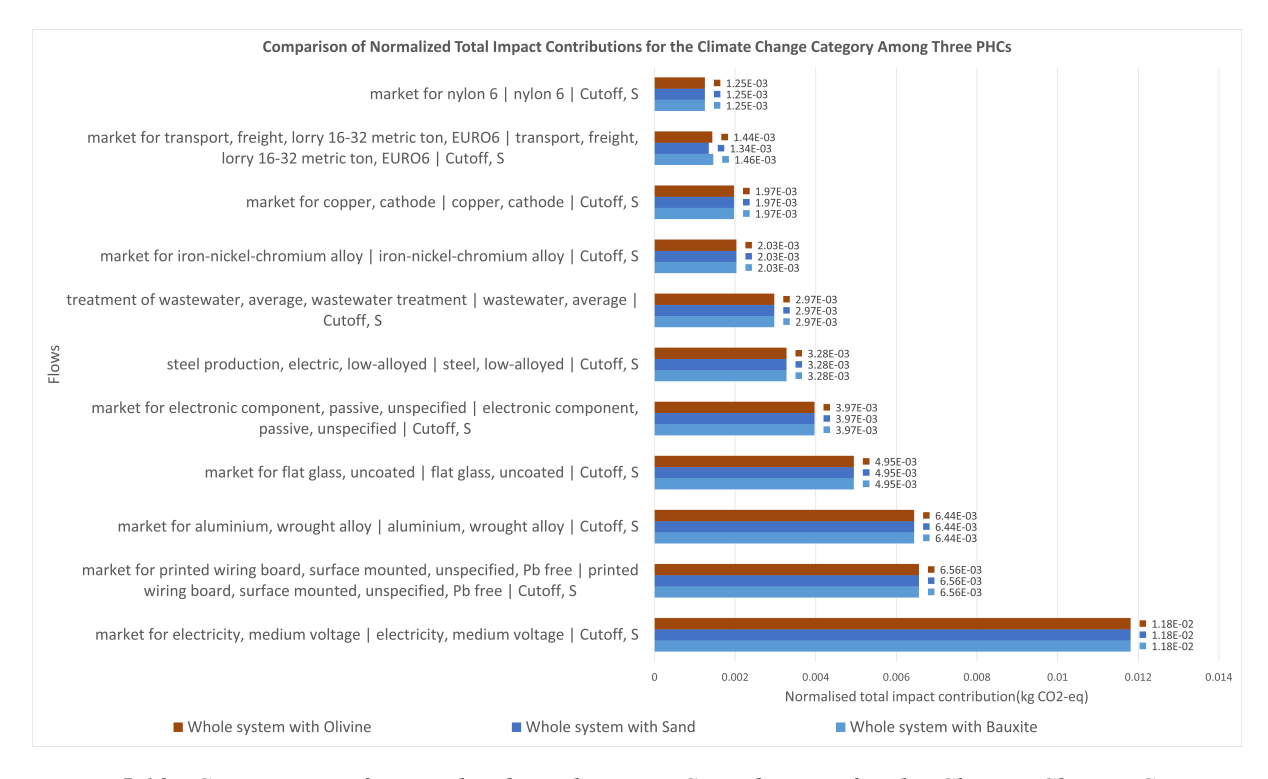


Figure 5.10: Comparison of Normalized Total Impact Contributions for the Climate Change Category Among Three PHCs.

Across all three scenarios, a clear and consistent pattern emerges. The market for electricity, medium voltage represents the single most dominant contributor, with a normalized impact of approximately 0.0118 in each case. This underscores the significance of electricity consumption as a driver of climate-related impacts, highlighting its overarching influence regardless of the particle type considered. Following electricity, the market for printed wiring boards (surface-mounted, Pb-free, unspecified) consistently appears as the second most impactful process, while aluminium (wrought alloy) and flat glass (uncoated) also demonstrate high levels of contribution. Collectively, these processes represent core material- and energy-intensive stages of the system, reflecting the environmental burden associated with electronics and structural materials.

Processes such as the market for passive electronic components, steel production (low-alloyed,

electric), and the treatment of wastewater (average) emerge as intermediate contributors. Although their normalized values are smaller than those of the top four contributors, their consistent presence across all scenarios indicates their role as secondary hotspots. Metals such as copper cathodes and iron-nickel-chromium alloys contribute at lower levels but remain relevant to the total system burden. At the bottom end of the top eleven, the market for transport (freight, lorry 16–32 metric ton, EURO6) and nylon 6 or concrete (30 MPa) make relatively small contributions.

When comparing across particle scenarios, the overall magnitude of normalized contributions is nearly identical. The normalized values for electricity supply in each system are very close (0.011809396 for Bauxite, 0.011809707 for Sand, and 0.011809084 for Olivine), showing that the choice of particle has negligible influence on the climate change profile. The variation is most noticeable in the lower-ranked contributors: while the Bauxite scenario includes nylon 6 within the top eleven, both the Sand and Olivine scenarios instead feature concrete (30 MPa). Additionally, the contribution of transport (freight, lorry, EURO6) is slightly lower in the Sand system, which can be attributed to the shorter distance between the supplier and the site, thereby reducing transport-related emissions.

From an interpretive perspective, the findings demonstrate that the main environmental hotspots are not directly linked to the particle substitution itself, but rather to system-level processes such as electricity consumption, material production, and electronics manufacturing. This has important implications: first, it indicates that decarbonization of the electricity grid would offer the most significant potential to reduce climate change impacts across all systems. Second, the prominence of printed wiring boards, aluminium, and flat glass suggests that material efficiency, recycling, and substitution strategies are critical levers for impact reduction. Finally, transport-related emissions, while comparatively small, reveal how supply chain logistics (e.g., shorter transport distances as in the Sand system) can still contribute to incremental reductions in climate change impacts.

In summary, the comparative analysis shows that the substitution of bauxite, sand, or olivine particles does not significantly alter the relative distribution of impacts in the climate change category. Instead, the results highlight the dominance of electricity and material-intensive processes as key drivers, while also pointing to the role of supply chain optimization (shorter transport distances) as a potential secondary lever for reducing emissions.

Energy resources: non-renewable, fossil (kg oil-eq)

The category of non-renewable fossil energy resources reflects the cumulative consumption of oil-equivalents across the product systems. Figure 5.11 presents the results for the three scenarios—*Whole system with Bauxite*, *Whole system with Sand*, and *Whole system with Olivine*—highlighting the twelve processes with the largest contributions.

The results show a clear dominance of electricity supply, with the process *market for electricity, medium voltage* (Germany) contributing approximately 0.00298 kg oil-eq in all scenarios. This makes electricity the single most significant driver of fossil energy use. This finding aligns with the well-documented dependence of electricity generation in Europe on fossil-based energy carriers, particularly natural gas and coal, despite ongoing increases in renewable energy integration.

The second-largest contribution stems from *printed wiring boards*, *surface mounted*, *Pb-free* (0.00162 kg oil-eq), followed by aluminium (wrought alloy, 0.00135 kg oil-eq), flat glass (0.00115 kg oil-eq), and passive electronic components (0.00105 kg oil-eq). Collectively, these processes underline the energy intensity of electronic and alloy material production, which remains strongly linked to fossil energy due to their electricity- and heat-intensive nature. Additional but smaller contributions arise from steel production (low-alloyed, 0.00066 kg oil-eq), wastewater treatment (0.00055 kg oil-eq), *iron-nickel-chromium* alloy (0.00053 kg oil-eq), and copper cathode (0.00050 kg oil-eq). In the lower range, freight transport with EURO6 lorries, nylon 6 production, and concrete (30 MPa) contribute between 0.00018 and 0.00046 kg oil-eq, indicating the broad but relatively modest fossil energy dependence of supporting supply-chain activities.

When comparing the three scenarios, the profiles are nearly indistinguishable, with only marginal variations in the contribution from freight transport. Specifically, the Bauxite system registers 0.00046 kg oil-eq, the Sand system 0.00042 kg oil-eq, and the Olivine system 0.00045 kg oil-eq. These small deviations are linked to logistical differences in particle sourcing and delivery, with Sand showing the lowest transport contribution due to the shorter distance between local supply points and the site. All other major contributors remain constant across scenarios, indicating that the choice of particle (bauxite, sand, or olivine) exerts negligible influence on fossil energy demand.

From an interpretive perspective, the analysis highlights two main conclusions. First, the electricity system is the dominant hotspot in fossil energy consumption, vastly outweighing contributions from other processes. This suggests that transitioning electricity generation toward renewable sources is the most effective lever for reducing fossil energy demand in the studied systems. Second, material production (aluminium, electronics, glass, and steel) constitutes a cluster of secondary but still significant hotspots, reflecting the persistent fossil dependency of energy-intensive industries.

Overall, the fossil energy demand of the studied systems is largely determined by electricity generation and industrial materials production, with transport and concrete playing minor roles. Importantly, the substitution between bauxite, sand, and olivine has minimal effect on this impact category, reinforcing that system-level reductions in fossil energy use must primarily target energy supply decarbonization and efficiency improvements within materials industries, rather than the choice of particle inputs.

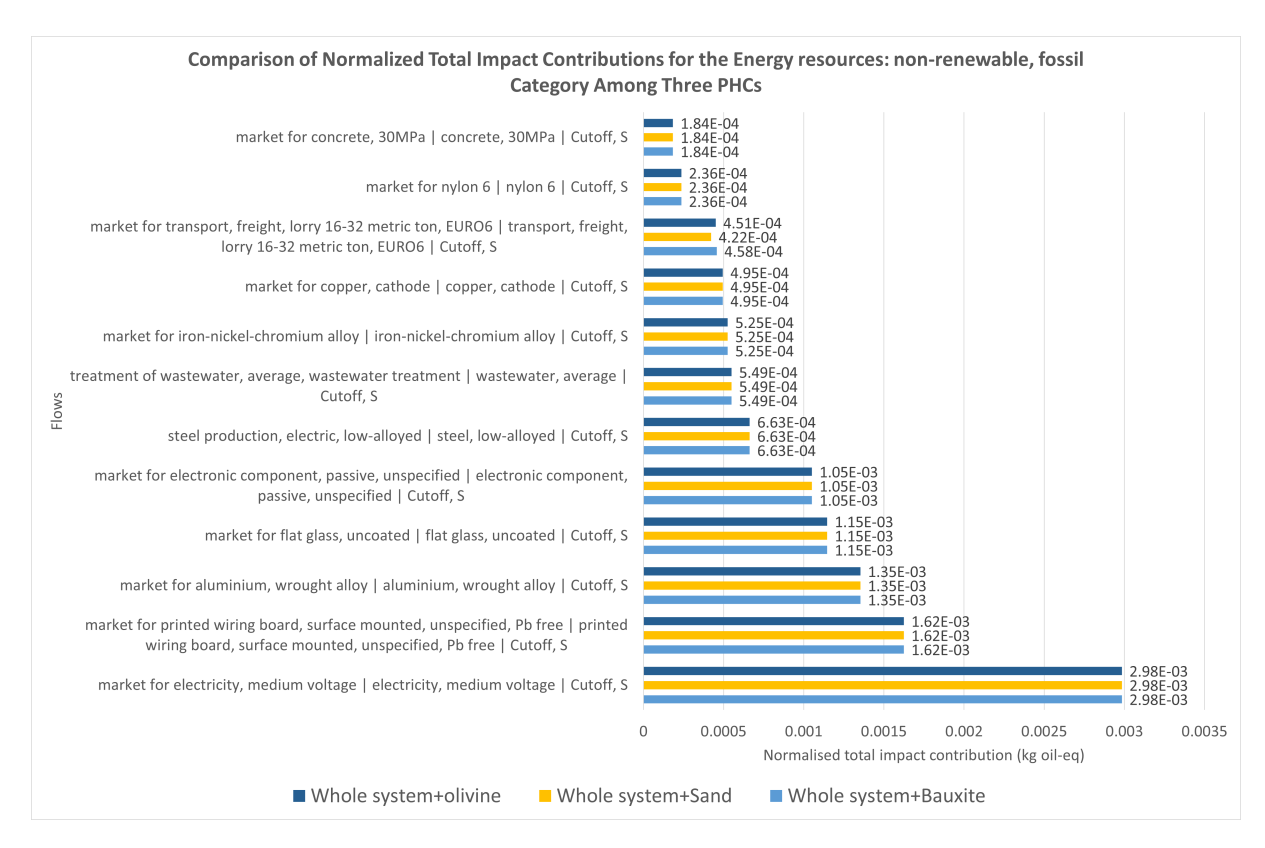


Figure 5.11: Comparison of Normalized Total Impact Contributions for the Energy resources: non-renewable, fossil Category Among Three PHCs.

Material resources (kg Cu-eq)

The assessment of material resource depletion, measured in kilograms of copper equivalents (kg Cu-eq), provides insights into the extent to which the studied systems rely on scarce raw materials. Figure 5.12 illustrates the relative contribution of each process under the three mineral input scenarios: Whole system + Bauxite, Whole system + Sand, and Whole system + Olivine. Across all three systems, the dominant contributions arise from metal production and electronics-related processes. The most significant hotspots include copper cathode production (5.02 × 10^{-4} kg Cu-eq), iron-nickel-chromium alloy production (4.57 × 10^{-4} kg Cu-eq), and passive electronic components (3.73 × 10^{-4} kg Cu-eq). Collectively, these account for the majority of the material resource impact, reflecting the high criticality of copper, nickel, and specialty alloys in modern manufacturing.

Additional important contributors are printed wiring boards, Pb-free $(2.74 \times 10^{-4} \text{ kg Cu-eq})$, and refractory materials $(2.18 \times 10^{-4} \text{ kg Cu-eq})$. Bulk construction and structural materials such as low-alloyed steel $(1.81 \times 10^{-4} \text{ kg Cu-eq})$ and aluminium wrought alloys $(1.04 \times 10^{-4} \text{ kg Cu-eq})$ also play notable roles. Meanwhile, electricity generation, chromium steel (18/8, hot rolled), wastewater treatment, and flat glass production contribute at intermediate levels $(6 \times 10^{-5} \text{ to } 3 \times 10^{-5} \text{ kg Cu-eq})$.

The inclusion of mineral feedstock differentiates the three scenarios. In the Bauxite scenario, a direct contribution from bauxite market inputs is observed (8.8×10^{-5} kg Cu-eq), representing a non-negligible fraction of the total material resource burden. This additional load reflects the relatively high depletion potential of bauxite mining due to its link with aluminium produc-

tion. In contrast, in both the Sand and Olivine scenarios, this contribution is effectively zero, indicating that the extraction of these mineral inputs is not associated with substantial copper-equivalent burdens in the inventory model.

Apart from this distinction, the overall impact profiles are nearly identical across scenarios, as the hotspots remain linked to copper, alloys, and electronic components. Minor deviations are visible in background processes such as flat glass and transport (EURO6 freight lorry), where values shift slightly depending on the mineral scenario, but these remain at the lower order of magnitude and do not significantly affect the overall interpretation.

From an interpretive perspective, two main findings emerge. First, the dominance of copper cathode and nickel-chromium alloys underscores the systemic dependency on critical raw materials. This aligns with broader trends in resource criticality, where copper and nickel are highlighted as strategic due to their demand in electronics, renewable energy, and infrastructure applications. Second, the choice of mineral feedstock only significantly affects the result in the case of bauxite, where a measurable additional burden appears. Conversely, sand and olivine exert negligible influence on material resource depletion.

To sum up, material resource depletion is overwhelmingly driven by metal extraction and electronics manufacturing, while the selection of sand or olivine as aggregate alternatives has no meaningful effect. Only bauxite introduces an additional burden, linked to its critical role in the aluminium supply chain. Therefore, mitigation strategies should focus on metal recycling, alloy substitution, and circular economy approaches in electronics, rather than on aggregate replacement.

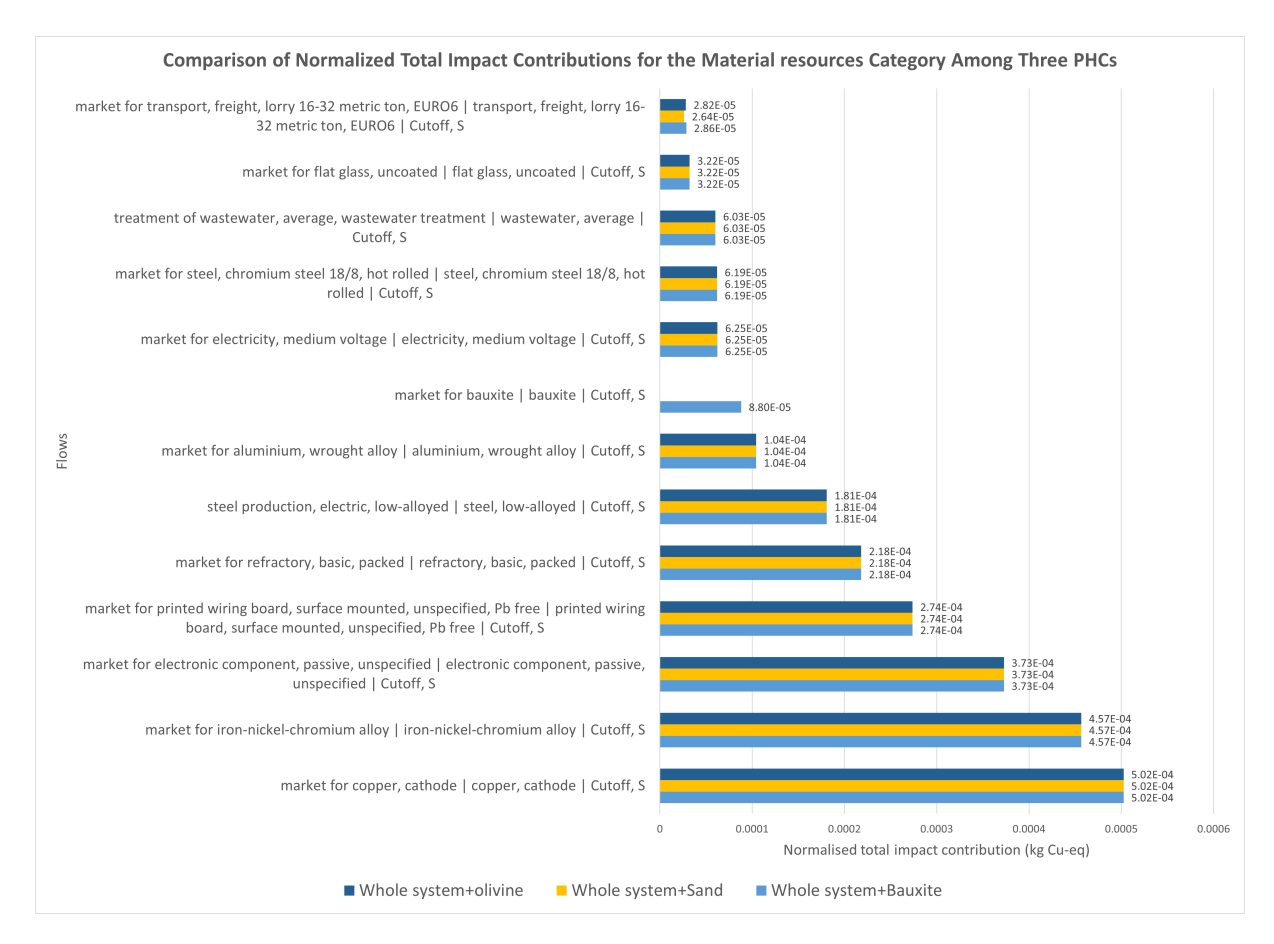


Figure 5.12: Comparison of Normalized Total Impact Contributions for the Material resources Category Among Three PHCs.

Land use (m²a crop-eq)

The land use assessment, expressed in square meters per annum of crop-equivalent (m²a crop-eq), highlights the extent to which the studied systems depend on land occupation for biomass provision and agricultural equivalence. Figure 5.13 presents the comparative results for the three mineral input scenarios: Whole system with Bauxite, Whole system with Sand, and Whole system with Olivine.

Across all scenarios, the most significant contributors are associated with copper production, electricity supply, and electronic components. Copper cathode production emerges as the dominant hotspot with a contribution of 3.16×10^{-4} m²a crop-eq, followed by electricity, medium voltage (DE mix) $(2.51\times10^{-4}$ m²a crop-eq), and passive electronic components $(2.11\times10^{-4}$ m²a crop-eq). Additionally, printed wiring boards (Pb-free) $(2.10\times10^{-4}$ m²a crop-eq) and flat glass production $(9.88\times10^{-5}$ m²a crop-eq) also represent notable contributors. Structural materials such as low-alloyed steel $(9.26\times10^{-5}$ m²a crop-eq) and aluminium wrought alloys $(7.17\times10^{-5}$ m²a crop-eq) provide secondary but non-negligible impacts.

Lower-order contributions are observed for wastewater treatment $(8.33 \times 10^{-5} \text{ m}^2\text{a} \text{ crop-eq})$ and waste mixed aggregates from demolition, which exhibit very small values across all scenarios $(10^{-8} \text{ to } 10^{-7} \text{ m}^2\text{a} \text{ crop-eq})$. Although marginal in absolute terms, these processes are relevant as indicators of waste handling within the system boundary.

The differences between the three mineral input scenarios stem from the treatment of bauxite, silica sand, and olivine. In the *Bauxite* scenario, an additional land occupation of 4.75×10^{-7} m²a crop-eq is recorded, reflecting land use associated with bauxite mining. In the *Sand* scenario, this contribution is slightly higher at 2.05×10^{-6} m²a crop-eq, indicating that although sand extraction is perceived as low-impact, it carries a measurable land occupation footprint. Conversely, in the *Olivine* scenario, no land use burden is allocated to mineral extraction, and the only additional effect is the negligible contribution of waste mixed aggregates $(1.47 \times 10^{-8} \text{ m}^2\text{ a crop-eq})$.

Overall, the land use profile remains largely invariant across the three scenarios, with dominant hotspots consistently linked to copper production, electricity, and electronics manufacturing. The introduction of bauxite or sand marginally increases land use burdens by approximately 0.1–0.6% relative to total results, whereas olivine substitution exerts virtually no additional effect.

From a systems perspective, these results suggest that land occupation impacts in this study are primarily driven by energy and metals supply chains rather than the choice of mineral input for aggregate substitution. Therefore, strategies aimed at reducing land use burdens should focus on improving copper supply, increasing renewable electricity integration, and adopting circular approaches for electronics, rather than on aggregate material substitution.

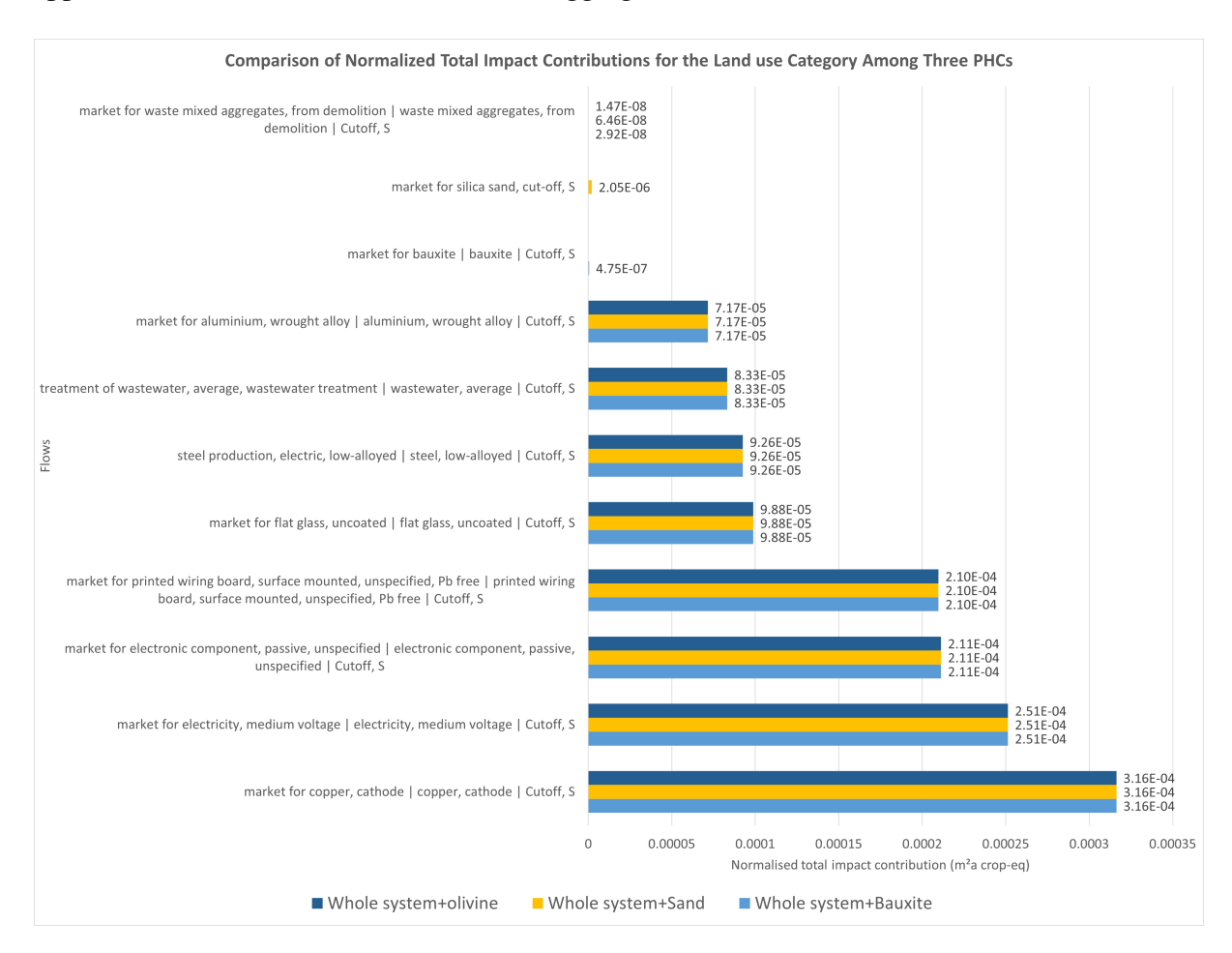


Figure 5.13: Comparison of Normalized Total Impact Contributions for the Land use Category Among Three PHCs.

Water use (m³)

The water use assessment, expressed in cubic meters, evaluates the total freshwater consumption associated with the production and life cycle of the studied systems, including both direct and upstream processes. Figure 5.14 presents the comparative results for the three scenarios: Whole system with Bauxite, Whole system with Sand, and Whole system with Olivine.

Across all scenarios, the largest contributions to water use originate from the production of iron-nickel-chromium alloy $(1.37 \times 10^{-4} \text{ m}^3)$ and electricity supply (DE mix) $(5.54 \times 10^{-5} \text{ m}^3)$. These findings underscore that metal extraction and energy generation remain the primary drivers of freshwater consumption within the system. Secondary contributors include printed wiring boards (Pb-free) $(4.76 \times 10^{-5} \text{ m}^3)$, low-alloyed steel production $(3.75 \times 10^{-5} \text{ m}^3)$, and copper cathode production $(3.71 \times 10^{-5} \text{ m}^3)$.

Other components, such as aluminium wrought alloys, wastewater treatment, and passive electronic components, contribute moderately to the overall water footprint, ranging from 2.98×10^{-5} m³ to 2.45×10^{-5} m³. Minor contributions are associated with nylon 6, steel 18/8, concrete, glass wool mat, and transport, with values in the order of 10^{-6} to 10^{-9} m³. The inclusion of bauxite extraction in the *Bauxite* scenario adds only a negligible contribution $(1.60 \times 10^{-9} \text{ m}^3)$, reflecting the relatively minor water demand linked to bauxite mining within the system boundary.

When comparing the three mineral scenarios, the water use profiles are notably consistent, with only slight variations introduced by the specific mineral added. For example, in the *Sand* scenario, water use from bauxite is absent, and a very small contribution arises from sand supply chain $(3.54 \times 10^{-9} \text{ m}^3)$. Similarly, in the *Olivine* scenario, minimal contributions from mineral-specific flows $(8.08 \times 10^{-10} \text{ m}^3)$ indicate that olivine extraction is effectively water-neutral in this context

Overall, the dominant factors influencing water use across all systems are metal production and electricity supply. The choice of mineral additive—bauxite, sand, or olivine—has a negligible impact on total freshwater consumption. These results suggest that mitigation strategies should primarily target reducing water intensity in metal processing and electricity generation rather than altering mineral input choices.

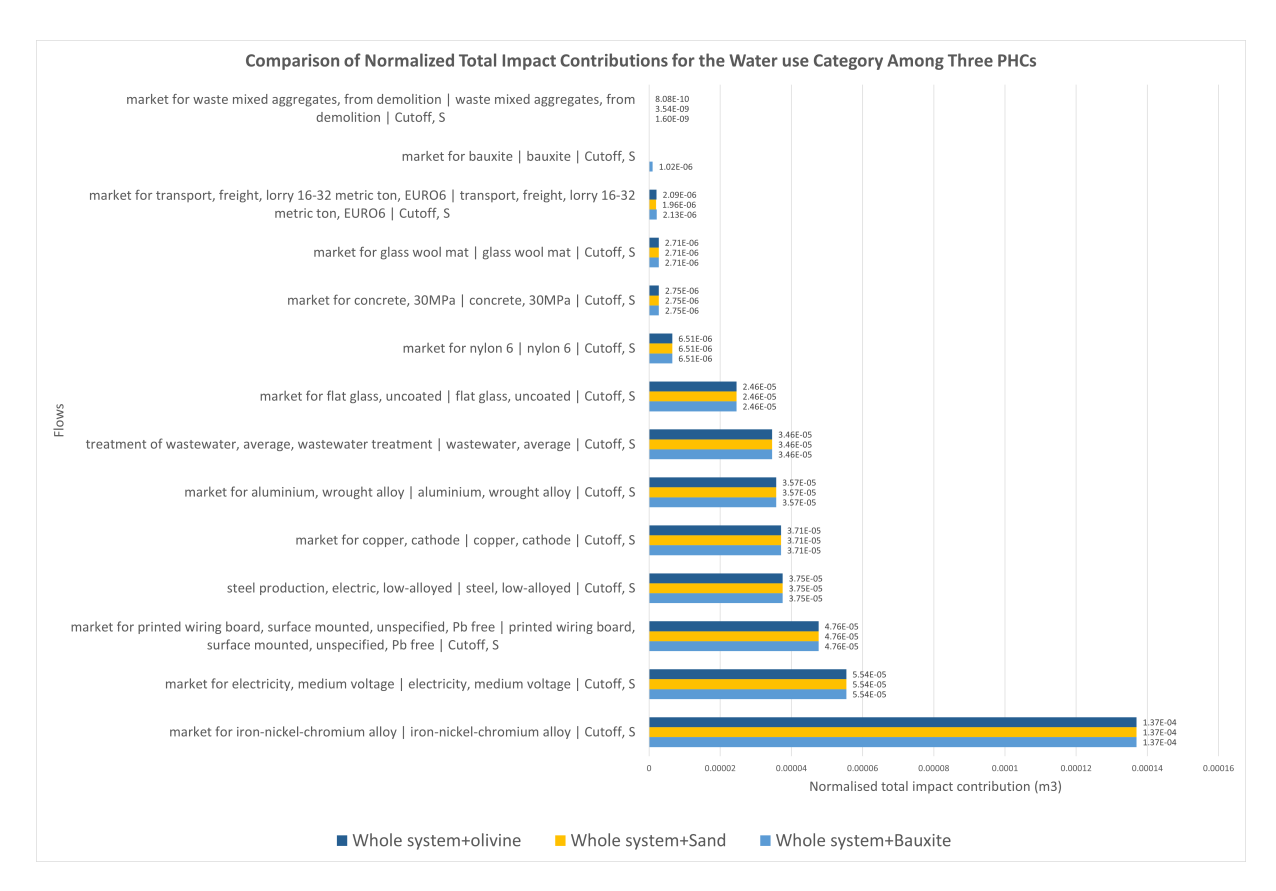


Figure 5.14: Comparison of Normalized Total Impact Contributions for the Water use Category Among Three PHCs.

Human toxicity (kg 1,4-DCB-eq)

In the human toxicity category, the normalized total impact contributions were examined for the three scenarios: Whole system with Bauxite, Whole system with Sand, and Whole system with Olivine. The analysis considered the eleven processes with the highest contributions, which together account for the majority of toxicological impacts across the system. The results are presented in Figure 5.15.

Across all scenarios, the results are dominated by a single process: *steel production, electric, low-alloyed* (Europe without Switzerland and Austria), with a normalized contribution of 0.1745. This value is markedly higher than that of all other processes, making steel production the clear hotspot for human toxicity. This strong influence reflects the intensive resource extraction, metallurgical processing, and associated emissions of heavy metals and other toxic substances that occur during steelmaking.

Following steel production, the next most important contributors—though at much smaller magnitudes—are the market for iron-nickel-chromium alloys (0.00425), aluminium production (wrought alloy, 0.00413), passive electronic components (0.00355), and steel chromium 18/8 hot rolled (0.00346). Together, these processes highlight the central role of metal extraction and processing in shaping the toxicity profile. The copper cathode market (0.00265) also contributes noticeably, further reinforcing the influence of base and alloy metals.

Other contributors include electricity supply (medium voltage, 0.00159), printed wiring boards (0.00104), wastewater treatment (0.00082), flat glass production (0.00038), and freight trans-

port (lorry, 16–32 metric tons, EURO6), which appears as the lowest-ranking process within the top eleven. Although these contributions are relatively minor compared to steelmaking, they demonstrate that the toxicity burden is spread across a wide range of supply-chain activities, from energy provision to infrastructure materials.

When comparing across the three particle scenarios, the overall profile remains nearly identical. The normalized contributions for the dominant steel production process are exactly the same across Bauxite, Sand, and Olivine systems, while values for the other processes vary only in the third or fourth decimal place. This indicates that the choice of particle (bauxite, sand, or olivine) has no meaningful effect on the human toxicity results. Instead, the toxicological profile is determined almost entirely by upstream material- and metal-intensive processes that are common to all systems.

From an interpretive perspective, the findings clearly demonstrate that human toxicity impacts are driven overwhelmingly by the steel sector, with additional but smaller contributions from alloy, aluminium, and copper production. This outcome suggests that effective strategies to reduce toxicity impacts should focus on:

- Decarbonizing and detoxifying metallurgical processes, through improved emission control technologies in steelmaking and alloy production.
- Enhancing material circularity, particularly by increasing the use of recycled metals, which would reduce the toxic emissions associated with primary extraction and refining.
- Optimizing supply chains and product design, to minimize the need for high-toxicity materials without compromising product functionality.

In summary, the human toxicity results indicate that while particle substitution (bauxite, sand, or olivine) does not materially change the impact distribution, metallurgical processes—especially steel production—are the primary drivers of toxicological burdens. As such, system-level improvements in the sourcing and processing of metals offer far greater potential for reducing human toxicity than the selection of alternative particles.

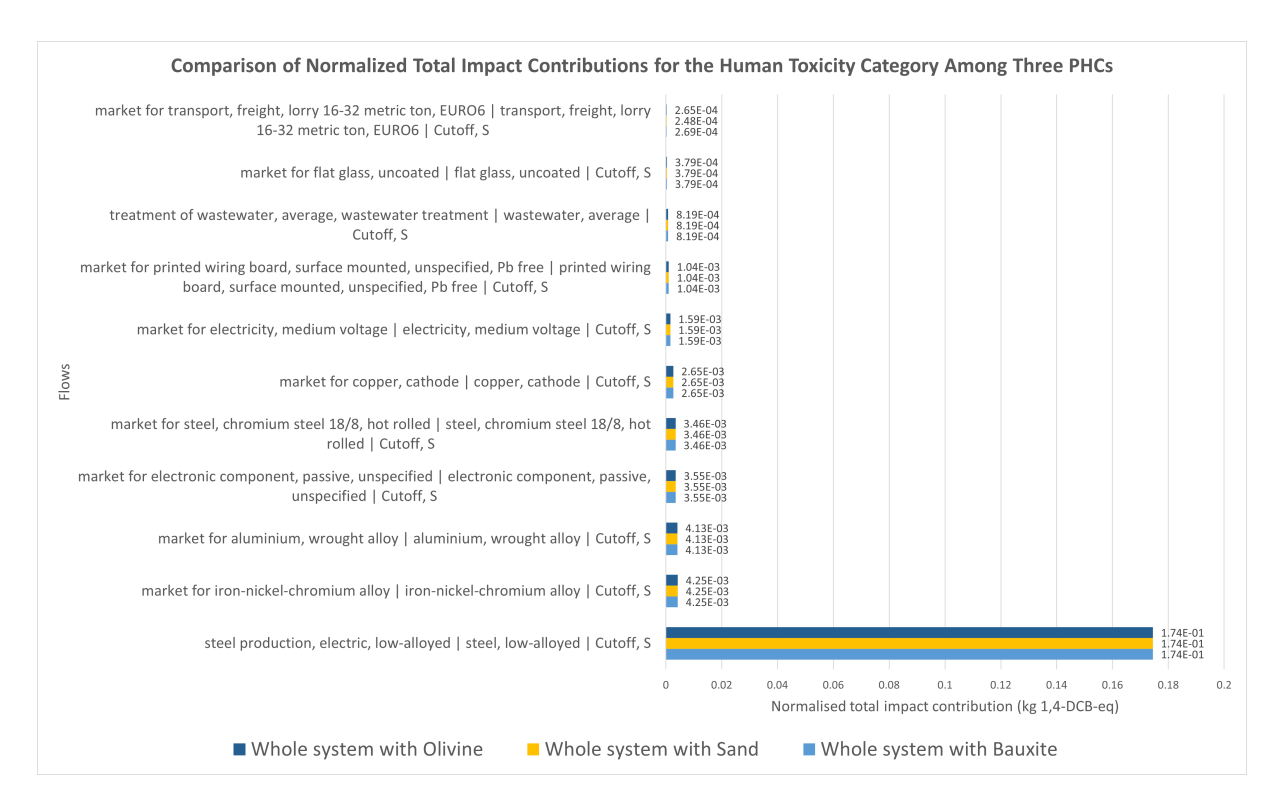


Figure 5.15: Comparison of Normalized Total Impact Contributions for the Human Toxicity Category Among Three PHCs.

5.4 Hotspot Analysis with Sankey Diagrams

To gain a deeper understanding of the processes driving environmental impacts, Sankey diagrams were developed for both the Human Toxicity and Climate Change categories across the three PHC scenarios. These diagrams provide a visual breakdown of burdens across life cycle stages, where the thickness of each flow corresponds to the relative contribution of a process or material. It is important to note that the amounts shown in the diagrams represent pre-normalization values. The raw LCIA results were initially calculated for the entire system lifetime, corresponding to the delivery of 98,550 kWh of useful thermal energy. Since the functional unit of this study is defined as 1 kWh of useful heat delivered to the kiln bed, the total impacts were normalized by dividing these values by 98,550. By doing so, the Sankey diagrams complement the quantitative tables presented earlier by illustrating how impacts accumulate throughout the supply chains and infrastructure, rather than arising directly from kiln operation.

5.4.1 Bauxite

I. Bauxite: Human Toxicity Hotspot Analysis with Sankey Diagram

As shown in Figure 5.16,the life cycle assessment of the Bauxite-PHC system reveals that human toxicity emissions are heavily concentrated in upstream processes, with total impacts reaching 1.943×10^4 kg 1,4-DCB-eq. This figure represents the full burden of the system, and the analysis makes clear that heliostat operation is the dominant contributor. With 1.710×10^4 kg 1,4-DCB-eq (around 88% of the total), the heliostat subsystem reflects the intensive mate-

rial and energy demands associated with commissioning, installation, and operational support. Closely linked to this is steel production—particularly low-alloy electric steel—which contributes a nearly equivalent burden of 1.719×10^4 kg 1,4-DCB-eq (approximately 88.5%). The overlap between these two hotspots highlights how deeply the heliostat system is tied to steel inputs.

Breaking the heliostat subsystem down further, the greatest shares of toxicity are tied to the early lifecycle stages. Commissioning, transportation, installation, and frame assembly each register around 1.497×10^4 kg (approximately 77%), showing how resource-intensive the deployment phase is. Substantial, though comparatively smaller, burdens arise from foundation and support structures (7.065×10^3 kg, approximately 36.4%), mirror module fabrication (4.062×10^3 kg, approximately 20.9%), and the drive and control systems (3.352×10^3 kg, approximately 17.3%). These figures emphasize that toxicity impacts are not just embedded in raw materials, but also in the processes that enable large-scale installation and operation.

At the material level, certain components emerge as notable hotspots. Small electric motors contribute 1.830×10^3 kg (approximately 9.42%), making them one of the single largest material-level sources. Other significant contributors include iron–nickel–chromium alloys $(4.184 \times 10^2 \text{ kg})$, approximately 2.15%), aluminium wrought alloys $(4.067 \times 10^2 \text{ kg})$, approximately 2.09%), and copper cathodes $(2.607 \times 10^2 \text{ kg})$, approximately 1.34%). Printed wiring boards $(1.027 \times 10^2 \text{ kg})$, approximately 0.53%) and flat uncoated glass (37.322 kg), approximately 0.19%) contribute smaller fractions, but nonetheless illustrate the wide range of materials that feed into the overall toxicity profile. Even more marginal are flows such as glass wool mats (15.482 kg), approximately 0.08%) and concrete (12.881 kg), approximately 0.066%), which play only a minor role.

Rotary kiln construction also represents an important source of toxicity emissions. Contributions from material preparation, rolling/forming, machining, and welding/assembly are all in a similar range—between 2.276×10^3 and 2.291×10^3 kg (approximately 11.7–11.8%). While less dominant than heliostat operation, these stages reflect the persistent influence of energy-and resource-intensive industrial processes on the overall system profile.

Beyond these major contributors, several smaller flows collectively add to the picture. These include electronic components $(3.501 \times 10^2 \text{ kg}, \text{ approximately } 1.80\%)$, wastewater treatment (80.706 kg, approximately 0.42%), freight transport (26.483 kg, approximately 0.14%), municipal waste glass treatment (12.357 kg, approximately 0.064%), rotary kiln end-of-life treatment (6.989 kg, approximately 0.036%), and medium-voltage electricity $(1.565 \times 10^2 \text{ kg}, \text{ approximately } 0.805\%)$. Interestingly, the direct contribution of bauxite itself is minimal. Processed bauxite adds only 3.196 kg (approximately 0.016%), while the initial bauxite stock contributes 2.973 kg (approximately 0.015%).

Taken together, these results show that the human toxicity profile of the Bauxite-PHC system is strongly skewed toward heliostat operation and steel production, which together account for nearly 88% of total emissions. Additional burdens from rotary kiln construction and specific materials—such as motors, aluminium, and specialty alloys—are also significant, whereas the contribution of raw bauxite is negligible. This highlights the importance of adopting a comprehensive life cycle perspective: while bauxite is central to the system conceptually, its direct toxicity footprint is minor compared to the infrastructure and supporting materials. From a mit-

igation perspective, the most effective strategies will likely involve reducing the material and energy intensity of heliostat logistics, improving the efficiency of steel and component manufacturing, and optimizing construction processes for the rotary kiln.

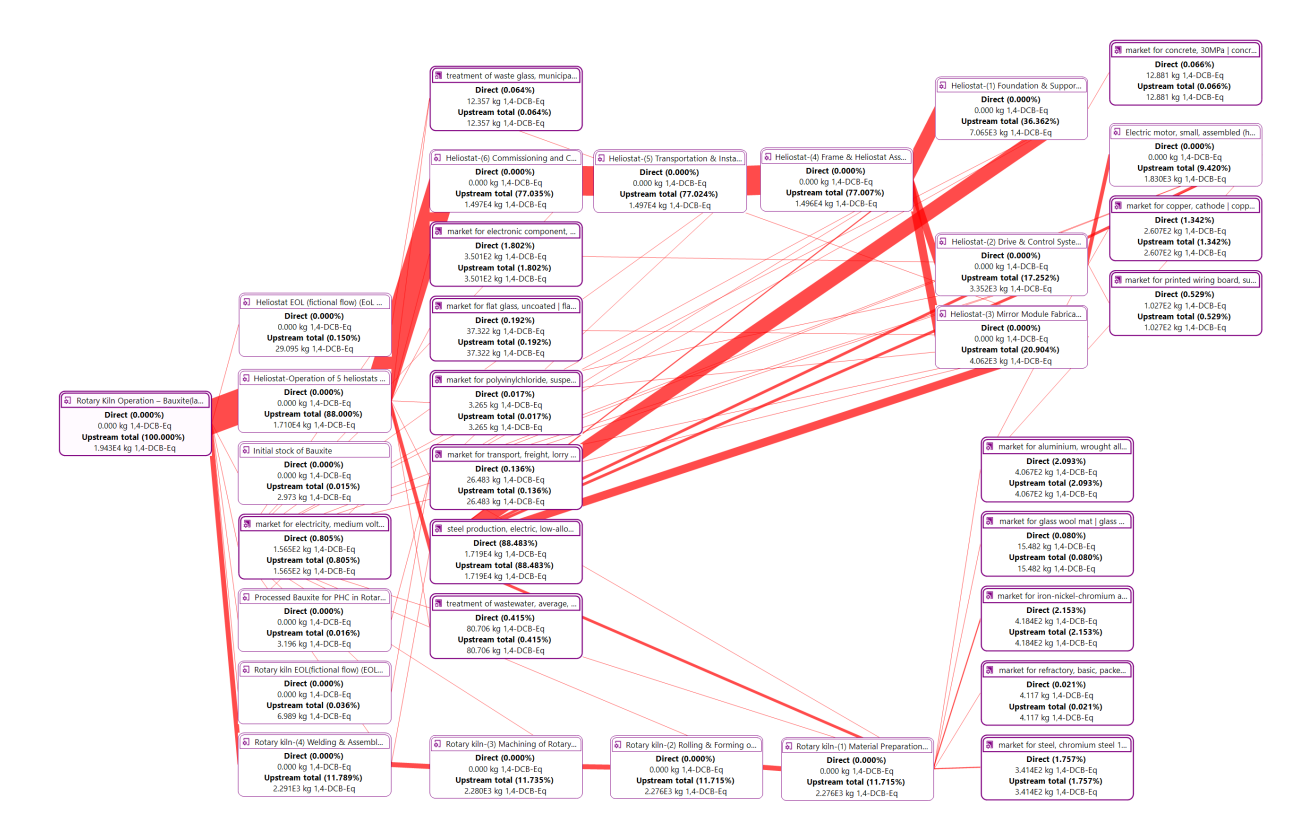


Figure 5.16: Human Toxicity Hotspot Analysis with Sankey Diagram Using Bauxite as the PHC.

II. Bauxite: Climate Change Hotspot Analysis with Sankey Diagram

The climate change impacts of the Bauxite-based PHC system amount to 4.971×10^3 kg CO₂-equivalents (CO₂-Eq), representing the full upstream greenhouse gas emissions associated with material production, component manufacturing, assembly, transport, operation, and end-of-life management. At the system level, heliostat operation emerges as the dominant contributor, responsible for 4.099×10^3 kg CO₂-Eq, or approximately 82% of the total footprint. This concentration reflects the energy- and material-intensive requirements of deploying, commissioning, and managing heliostat systems.

As illustrated in Figure 5.17 below, Within the heliostat chain, the largest contributions stem from commissioning and control (2.842×10^3 kg CO₂-Eq, approximately 57%), followed closely by transportation and installation (2.826×10^3 kg CO₂-Eq, approximately 57%) and frame assembly (2.808×10^3 kg CO₂-Eq, approximately 56%). The similarity in these values underscores that emissions are heavily clustered in logistics, assembly, and early operational stages rather than during disposal. Other relevant subsystems include the drive and control system (1.841×10^3 kg CO₂-Eq, approximately 37%), mirror module fabrication (6.640×10^2 kg CO₂-Eq, approximately 13%), and foundation and support structures (2.667×10^2 kg CO₂-Eq, approximately 5%). End-of-life treatment of heliostats, represented as a notional flow, accounts

for only 1.945×10^2 kg CO₂-Eq (approximately 4%), confirming that climate burdens are overwhelmingly front-loaded in the heliostat lifecycle.

The rotary kiln fabrication and assembly chain also contributes significantly to the overall emissions profile. Each stage contributes in a fairly uniform manner: material preparation $(5.608 \times 10^2 \text{ kg CO}_2\text{-Eq}, \text{ approximately } 11.3\%)$, rolling and forming $(5.618 \times 10^2 \text{ kg CO}_2\text{-Eq}, \text{ approximately } 11.3\%)$, machining $(5.901 \times 10^2 \text{ kg CO}_2\text{-Eq}, \text{ approximately } 11.9\%)$, and welding and assembly $(5.915 \times 10^2 \text{ kg CO}_2\text{-Eq}, \text{ approximately } 11.9\%)$. This even distribution suggests no single stage dominates, and improvements in any part of the kiln construction process could yield meaningful reductions in emissions. Conversely, end-of-life treatment of the rotary kiln contributes only $5.489 \times 10^1 \text{ kg CO}_2\text{-Eq}$ (approximately 1.1%). The processed bauxite input used within the kiln adds just $1.846 \times 10^1 \text{ kg CO}_2\text{-Eq}$ (approximately 0.37%), reinforcing that raw feedstock itself plays a minor role in climate impacts.

Material- and component-level analysis further clarifies key drivers of emissions. Medium-voltage electricity is the single largest contributor, responsible for 1.164×10^3 kg CO₂-Eq (approximately 23%). Small electric motors follow closely with 9.806×10^2 kg CO₂-Eq (approximately 20%). Other significant contributors include printed wiring boards (6.464×10^2 kg CO₂-Eq, approximately 13%), aluminium wrought alloy (6.345×10^2 kg CO₂-Eq, approximately 13%), and flat uncoated glass (4.875×10^2 kg CO₂-Eq, approximately 10%). Passive electronic components add 3.912×10^2 kg CO₂-Eq (around 8%), while steel production, particularly low-alloy electric steel, accounts for 2.928×10^2 kg CO₂-Eq (about 6%). Other contributors include copper cathodes (2.002×10^2 kg CO₂-Eq, approximately 4%) and iron–nickel–chromium alloys (1.945×10^2 kg CO₂-Eq, approximately 4%). Smaller yet measurable flows arise from concrete (1.230×10^2 kg CO₂-Eq, about 2.5%), nylon-6 (91.444 kg, approximately 1.8%), chromium steel (60.499 kg, approximately 1.2%), refractory materials (35.595 kg, approximately 0.7%), and glass wool mats (32.790 kg, approximately 0.7%).

Additional flows, though individually modest, collectively reinforce the importance of a full lifecycle perspective. Wastewater treatment contributes 3.228×10^2 kg CO₂-Eq (approximately 6.5%), lorry transport adds 1.437×10^2 kg CO₂-Eq (approximately 2.9%), hazardous waste mineral oil treatment accounts for 30.626 kg CO₂-Eq (about 0.6%), and heat production from natural gas furnaces adds 23.806 kg CO₂-Eq (about 0.5%).

In summary, the climate change profile of the Bauxite-PHC system is highly skewed toward heliostat-related processes, with the majority of upstream emissions arising during commissioning, transportation, and assembly stages. Large-scale material and component flows—particularly electricity consumption, small motors, aluminium, and wiring—are significant contributors. In contrast, bauxite-specific contributions are negligible, supporting the earlier conclusion that raw material impacts are minor compared to infrastructure deployment, manufacturing, and energy use. From a mitigation standpoint, strategies should focus on reducing the carbon intensity of electricity across the supply chain, improving material efficiency in high-impact components, and streamlining heliostat deployment processes to substantially lower the system's overall climate burden.

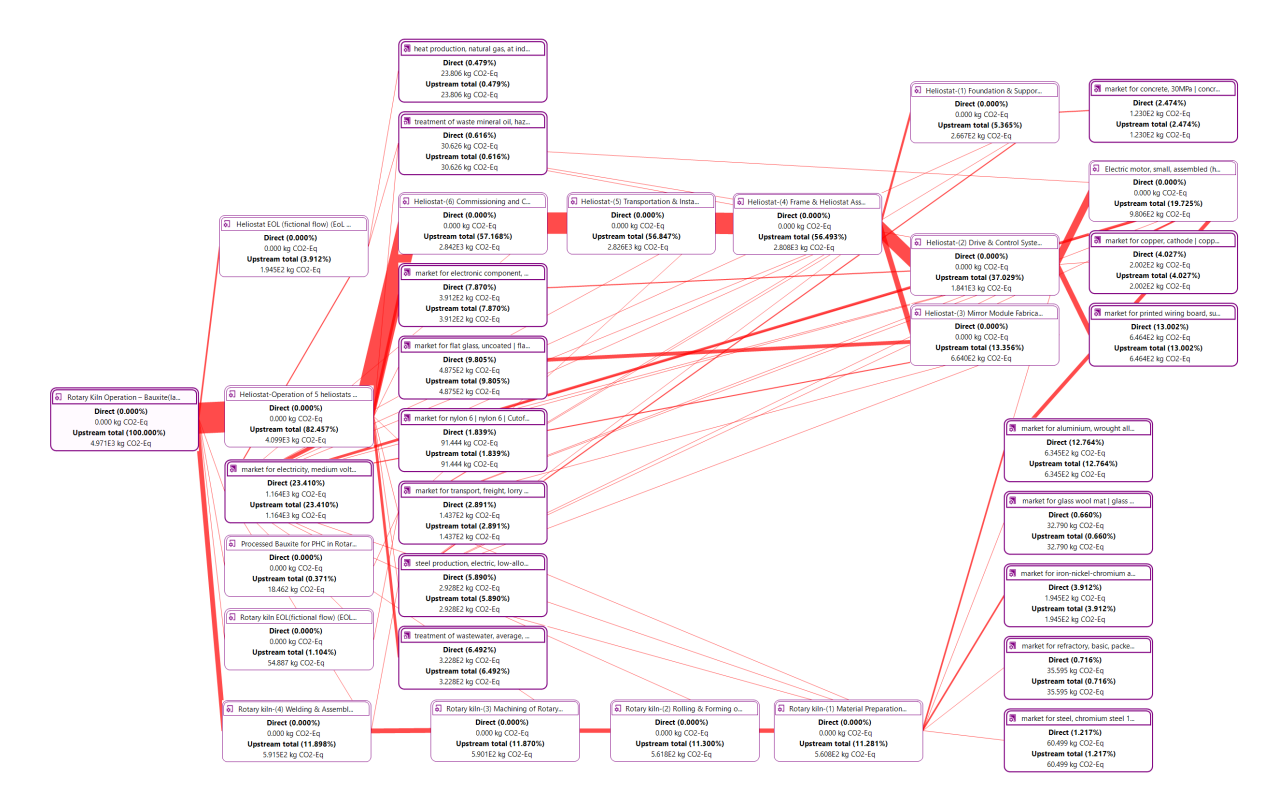


Figure 5.17: Climate Change Hotspot Analysis with Sankey Diagram Using Bauxite as the PHC.

5.4.2 Sand

I. Sand: Human Toxicity Hotspot Analysis with Sankey Diagram

The human toxicity assessment of the sand-based solar system, visualized through a Sankey diagram 5.18, reveals a clear pattern: the rotary kiln itself contributes nothing directly to toxicity impacts. The central node, Rotary Kiln Operation (Sand), shows a 0.000% direct contribution, while its upstream share reaches 100%. This demonstrates that all toxicity burdens are inherited from the broader supply chain and infrastructure requirements, rather than from the kiln's direct operation.

Within this upstream profile, the heliostat infrastructure dominates. Heliostat operation alone is responsible for 88.0% of the total burden, underlining the material- and energy-intensive nature of commissioning, installing, and maintaining a heliostat field. Deployment stages further amplify this impact: commissioning and construction contribute 77.0%, transportation and installation 77.0%, and frame assembly 77.0%. Even secondary subsystems such as foundations (36.4%) and drive and control systems (17.3%) add significant shares. At the component level, small electric motors stand out, contributing 9.4% of total toxicity, despite their modest scale within the overall system.

Tracing the Sankey flows upstream highlights the material and industrial origins of these burdens. Flat uncoated glass contributes 0.19%, reflecting the emissions embedded in mirror production. Electronics also play a role, with copper cathodes accounting for 1.34% and printed wiring boards for 0.59%, linked to refining and semiconductor manufacturing. Even seemingly marginal inputs, such as polyvinyl chloride (0.017%), reveal the influence of plastics in wiring and insulation.

The strongest signal, however, comes from metals. Steel production, particularly low-alloy electric arc furnace steel, accounts for 88.5% of total human toxicity—a single overwhelming hotspot. Aluminium wrought alloys add 2.1%, while chromium steel contributes 1.75%. Electricity use is comparatively minor, with medium-voltage electricity accounting for only 0.8%. These results suggest that metallurgy and large-scale material processing, rather than direct energy consumption, define the system's toxicity profile.

Other flows, though small, provide a more complete picture. The welding and assembly stage of the rotary kiln contributes 11.8%, while end-of-life processes remain negligible: rotary kiln disposal adds just 0.036%, waste glass treatment 0.064%, and concrete (30 MPa) 0.066%. Freight transport makes only a modest contribution at 0.13%. Most importantly, the contribution of the heat carrier itself—processed sand—is virtually zero, at just 0.0025%.

In summary, the human toxicity burden of the sand-based solar system is driven almost entirely by materials and infrastructure, particularly steel, aluminium, glass, and electronic components. The sand itself plays no meaningful role. Mitigation strategies should focus on developing cleaner steelmaking routes, improving glass and aluminium production processes, promoting more sustainable electronics and copper supply chains, and streamlining installation logistics. This analysis reinforces the conclusion that toxicity impacts are predominantly infrastructure-driven rather than fuel-driven.

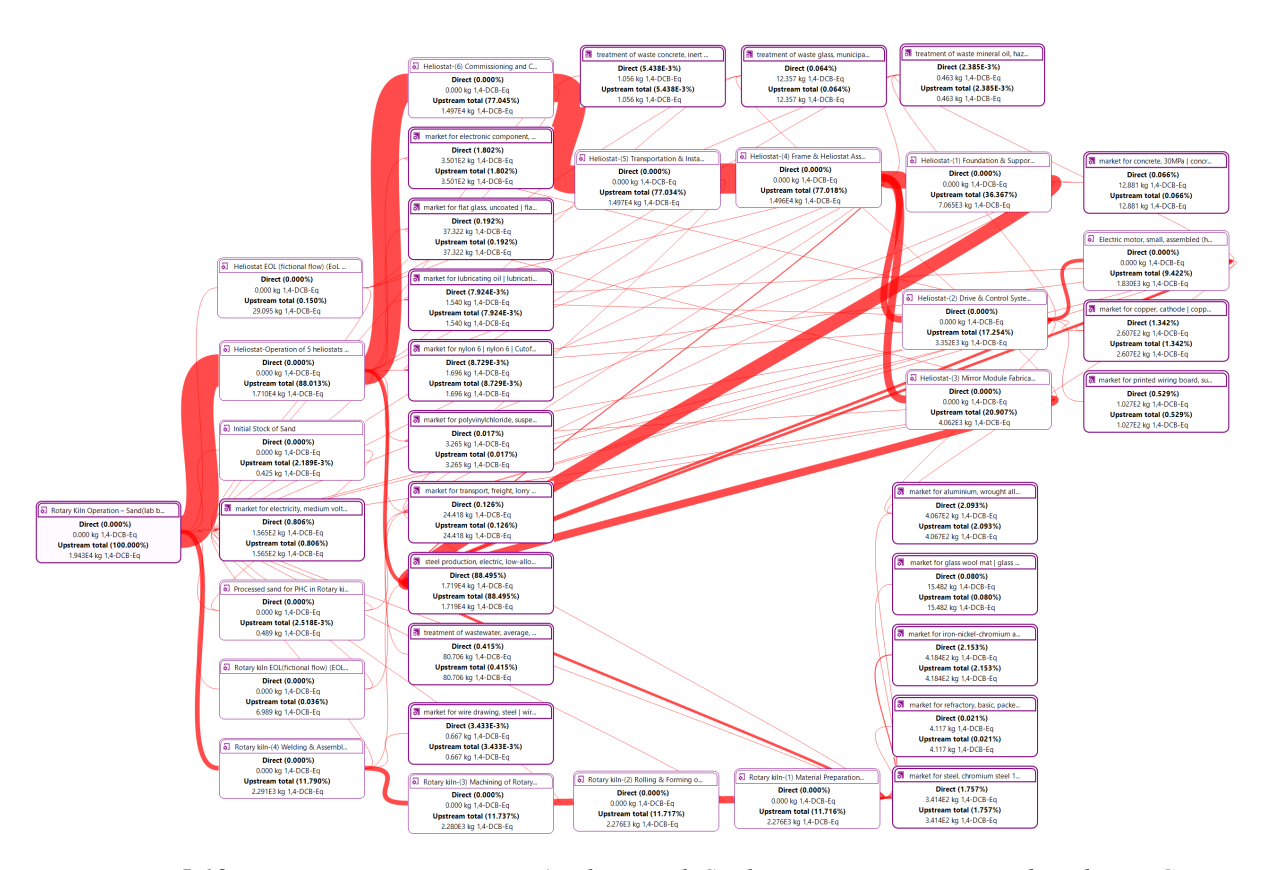


Figure 5.18: Human Toxicity Hotspot Analysis with Sankey Diagram Using sand as the PHC.

II. Sand: Climate Change Hotspot Analysis with Sankey Diagram

The climate change analysis of the sand-based solar system further reinforces the finding that impacts are rooted in infrastructure rather than in the kiln itself. The Sankey diagram in Figure 5.19 shows that Rotary Kiln Operation (Sand) contributes 0.000% directly, with the entire 100% burden inherited upstream. This indicates that greenhouse gas emissions arise entirely from the processes enabling system operation—material production, heliostat assembly, electronics manufacturing, and associated logistics.

The heliostat subsystem again emerges as the primary hotspot, responsible for 82.6% of upstream emissions. Within this, commissioning and construction contribute 57.2%, transportation and installation 56.9%, and frame assembly 56.6%. The drive and control system adds a further 37.1%, highlighting the embodied carbon in precision actuators and electronics. Mirror module fabrication contributes 13.4%, while foundations and supports add 5.4%. In contrast, end-of-life treatment of heliostats accounts for only 3.9%, confirming that operational phases dominate over disposal.

Electricity supply is another major driver, with medium-voltage electricity responsible for 23.4% of the total footprint. This underscores the system's strong dependence on the carbon intensity of grid electricity: adopting renewable or low-carbon electricity sources would directly lower emissions.

Materials and electronics also make significant contributions: printed wiring boards account for 13.0%, aluminium wrought alloy 12.8%, flat uncoated glass 9.8%, and passive electronic components 7.9%. Steel, via low-alloy electric arc furnace routes, contributes 5.9%, while copper cathodes (4.0%) and iron–nickel–chromium alloys (3.9%) are notable hotspots. At the subsystem level, small electric motors contribute 19.8%—a striking figure given their small size, but one that reflects the energy- and material-intensive nature of their manufacturing. Supporting flows such as logistics and conventional construction materials add further, though smaller, contributions: freight transport by lorry contributes 2.7%, concrete (30 MPa) 2.5%, nylon-6 1.8%, and PVC 0.3%. End-of-life treatment of the rotary kiln adds 1.1%, while sand itself contributes just 0.2%. Residual flows include wastewater treatment (6.5%), hazardous mineral oil treatment (0.6%), waste glass incineration (0.3%), and upstream natural gas use (0.5%).

Overall, the climate footprint of the sand-based system is overwhelmingly infrastructure-driven, with heliostat operation, materials production, electricity supply, and electronic components defining the majority of emissions. The sand itself contributes negligibly. Mitigation strategies should therefore focus on decarbonizing steel, aluminium, and glass production, expanding recycling in metals, transitioning to low-carbon electricity, and optimizing electronics and logistics. In short, reducing the climate burden depends less on the choice of heat carrier and more on improving the sustainability of the infrastructure that enables solar concentration.

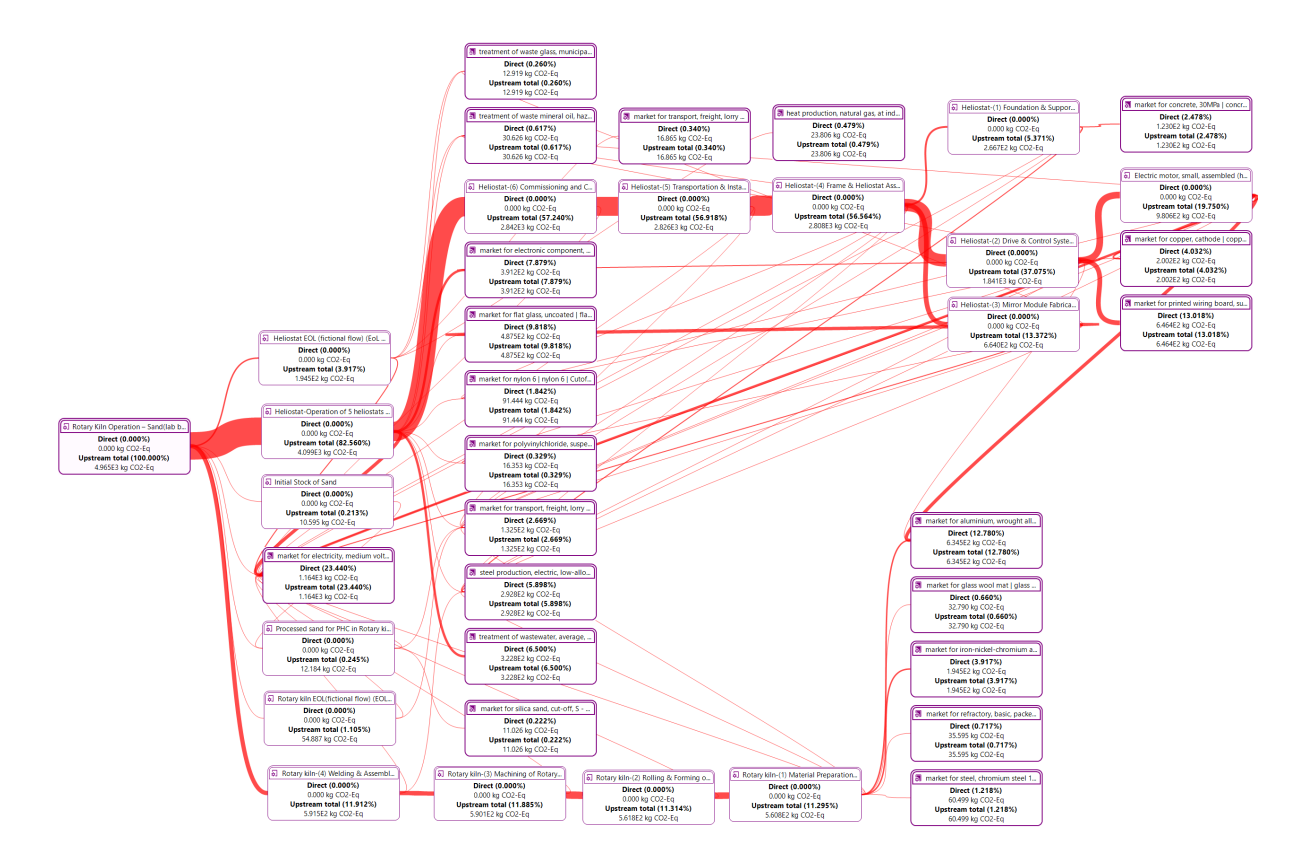


Figure 5.19: Climate Change Hotspot Analysis with Sankey Diagram Using sand as the PHC.

Olivine

I. Olivine: Human Toxicity Hotspot Analysis with Sankey Diagram

The human toxicity profile of the system using olivine as the primary heat carrier (PHC) amounts to 1.94×10^4 kg 1,4-DCB-Eq. As with other PHC systems, this burden is overwhelmingly shaped by upstream processes rather than direct kiln operation. The Sankey diagram (Figure 5.20) clearly illustrates that steel production and heliostat infrastructure dominate the overall profile.

Steel production, particularly low-alloy electric steel, emerges as the single largest hotspot, contributing 1.72×10^4 kg 1,4-DCB-Eq—equivalent to 88.5% of the system total. Steel is integral both to rotary kiln construction (welding, machining, rolling, and material preparation) and to heliostat subsystems such as frames, foundations, and support structures. Consequently, all downstream processes relying on steel inherit substantial indirect toxicity burdens. For example, each of the four kiln construction stages contributes approximately 2.28×10^3 kg ($\approx 11.7\%$), while the heliostat foundation alone adds 7.07×10^3 kg ($\approx 36.4\%$).

Within the heliostat subsystem, mirror module fabrication accounts for 4.06×10^3 kg ($\approx 20.9\%$), and the drive and control system contributes 3.35×10^3 kg ($\approx 17.3\%$). Other lifecycle phases, such as transportation, commissioning, and frame assembly, each contribute around 1.50×10^3 kg ($\approx 7.7\%$). In contrast, end-of-life stages are negligible: heliostat disposal adds only 29.1 kg ($\approx 0.15\%$), and kiln end-of-life just 6.99 kg ($\approx 0.04\%$).

Secondary material inputs, though smaller, are still notable: aluminium wrought alloy con-

tributes 4.07×10^2 kg ($\approx 2.1\%$), iron–nickel–chromium alloys 4.18×10^2 kg ($\approx 2.2\%$), and copper cathodes 2.61×10^2 kg ($\approx 1.3\%$). Electronics add further to the toxicity burden: printed wiring boards contribute 1.03×10^2 kg ($\approx 0.53\%$), and other electronic components contribute 3.50×10^2 kg ($\approx 1.8\%$). Glass-based materials, both flat and wool, contribute less than 0.2%, while cement and concrete inputs are around 0.07%. Waste management processes, such as municipal glass incineration (12.4 kg; $\approx 0.06\%$) and wastewater treatment (80.7 kg; $\approx 0.42\%$), are similarly minor.

Most strikingly, the contribution of olivine itself is negligible. The processed olivine used as PHC (1.85 kg; $\approx 0.01\%$) and the initial stock (1.77 kg; $\approx 0.01\%$) together account for less than 0.02% of the total impact. Although olivine is central to the kiln's function, its direct role in human toxicity is insignificant.

The human toxicity (cancer) category, measured in kg 1,4-DCB-Eq, reflects the potential risks to human health from toxic emissions linked to industrial processes. High values indicate emissions of carcinogenic substances such as heavy metals (chromium, nickel, arsenic), persistent organic pollutants, or by-products from smelting and energy-intensive manufacturing.

The results clearly identify structural materials—steel, aluminium, and specialty alloys—as the main drivers of toxicity, along with electronics. This aligns with the environmental record of metallurgical and electronic industries, where mining, smelting, and chemical processing frequently release carcinogenic pollutants. Conversely, kiln operation and the olivine material itself make no meaningful contribution to the toxicity profile.

The system's human health footprint is overwhelmingly determined by infrastructure and material supply chains rather than the choice of heat carrier, indicating that mitigation efforts should focus on reducing toxicity in steel and electronics manufacturing, improving supply chain sustainability, and minimizing upstream emissions.

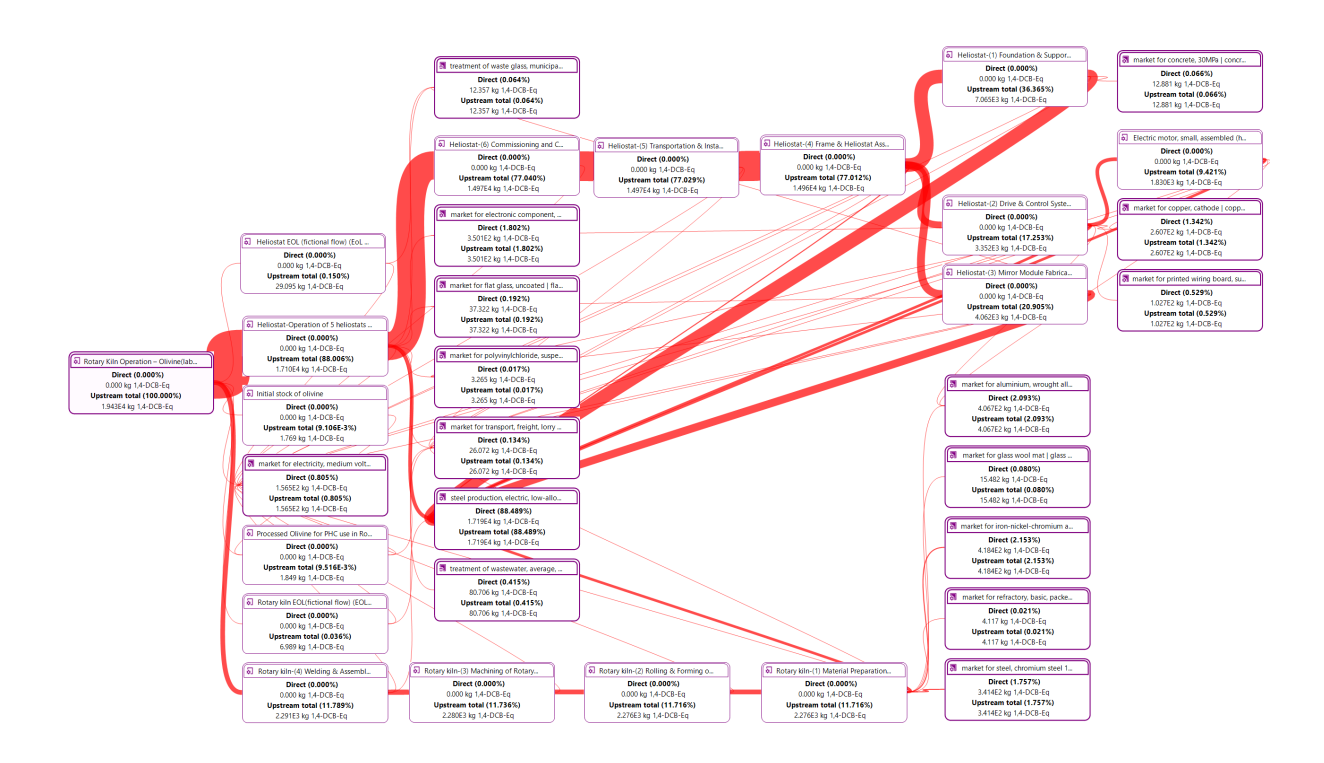


Figure 5.20: Human Toxicity Hotspot Analysis with Sankey Diagram Using Olivine as the PHC.

II. Olivine: Climate Change Hotspot Analysis with Sankey Diagram

The climate change assessment of the olivine-based PHC system quantifies upstream green-house gas emissions at 4.963×10^3 kg CO₂-equivalents, encompassing all stages from material extraction and manufacturing to assembly, transportation, operation, and end-of-life treatment (Figure 5.21). This comprehensive approach allows identification of the most significant contributors to the system's carbon footprint.

At the system level, the operation of the five heliostats dominates emissions, contributing 4.099×10^3 kg CO₂-Eq, or approximately 82.6%. This highlights that heliostat deployment, commissioning, and ongoing operation are highly energy-intensive processes. Within the heliostat subsystem, commissioning activities, transportation, and frame assembly account for the largest shares, suggesting that improvements in these stages—through design optimization or efficiency measures—could substantially reduce emissions.

Electricity consumption at the medium-voltage level contributes 1.164×10^3 kg CO₂-Eq ($\approx 23.4\%$), underscoring the system's sensitivity to energy sourcing. Transitioning to low-carbon electricity or enhancing operational energy efficiency could therefore significantly lower the overall footprint. Smaller but relevant contributors include heliostat end-of-life treatment (1.945×10^2 kg, $\approx 3.9\%$), rotary kiln end-of-life (5.489×10^1 kg, $\approx 1.1\%$), industrial heat from natural gas (2.381×10^1 kg, $\approx 0.48\%$), and freight transport by lorry (1.686×10^1 kg, $\approx 0.34\%$). Collectively, these minor flows emphasize the importance of a full lifecycle perspective. The rotary kiln manufacturing process is divided into four stages, each contributing nearly equally: material preparation (5.608×10^2 kg, $\approx 11.3\%$), rolling and forming (5.618×10^2

kg, $\approx 11.3\%$), machining (5.901 \times 10² kg, \approx 11.9%), and welding/assembly (5.915 \times 10² kg, \approx 11.9%). This uniform distribution suggests that incremental efficiency gains across any stage could cumulatively reduce emissions, rather than focusing solely on one process.

Material-level contributions within the heliostat subsystem further clarify the dominant sources of emissions. Small electric motors contribute 9.806×10^2 kg CO_2 -Eq ($\approx 19.8\%$), printed wiring boards 6.464×10^2 kg ($\approx 13.0\%$), and aluminium wrought alloys 6.345×10^2 kg ($\approx 12.8\%$). Copper cathodes add 2.002×10^2 kg ($\approx 4.0\%$), and flat uncoated glass 4.875×10^2 kg ($\approx 9.8\%$). Secondary materials—chromium steel (6.050×10^1 kg, $\approx 1.2\%$), iron—nickel—chromium alloys (1.945×10^2 kg, $\approx 3.9\%$), Nylon-6 (9.144×10^1 kg, $\approx 1.8\%$), glass wool mats (3.279×10^1 kg, $\approx 0.66\%$), and concrete (1.230×10^2 kg, $\approx 2.5\%$)—also contribute modestly. Additional flows such as freight transport (1.415×10^2 kg, $\approx 2.85\%$), wastewater treatment (3.228×10^2 kg, $\approx 6.5\%$), and hazardous mineral oil treatment (3.063×10^1 kg, $\approx 0.6\%$) demonstrate the importance of auxiliary processes.

Collectively, these results indicate that emissions are concentrated in a few key components and processes. Heliostat assembly, commissioning, drive systems, and electricity use dominate the carbon footprint, while other materials and lifecycle stages, though smaller individually, cumulatively shape the total impact. Improving the largest contributors is likely to yield the most significant reductions, with additional benefits achievable through incremental gains in kiln manufacturing and end-of-life management.

The olivine-based PHC system exhibits a highly concentrated climate impact profile, with a small set of processes and materials responsible for the majority of upstream emissions. Mitigation opportunities primarily involve optimizing heliostat-related operations, enhancing component efficiency, and transitioning to low-carbon electricity sources, rather than modifications to the olivine heat carrier itself.

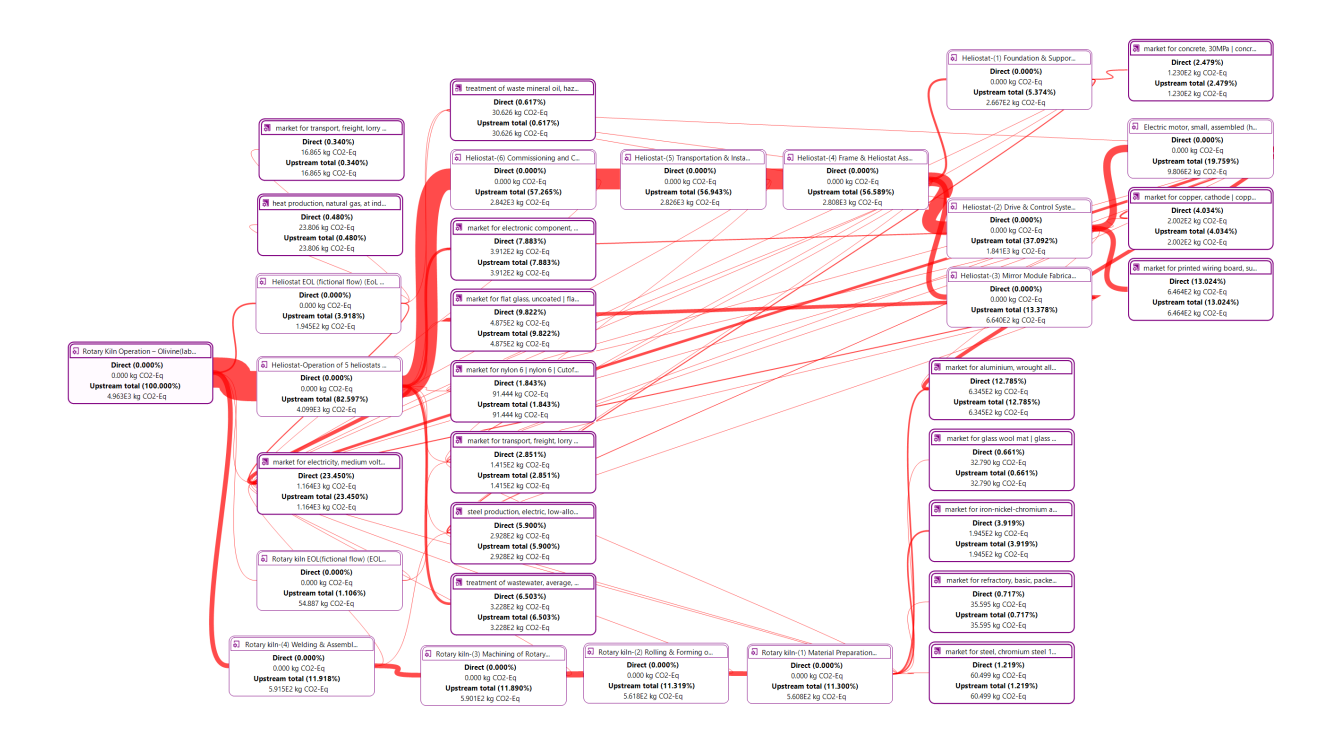


Figure 5.21: Climate Change Hotspot Analysis with Sankey Diagram Using Olivine as the PHC.

5.5 Summary of Results

Comparing the three particle heat carriers—bauxite, sand, and olivine—gives clear insight into the environmental impacts of the PYSOLO system. Across categories like climate change, human toxicity, material and energy use, land use, and water consumption, the heliostat subsystem—especially during construction—stands out as the largest contributor. No matter which particle is used, the heliostat field produces more than half of the greenhouse gas emissions and over three-quarters of the human toxicity impacts. This shows how material-intensive the heliostat is, due to steel, aluminum, copper, and electronic components.

The choice of particle has only a small effect on overall environmental impacts. Bauxite shows the largest differences in material use because it is mined directly, while sand and olivine mainly affect land use and water consumption slightly. Interestingly, sand, often considered low-impact, actually has a notable land-use footprint because of aggregate extraction. Olivine is similar to bauxite but does not change the overall impact distribution much.

Pie charts for each scenario—bauxite (climate change, human toxicity, material use), sand (climate change, human toxicity, land use), and olivine (climate change, human toxicity)—show very similar patterns. In all cases, heliostat construction is the main contributor, followed by heliostat operation and rotary construction. End-of-life impacts are smaller but still significant, pointing to opportunities for recycling and material recovery.

In summary, changing the particle alone does little to improve the system's life-cycle performance. The best way to reduce environmental impacts is through design improvements and using materials more efficiently in the heliostat subsystem.

6 Discussion and Optimization

This study points to several ways the PYSOLO system could lower its environmental impacts. It is important to note that many numbers are based on scaled assumptions, so the exact values are uncertain. Still, the trends are clear. Heliostat materials were estimated from literature and reference systems, kiln materials from engineering equations, and energy use and PHC losses from earlier studies and technical judgment.

6.1 Material and Design Efficiency

Reducing material use is one of the best ways to lower impacts. Using lighter heliostat supports, replacing primary alloys with recycled ones, and choosing modular designs could reduce climate and toxicity impacts. A more efficient kiln design could also save materials, even though the exact savings are not known.

6.2 Operational Improvements

Improving operation can also make a difference. Better heliostat tracking, reducing unnecessary electricity use, and relying on cleaner electricity sources would cut emissions. Even though energy and PHC loss data were estimated, applying these improvements in practice could strengthen the sustainability of the system.

6.3 End-of-Life and Circularity

Designing components for reuse and recycling can reduce the material footprint. Planning from the start for disassembly and recovery of metals would make the system more circular. The exact effect is uncertain, but this direction clearly offers benefits.

6.4 Net-Negative Emissions Potential

Beyond reducing impacts, PYSOLO has the potential to achieve net-negative emissions through biochar production. This depends on the long-term stability of carbon in biochar and its ability to replace fossil-based inputs like synthetic fertilizers or activated carbon. Optimizing the heliostat subsystem, along with material efficiency, operational improvements, and circular end-of-life strategies, can minimize the solar subsystem's material-related impacts relative to the carbon sequestration and emissions avoided through biochar. Even with the uncertainties inherent in the scaled assumptions, PYSOLO shows strong promise as a scalable technology for climate mitigation.

6.5 Interpretation (ISO 14044)

The results show that heliostat construction dominate most impact categories, particularly climate change and resource use. The choice of PHC makes only a minor difference.

The system model is considered complete within the defined boundaries. Very small flows were excluded according to the cut-off rules described in Chapter 4. The same functional unit,

boundaries, allocation procedure, and impact method (ReCiPe 2016 Midpoint H) were applied consistently.

No sensitivity analysis was carried out, but key uncertainties such as PHC attrition, lifetimes, and electricity demand are acknowledged. These may shift absolute values but do not change the main conclusion that heliostat construction is the major contributor.

7 Conclusion and Future work

7.1 Summary of Contributions

This thesis presented the first life-cycle assessment of the PYSOLO solar subsystem, comparing three PHCs: bauxite, sand, and olivine. The analysis shows that heliostat construction is the dominant source of environmental impacts, followed by heliostat operation and kiln construction. PHC choice has only minor influence on overall results.

Material and energy values were estimated from literature, engineering calculations, and prior technology data. Although these assumptions introduce uncertainty, the results provide a clear picture of the relative contributions of different subsystems. The study highlights where design improvements, operational changes, and circular end-of-life strategies could bring the largest benefits.

7.2 Limitations of the Study

The main limitation of this study is that it relies on scaled data rather than measured operational values. Heliostat materials were estimated from reference designs, rotary kiln materials and particle heat carrier (PHC) flows were calculated using engineering equations, and some assumptions were based on previous studies. This means the results are indicative rather than exact. The study also did not include the benefits of biochar use, such as carbon storage or soil improvement, and it focused only on the solar subsystem, without considering interactions with the rest of the plant.

7.3 Recommendations for Future Research

Future work should focus on replacing assumptions with real data, such as measured energy use, detailed bills of materials, and actual PHC attrition rates. Studies in different regions would help improve estimates for electricity mixes and supply chain impacts. Research on modular and recyclable heliostat designs could further improve circularity. Most importantly, subsystem results should be integrated into full plant assessments, including biochar carbon permanence and avoided emissions. Finally, economic and policy studies are needed to evaluate the practical feasibility of scaling up PYSOLO as a net-negative technology.

In conclusion, the PYSOLO solar subsystem shows clear ways to reduce environmental impacts through improvements in design, operation, and circularity. Heliostat construction is the main driver of impacts, while the choice of particle heat carrier has only a minor effect. Although this study relied on assumptions rather than measured data, it provides a solid foundation for future validation and optimization. Combining these subsystem results with whole-plant assessments, including biochar carbon storage, will be important to determine PYSOLO's potential as a scalable net-negative technology. Overall, the findings offer a roadmap for developing sustainable, low-impact solar thermochemical processes.

Bibliography

- [1] International Energy Agency. World energy investment 2023. Technical report, International Energy Agency, Paris, 2023. Licence: CC BY 4.0.
- [2] International Energy Agency. Global energy review 2025. Technical report, International Energy Agency, Paris, France, 2025. Revised version, March 2025. Information notice at: https://www.iea.org/corrections.
- [3] Werner Weiss and Monika Spörk-Dür. Solar heat worldwide: Global market development and trends 2023 detailed market figures 2022, 2024 edition. Technical report, AEE Institute for Sustainable Technologies, Gleisdorf, Austria, 2024. Supported by the IEA Solar Heating Cooling Programme; DOI: 10.18777/ieashc-shww-2024-0001.
- [4] International Energy Agency (IEA). Technology roadmap: Concentrating solar power. Technical report, International Energy Agency, Paris, France, 2010.
- [5] HORIZON-CL5-2022-D3-02. Pyrolysis of biomass by concentrated solar power. Technical report, HORIZON Action Grant Budget-Based, 2022. Technical description (Part B).
- [6] Marco Tomatis, Harish Jeswani, Laurence Stamford, and Adisa Azapagic. High temperature solar-heated reactors for industrial production of reactive particulates. Deliverable D6.3, European SOLPART Project, 2020. Grant Agreement number 654663; WP6 Environmental Life Cycle Assessment of the Solar Process and Comparison to the Standard Technology; Development of an open-source LCA model of the SOLPART and standard systems.
- [7] Z. Bai et al. Applying the solar solid particles as heat carrier to enhance biomass gasification. *Energy Conversion and Management*, 2023.
- [8] V. M. Maytorena et al. Worldwide developments and challenges for solar pyrolysis. *Renewable and Sustainable Energy Reviews*, 2024.
- [9] A. I. Osman et al. Conversion of biomass to biofuels and life cycle assessment. *Environmental Chemistry Letters*, 19:4075–4118, 2021.
- [10] Xiefei Zhu, Claudia Labianca, Mingjing He, Zejun Luo, Chunfei Wu, Siming You, and Daniel C.W. Tsang. Life-cycle assessment of pyrolysis processes for sustainable production of biochar from agro-residues. *Bioresource Technology*, 2022. Available online 11 July 2022.
- [11] J. Cheng et al. Assessing the sustainable abilities of a pilot hybrid solar-pyrolysis energy system. *Energy Reports*, 2020.
- [12] Keith Lovegrove and Wes Stein. Introduction to concentrating solar power (csp) technology. In *Concentrating Solar Power Technology: Principles, Developments and Applications*, pages 3–17. Woodhead Publishing, 2012.
- [13] Manuel Romero and José González-Aguilar. Solar thermal csp technology. *WIREs Energy and Environment*, 3(1):42–59, 2014.
- [14] Gemma Gasa, Antón LopezRoman, Cristina Prieto, and Luisa F. Cabeza. Life cycle assessment (lca) of a concentrating solar power (csp) plant in tower configuration with and without thermal energy storage (tes). *Sustainability*, 13(7):3672, 2021.
- [15] Peter Viebahn, Yolanda Lechón, and Franz Trieb. The potential role of concentrated solar power (csp) in africa and europe—a dynamic assessment of technology development, cost development and lifecycle inventories until 2050. *Energy Strategy Reviews*, in press.
- [16] Gilles Flamant, Hadrien Benoit, Martin Jenke, et al. Solar processing of reactive particles up to 900°c, the solpart project. In *AIP Conference Proceedings*, volume 2033, page 020004. AIP Publishing, 2018. Published online 08 November 2018.

[17] J. P. Rincon Duarte, S. Tescari, T. Fend, M. Roeb, and C. Sattler. Solar rotary kiln for thermal storage applications. 2020. Affiliations: German Aerospace Center (DLR), Institute of Solar Research, Linder Hoehe, 51147 Cologne, Germany; TU Dresden, Faculty of Mechanical Science and Engineering, Institute of Power Engineering, Solar Fuel Production, 01062 Dresden, Germany.

- [18] Muhammad Ahsan Amjed, Marco Colombi, Juan Pablo Rincon Duarte, et al. Techno-economic analysis of a solar-driven biomass pyrolysis plant for bio-oil and biochar production. *Sustainable Energy Fuels*, 8(18):4243–4262, 2024.
- [19] A. Gallo, A. Guandalini, C. Soares, et al. Considerations for using a rotary kiln for high temperature industrial processes with and without thermal storage, 2016.
- [20] B. Bisulandu and F. Huchet. Rotary kiln process: An overview of physical mechanisms, models and applications. *Applied Thermal Engineering*, 221:119637, 2023.
- [21] C. R. Jones, A. Corona, C. Amador, and P. J. Fryer. Dynamics of fabric and dryer sheet motion in domestic clothes dryers. *Drying Technology*, 40(10):2087–2104, 2022.
- [22] Stefania Tescari, Gkiokchan Moumin, Brendan Bulfin, Lamark de Oliveira, Stefan Schaefer, Nicolas Overbeck, Christian Willsch, Carsten Spenke, Martin Thelen, Martin Roeb, and Christian Sattler. Experimental and numerical analysis of a solar rotary kiln for continuous treatment of particle material. *Unspecified Journal or Conference*, 2019. German Aerospace Center (DLR), Linder Hoehe, Cologne 51147, Germany. Corresponding author: Stefania.Tescari@dlr.de.
- [23] E. Alonso, A. Gallo, M. I. Roldán, C. A. Pérez-Rábago, and E. Fuentealba. Use of rotary kilns for solar thermal applications: Review of developed studies and analysis of their potential. *Solar Energy*, 144:90–104, 2017.
- [24] Xenon lamps of the solar simulator in cologne. https://www.dlr.de/de/bilder/2014/3/xenon-lampen-des-strahlers-in-koeln_15670.
- [25] Deutsches Zentrum für Luft- und Raumfahrt (DLR). Solarer strahlungsempfänger centrec. https://event.dlr.de/en/hmi2022-energie/solarer-strahlungsempfaenger-centrec/, 2022. Accessed: 2024-04-27.
- [26] Reiner Buck et al. Techno-economic analysis of candidate oxide materials for thermochemical storage in concentrating solar power systems. *Frontiers in Energy Research*, 9:694248, 2021. Edited by: Juan M. Coronado, Institute of Catalysis and Petrochemistry, Spain. Reviewed by: Alfonso Chinnici, University of Adelaide, Australia; George Karagiannakis, Centre for Research and Technology Hellas, Greece. Correspondence: Reiner Buck, reiner.buck@dlr.de. Submitted to: Solar Energy section of Frontiers in Energy Research. Received: 12 April 2021. Accepted: 07 June 2021. Published: 12 July 2021.
- [27] Hans O. A. Fredriksson, Remco J. Lancee, Peter C. Thüne, Hubert J. Veringa, and J. W. (Hans) Niemantsverdriet. Olivine as tar removal catalyst in biomass gasification: Catalyst dynamics under model conditions. *Fuel Processing Technology*, 101:1–10, October 2012. Article history: Received 26 July 2012; Revised 10 October 2012; Accepted 14 October 2012; Available online 29 October 2012.
- [28] Re-cord. https://www.re-cord.org/.
- [29] Dlr space administration. https://www.dlr.de/en/sf.
- [30] Politecnico di torino. https://www.polito.it/.
- [31] Politecnico di milano. https://www.polimi.it/.

[32] Clarisse Lorreyte, Juan Pablo Rincon Duarte, Martin Roeb, and Megan Kirschmeier. Heat carrier characterization for solar operation. Deliverable D3.1, DLR, Germany, 2024. HORIZON Research and Innovation Actions, Grant Agreement No. 101118270, Call: HORIZON-CL5-2022-D3-02.

- [33] Deutsches Zentrum für Luft- und Raumfahrt (DLR). Solar towers in jülich, 2023. Credit: DLR (CC BY-NC-ND 3.0).
- [34] Felix Göhring. Test opportunities at the jülich solar towers. mailto:felix. goehring@dlr.de, 2020.
- [35] Kraftanlagen München (KAM). Solar heliostat manufacturers.
- [36] F. Göhring, O. Kaufhold, D. Maldonado Quinto, M. Sibum, and M. Wirger. Operational experiences with the heliostat field at the juelich solar towers. In *Proc. SPIE 12671, Advances in Solar Energy: Heliostat Systems Design, Implementation, and Operation*, volume 12671, page 1267109, 2023.
- [37] Deutsches Zentrum für Luft- und Raumfahrt (DLR). Jülich solar towers, 2023. Credit: DLR (CC BY-NC-ND 3.0).
- [38] Andreas Pfahl, Joe Coventry, Marc Röger, Fabian Wolfertstetter, Juan Felipe Vásquez-Arango, Fabian Gross, Maziar Arjomandi, Peter Schwarzbözl, Mark Geiger, and Phillip Liedke. Progress in heliostat development. *Solar Energy*, 152:3–37, 2017. Open access under CC-BY-NC-ND 4.0 license.
- [39] Parthiv Kurup, Sertaç Akar, Stephen Glynn, Chad Augustine, and Patrick Davenport. Cost update: Commercial and advanced heliostat collectors. Technical Report NREL/TP-7A40-80482, National Renewable Energy Laboratory (NREL), Golden, CO, February 2022.
- [40] Andreas Pfahl and Volkmar Dohmen. Low-cost materials for heliostats: Cost comparison of extensive or moderate use of timber, concrete, and polymers. In *SolarPACES 2023*, *Solar Collector Systems 3*, Germany, 2023. German Aerospace Center (DLR), Institute of Solar Research, Solar Power Plant Technology, WILL BE FILLED IN BY TIB Open Publishing. © Authors. This work is licensed under a Creative Commons Attribution 4.0 International License.
- [41] Flabeg, 2023. Accessed: 2023-10-04.
- [42] Deutscher Wetterdienst. The weather in germany in year 2023, 2023. Accessed: 2024-04-27.
- [43] Le Quyen Luu, Maurizio Cellura, Sonia Longo, and Francesco Guarino. A comparison of the life-cycle impacts of the concentrating solar power with the product environmental footprint and recipe methods. *Unpublished or specify journal if available*, 2021. Authors' affiliations: Department of Engineering, University of Palermo, Italy.
- [44] Liberty Steel Group. Carbon steel reinforcing bar (secondary production route scrap). Technical report, Liberty Steel, 2021.
- [45] Nick Thow Ann Austin Donato D'Angola Dr Dia Adhikari Smith Abigail Heywood, Nicholas Wensley. The electric edge: Energy, emissions and cost benefits of electric concrete pumping comparing energy use, carbon emissions, and costs for electric and diesel concrete pumping at one sydney harbour. Technical report, 2024.
- [46] ITeC. Energy consumption assessment for internal concrete vibrators. Technical report, 2014.
- [47] Elaine Toogood. White collar kid: What derwent's latest loose-fit office learnt from the factory next door. *Concrete Quarterly*, 282, Spring 2023.

[48] Keehoon Kwon, Doyeong Kim, and Sunkuk Kim. Cutting waste minimization of rebar for sustainable structural work: A systematic literature review. *Sustainability*, 13:5929, 2021. Open Access under CC BY 4.0 License.

- [49] Johannes Auer and Anna Meincke. Comparative life cycle assessment of electric motors with different efficiency classes: a deep dive into the trade-offs between the life cycle stages in ecodesign context. *International Journal of Life Cycle Assessment*, 23(8):1590–1608, 2018. Department for Environment, Health & Safety, Process Industries & Drives Division, Siemens AG; Department of Management Engineering, Division for Quantitative Sustainability Assessment, Technical University of Denmark; Department of Environmental and Climate Affairs, Sustainability, thyssenkrupp Steel Europe AG.
- [50] Sahil Sahni, Avid Boustani, Timothy Gutowski, and Steven Graves. Electric motor remanufacturing and energy savings. Technical report, Environmentally Benign Laboratory, Laboratory for Manufacturing and Productivity, Sloan School of Management. Sahil Sahni and Avid Boustani contributed equally to this study.
- [51] Danilo Ferreira de Souza, Pedro Paulo Fernandes da Silva, Ildo Luis Sauer, Aníbal Traça de Almeida, and Hédio Tatizawa. Life cycle assessment of electric motors a systematic literature review. *Journal of Cleaner Production*, 2023.
- [52] Guardian Industries. Guardian wet coated glass epd brazil, 2023. Accessed: 2023-10-04.
- [53] Bottero SpA. 352 bcsclassic numeric control cutting machine for flat glass. Technical report, Bottero SpA, Italy, July 2009. Technical data sheet, confidential, all images non-binding, modifications reserved.
- [54] Teknika Group. Genius ct-next cutting tables for float glass, 2025. Brochure for Genius CT-NEXT range, including features and specifications.
- [55] TWI. Eup directive and welding equipment energy consumption, 2023. Accessed: 2023-10-04.
- [56] Vicky Papaioannou, Stefano Pietrosanti, William Holderbaum, Victor M. Becerra, and Rayner Mayer. Analysis of energy usage for rtg cranes. 2024.
- [57] Mariusz Brzeziński, Dariusz Pyza, Joanna Archutowska, and Michał Budzik. Method of estimating energy consumption for intermodal terminal loading system design. *Energies*, 17(24):6409, 2024. Submission received: 16 November 2024 / Revised: 10 December 2024 / Accepted: 13 December 2024 / Published: 19 December 2024.
- [58] How much current does an overhead crane use? https://www.agcranes.com/product/how-much-current-does-an-overhead-crane-use, 2024. Accessed: 2024-12-19.
- [59] Thyssenkrupp Steel Europe. Circular steel: A system perspective on recycled content targets. Technical report, Thyssenkrupp Steel Europe, November 2023. White paper commissioned by Thyssenkrupp Steel Europe.
- [60] Rainer Remus, Miguel A. Aguado-Monsonet, Serge Roudier, and Luis Delgado Sancho. Best available techniques (bat) reference document for iron and steel production. Industrial Emissions Directive 2010/75/EU EUR 25521 EN, European Commission, Luxembourg, 2013. Integrated Pollution Prevention and Control.
- [61] Ning Ding, Feng Gao, Zhihong Wang, Xianzheng Gong, and Zuoren Nie. Environment impact analysis of primary aluminum and recycled aluminum. In *Proceedings of the 2011 Chinese Materials Conference*, Beijing, China, 2011. Chinese Materials Society, Chinese Materials Society. College of Material Science and Engineering, Beijing University of Technology.

[62] The global aluminium recycling committee (garc), 2009. Includes information on aluminium recyclability, statistics, and industry initiatives.

- [63] International Copper Association, Ltd. Copper recycling, 2021. Developed to provide information on copper recycling from publicly available sources. © 2021 International Copper Association, Ltd. Copper Alliance™ is a trademark of the International Copper Association, Ltd. All Rights Reserved. 10/20/17-ICA-BR-GL-HE-03-EN.
- [64] O. Choukri, Mohsine Ezzine, and S. Taibi. Industrial recycling of scrap copper cables and wires: Combining cold and hot treatments for maximum recovery and minimal emissions. *Archives of Foundry Engineering*, December 2024. Published December 2024.
- [65] Tong Wang, Peter Berrill, Julie Beth Zimmerman, Narasimha D. Rao, Jihoon Min, and Edgar G. Hertwich. Improved copper circularity as a result of increased material efficiency in the u.s. housing stock. *Environmental Science Technology*, 56(7):4565–4577, 2022.
- [66] P. Garcia-Gutierrez, A.M. Amadei, D. Klenert, S. Nessi, D. Tonini, D. Tosches, F. Ardente, and H. Saveyn. Environmental and economic assessment of plastic waste recycling: A comparison of mechanical, physical, chemical recycling and energy recovery of plastic waste. 2023.
- [67] Salman Pervaiz, Sathish Kannan, Ibrahim Deiab, and H. A. Kishawy. Role of energy consumption, cutting tool and workpiece materials towards environmentally conscious machining: A comprehensive review. *Proceedings of the Institution of Mechanical Engineers, Part B: Journal of Engineering Manufacture*, September 2019:1–20, 2019. Cited by 37, Read by 2,716.
- [68] Ceramic Manufacturing. Advance information about ceramic machining, 2023. Accessed: 2024-04-27.
- [69] A. Sharma, A. Babbar, Y. Tian, et al. Machining of ceramic materials: a state-of-the-art review. *International Journal of Interactive Design Manufacturing*, 17:2891–2911, 2023. Published: December 2023.
- [70] ecoinvent Association. ecoinvent database (version 3.10), 2023. Retrieved from https://ecoinvent.org.
- [71] Union Stahl. The company, 2024. Accessed: 2024-04-27.
- [72] Metallstore24. Stainless steel 316, 2024. Accessed: 2024-04-27.
- [73] Kalikund Steel Alloys. Inconel 600 plates supplier stockist in germany, 2024. Accessed: 2024-04-27.
- [74] ISOTEC Isolierungen. Ceramic fibre insulation superwool, 2024. Accessed: 2024-04-27.
- [75] Ceramaterials. Ceramic fiber 3-ply twisted rope, 2024. Accessed: 2024-04-27.
- [76] 4ming. Energy costs of punching, 2020. Accessed: 2024-04-27.
- [77] Nitesh Sihag and Kuldip Singh Sangwan. A systematic literature review on machine tool energy consumption. *Journal of Cleaner Production*, 275:123125, 2020.
- [78] International Energy Agency. Iron steel technology roadmap. Technical report, International Energy Agency, 2020. Accessed: 2024-04-27.
- [79] D.I. Bleiwas. Estimates of electricity requirements for the recovery of mineral commodities, with examples applied to sub-saharan africa. Technical Report Open-File Report 2011–1253, U.S. Geological Survey, 2011.

[80] Satyen Moray, Nathan Throop, John Seryak, Chris Schmidt, Chris Fisher, and Mark D'Antonio. Energy efficiency opportunities in the stone and asphalt industry. Technical report, Energy Resource Solutions, Inc., 2024. Details such as publication number or URL can be added if available.

- [81] Rob Banes and John Fifer. Aggregate energy consumption guide: Summary report. Technical report, Mineral Products Association, Gillingham House, 38-44 Gillingham Street, London SW1V 1HU. Prepared for Jerry McLaughlin, with contributions from SKM Enviros and Carbon Trust.
- [82] Quarzwerke GmbH. Frechen plant. https://quarzwerke.com. Accessed: 2024-04-27.
- [83] EKC AG. Ekc ag official website. https://www.ekc.ag/, 2024. Accessed April 27, 2024.
- [84] Hmc2070a-m model. Available at: https://maplesystems.com/product/modelname/hmc2070a-m/?srsltid= AfmBOopTYsmoPcc5MBQD9C1JQANkLRW7Y7CrspFBKxaIRPDF5HLnB9OM. Accessed: 2024-04-27.
- [85] Civil Testing Equipment. Laboratory rotary kiln 1300°c 1600°c. https://www.civil-testing-equipments.com/general-laboratory-equipment/drying-equipment/laboratory-rotary-kiln-1300c-1600c.html. Accessed: 2024-04-27.
- [86] Team Stainless. The global life cycle of stainless steels. Technical report, October 2020. Summary of a study quantifying the stocks and flows cycle of stainless steels.
- [87] Barbara Reck, Thomas E. Graedel, J. Johnson, and T. Wang. The energy benefit of stainless steel recycling. *Energy Policy*, 36(1):181–192, 2008.
- [88] Susana J. Castillo, Anna Hayes, Greg Colvin, Barrett G. Potter, Rongguang Liang, and Krishna Muralidharan. Characterization of recycled inconel 718 metal powder for assessing its reusability in the laser powder bed fusion process. *Clean Technologies and Recycling*, 2(1):32–46, 2022. Received: 10 November 2021; Revised: 23 January 2022; Accepted: 10 February 2022; Published: 23 February 2022.